

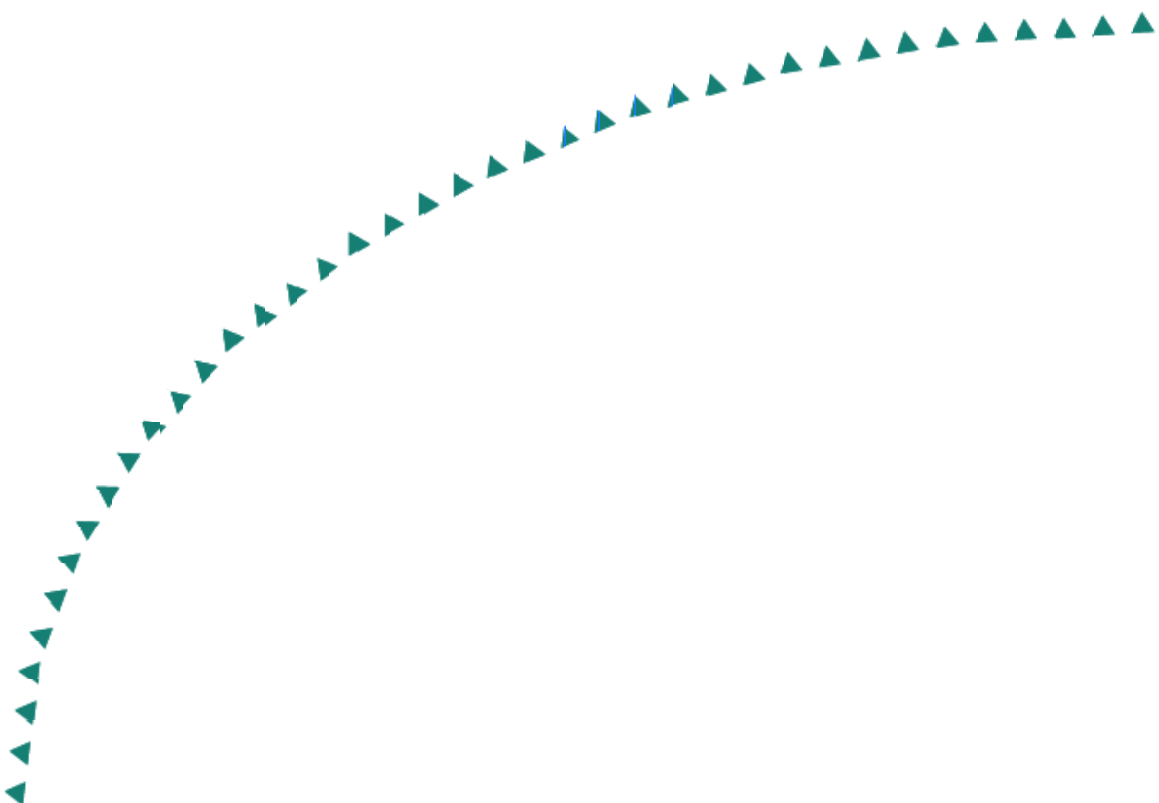
2003-10

Final Report

Enhancements and Verification Tests for Portable Deflectometers



Research



Technical Report Documentation Page

1. Report No. MN/RC – 2003-10	2.	3. Recipients Accession No.	
4. Title and Subtitle ENHANCEMENTS AND VERIFICATION TESTS FOR PORTABLE DEFLECTOMETERS		5. Report Date May 2003	
		6.	
7. Author(s) Olivier Hoffmann, Bojan Guzina and Andrew Drescher		8. Performing Organization Report No.	
9. Performing Organization Name and Address University of Minnesota Department of Civil Engineering 500 Pillsbury Drive S.E., Minneapolis, MN 55455-0220		10. Project/Task/Work Unit No.	
		11. Contract (C) or Grant (G) No. (c) 74708 (wo) 185	
12. Sponsoring Organization Name and Address Minnesota Department of Transportation 395 John Ireland Boulevard Mail Stop 330 St. Paul, Minnesota 55155		13. Type of Report and Period Covered Final Report: 2001-2003	
		14. Sponsoring Agency Code	
15. Supplementary Notes http://www.lrrb.gen.mn.us/PDF/200310.pdf			
16. Abstract (Limit: 200 words) In this study, the accuracy of the stiffness estimate from portable deflectometers is investigated, based upon the example of a particular device, PRIMA 100. The Beam Verification Tester (BVT) apparatus was developed at the University of Minnesota for the Minnesota Department of Transportation to: (i) verify the performance of the PRIMA device and (ii) to check the calibration factors of the sensors of the PRIMA device. The objective of such tests is to detect the potential occurrence of deterioration of the sensor's accuracy. Associated with the BVT apparatus, an enhanced setup for the portable device is examined. The inconsistency of the traditional data interpretation method using peak values of load and displacement time histories is pointed out by comparing the stiffness estimated from the PRIMA device against the known stiffness of the beam. An alternative method using Frequency Response Functions, spectral average, Single Degree of Freedom System analog, zero frequency estimates and curve fitting is proposed to extract the static stiffness from PRIMA measurements. Test results show good agreement between estimates based on the modified analysis and true beam stiffness. Implementation of both the alternative data interpretation method and the enhanced device setup to quality assurance field measurements are proposed.			
17. Document Analysis/Descriptors Portable deflectometer In-situ elastic modulus Accuracy of stiffness estimation		18. Availability Statement No restrictions. Document available from: National Technical Information Services, Springfield, Virginia 22161	
19. Security Class (this report) Unclassified	20. Security Class (this page) Unclassified	21. No. of Pages 101	22. Price

ENHANCEMENTS AND VERIFICATION TESTS FOR PORTABLE DEFLECTOMETERS

Final Report

Prepared by

Olivier Hoffmann
Bojan Guzina
and Andrew Drescher

University of Minnesota
Department of Civil Engineering

May 2003

Published by

Minnesota Department of Transportation
Office of Research Services
395 John Ireland Boulevard
Mail Stop 330
St. Paul, Minnesota 55155

The contents of this report reflect the views of the authors who are responsible for the facts and accuracy of the data presented herein. The contents do not necessarily represent the view or policy of the Minnesota Department of Transportation and/or the Center for Transportation Studies. This report does not contain a standard or specified technique.

The authors and the Minnesota Department of Transportation and/or Center for Transportation Studies do not endorse products or manufacturers. Trade or manufacturer's names appear here herein solely because they are considered essential to this report.

TABLE OF CONTENTS

CHAPTER 1 – INTRODUCTION	1
1.1 Background	1
1.2 Research issues and goals	2
1.3 Research approach	3
1.4 Report organization	3
 CHAPTER 2 - THEORETICAL BACKGROUND	 5
2.1 Soil modulus	5
2.2 Elastostatic model	7
2.3 Review of the Single Degree of Freedom system.....	8
2.4 Motion transducers	11
2.5 Frequency Response Function (FRF) for a SDOF system	13
2.5.1 Fourier transform	14
2.5.2 Mobility function $M(\omega)$	15
2.5.3 Dynamic stiffness function $K(\omega)$	16
2.5.4 Practical considerations	17
2.5.5 Estimation of FRF	18
2.6 FRF for a homogeneous elastic half-space model	20
2.6.1 Exact solution for the vertical compliance of a massless footing	20
2.6.2 Vertical compliance of a massive footing	22
 CHAPTER 3 - PFWD PRIMA 100 DEVICE	 23
3.1 Experimental setup	23
3.2 Measurement principle	25
3.3 Issues regarding the current PRIMA device.....	27
3.4 Enhancement of PRIMA device	28
 CHAPTER 4 - BEAM VERIFICATION TESTER: TRUE STIFFNESS OF THE BEAM VS. PRIMA ESTIMATES	 30
4.1 Setup for the BVT	30
4.1.1 Choice of the setup	30
4.1.2 Beam setup description	30
4.2 Static stiffness of the beam k_s	32
4.2.1 Theoretical static stiffness of the beam	32
4.2.2 Experimental Young's modulus of the steel.....	34
4.2.3 Experimental static stiffness of the beam K_{true}	35
4.3 Estimated beam stiffness k_{est} from PRIMA vs. k_s	36
4.4 Possible causes of the misfit between k_{est} and k_s	38
4.4.1 PRIMA sensors accuracy	38
4.4.2 Theoretical comparison of peak-based k_{est} vs. k_s	40

CHAPTER 5 - ENHANCEMENT OF BEAM STIFFNESS ESTIMATION USING PRIMA DEVICE	43
5.1 Consistent data interpretation	43
5.1.1 SDOF model for the beam	45
5.1.2 Frequency domain analysis tools	46
5.2 Experimental procedure and results	47
5.2.1 Data acquisition setup	47
5.2.2 Fitting process	49
5.2.3 Estimated k_{est} from PRIMA vs. k_s using the mobility function	49
5.2.4 Beam with additional damping	51
5.2.4.1 Auxiliary dampers.....	52
5.2.4.2 External damping setup	52
5.2.4.3 Experimental results	54
5.3 PFWD BVT apparatus: summary and practical applications	56
5.3.1 PFWD PRIMA	56
5.3.2 Other portable deflectometer devices	57
CHAPTER 6 – PRIMA DEVICE: ADDITIONAL CONSIDERATIONS AND RECOMMENDATIONS FOR FIELD USE	58
6.1 Theoretical comparison peak-based k_{est} vs. k_s for field profiles	58
6.1.1 Homogeneous half-space	58
6.1.2 Layered half-space	61
6.2 Proposal for PRIMA field-testing enhancements	62
6.2.1 Backcalculation analysis	62
6.2.2 Hardware	63
CHAPTER 7 – CONCLUSIONS	65
References	67
Appendix	A1

LIST OF FIGURES

	page
Fig. 2.1. Common in-situ test configuration.....	5
Fig. 2.2. Typical cyclic shear stress vs. cyclic shear strain curve (granular material).....	6
Fig. 2.3. Half-space loaded by a circular footing.....	7
Fig. 2.4. SDOF system - top force excitation.....	9
Fig. 2.5. SDOF system - base motion excitation.....	12
Fig. 2.6. Plot of the magnification factor for a SDOF system - base motion excitation	13
Fig. 2.7. Ideal single input/single output linear system	14
Fig. 2.8. Plot of the mobility function – theoretical example for a SDOF system.....	16
Fig. 2.9. Plot of the dynamic stiffness function – theoretical example for a SDOF system ...	17
Fig. 2.10. Relationships among FRFs	18
Fig. 2.11. Theoretical dimensionless compliance functions for the vertical mode of vibration of a massless rigid disk resting on an elastic half-space.....	21
Fig. 2.12. Steady-state forcing of the elastic half-space – massive rigid footing.....	21
Fig. 3.1. General illustration of PRIMA 100 device.....	23
Fig. 3.2. Detailed illustration of PRIMA 100 device.....	24
Fig. 3.3. Plot of PRIMA’s software output	26
Fig. 3.4. Modification of the setup of PRIMA device	29
Fig. 4.1. Sketch of the verification setup	31
Fig. 4.2. Verification setup.....	31
Fig. 4.3. Idealized beam model layout.....	33
Fig. 4.4. Four-point bending and static stiffness tests setup.....	35
Fig. 4.5. PRIMA measurements on the 70 cm span beam, using a rubber hammer	37
Fig. 4.6. Verification of PRIMA’s geophone output against an accelerometer.....	39
Fig. 4.7. Peak method applied to a theoretical SDOF system.....	41
Fig. 4.8. Influence of the pulse duration on peak-based stiffness estimation goodness - theoretical SDOF system	41
Fig. 5.1. BVT data acquisition	44
Fig. 5.2. SDOF analog for the BVT setup	46
Fig. 5.3. Typical measurement sequence and output..	48
Fig. 5.4. Measured data and fitted SDOF curves- example of a 60 cm span beam	50
Fig. 5.5. Fitted SDOF real part of $K(\omega)$ - example of a 60 cm span beam	50
Fig. 5.6. Simplified layout of the simply supported beam with damping devices located on the cantilever parts	53

Fig. 5.7. Layout of a damping device located at the end of the overhanging part of the beam..	53
Fig. 5.8. Testing setup for the BVT with additional damping	54
Fig. 5.9. Comparison of velocity time histories – undamped and damped beam setup	55
Fig. 6.1. Example of time history plots – homogeneous half-space	59
Fig. 6.2. Example of plot k_{est}/k_s vs. \bar{T} - homogeneous half-space.....	60
Fig. 6.3. Possible field testing setup for PRIMA device.....	64

LIST OF TABLES

Table 2.1. SDOF free vibration solutions.....	10
Table 2.2. Nomenclature for FRF	14
Table 4.1. Values of k_s using direct measurement and beam theory	36
Table 4.2. Average k_{est} from PRIMA: original (with small height drops) and enhanced configurations vs. k_s	37
Table 5.1. Static stiffness estimates via fitting of the mobility function – undamped beam.....	51
Table 5.2. Static stiffness estimates via fitting of the mobility function – beam with damping devices	56

LIST OF SYMBOLS

The following alphabetical list defines the main symbols associated with the main parameters used through the report.

Symbol	name
a	footing radius
a_1	distance between beam support and receptacle support
β	tuning ratio
b	beam width
c	damping coefficient
c_s	shear wave velocity
C_{vv}	vertical compliance half-space/rigid footing
\bar{C}_{vv}	non-dimensional vertical compliance half-space/rigid footing
Δt	sampling period
$\Delta \omega$	angular frequency resolution
d	distance between receptacle supports
ε	strain
E	Young's modulus
E_{max}	small strain or seismic elastic modulus
E_{true}	true Young's modulus of the beam
f	force time history
f_{peak}	peak of the force time history
F	Fourier transform of f
F_0	steady-state force amplitude
f	linear frequency
f_n	undamped natural linear frequency
FRF	Frequency Response Function
γ^2	coherence function
G	shear modulus
G_{max}	maximum or small strain shear modulus
$G_{\psi\psi}(\omega)$	one-sided auto-spectral density function of the signal $\psi(t)$
$G_{\theta\psi}(\omega)$	one-sided cross-spectral density function between $\psi(t)$ and $\theta(t)$
η	shape factor (for interface soil/footing stress distribution)
h	beam thickness
i	imaginary number
I	beam cross-sectional moment of inertia
$I(\omega)$	impedance function
k	spring coefficient (stiffness)
$K(\omega)$	dynamic stiffness

k_{est}	estimated static stiffness
k_{static}	static stiffness
k_s	static elastic stiffness of a system
L	beam (effective) span
m	mass
m_{eq}	equivalent mass for the SDOF system
$M(\omega)$	mobility function
\bar{M}	mass ratio
M_b	bending moment
ν	Poisson's ratio
p	half the total load applied to the beam
θ and Θ	linear system's arbitrary input time history and its Fourier transform
ρ	soil's mass density
σ	stress
S	cantilever (overhanging) part of the simply supported beam
SDOF	Single Degree of Freedom System
t	time
t_q	discrete sampling time
T	duration of force pulse f
\bar{T}	dimensionless period
T_n	SDOF system natural period
ω	angular frequency
$\bar{\omega}$	dimensionless frequency
ω_j	discrete sampling frequency
ω_n	undamped natural angular frequency
ω_d	damped natural angular frequency
ξ	damping ratio
u and U_o	steady-state ground displacement and its amplitude
x	displacement time history
x_{peak}	peak of the displacement time history
X	Fourier transform of x
X_0	steady-state displacement amplitude
\dot{x}	velocity time history
\dot{X}	Fourier transform of \dot{x}
\ddot{x}	acceleration time history
\ddot{X}	Fourier transform of \ddot{x}
ψ and Ψ	linear system's arbitrary output time history and its Fourier transform
y	position along the beam
z and Z	arbitrary time history and its Fourier transform

EXECUTIVE SUMMARY

Non-destructive testing is becoming more commonly used in field characterization of paved and unpaved subgrade profiles. In particular, its application to the quality assurance of newly constructed granular base (i.e. pavement foundation) layers has become more widespread.

Typically, portable nondestructive devices are used for an in-situ assessment of the elastic parameters (such as Young's modulus) of compacted soil layers on the basis of dynamic force and displacement measurements. This study deals with the reliability of stiffness estimates stemming from such portable tools. To this end, the performance of a particular device, Portable Falling Weight Deflectometer (PFWD) PRIMA 100, is examined and verified against the newly developed verification tester, the PFWD Beam Verification Tester (BVT). The BVT apparatus has been developed at the University of Minnesota for the Minnesota Department of Transportation (Mn/DOT). This apparatus is intended for verifying the performance of PRIMA 100 devices. Using the BVT associated with a spectral analysis method, tests also can be conducted to check whether the calibration factors of the PRIMA device sensors, as given by the manufacturer, are accurate. The objective of the verification tests is to detect the potential occurrence of deterioration of the sensor's accuracy during the life of the field-testing device.

The data interpretation method that is traditionally used in PFWD testing uses *peak* values of the dynamic force and displacement records in lieu of their static counterparts. By comparing the PRIMA 100 device to the BVT, it is shown that this "peak values" method fails to produce correct estimates of the static beam stiffness, with an error often exceeding 100 percent. Systematic error due to the peak method, observed experimentally for the beam, can be expected in the field situations as well.

To eliminate this major source of systematic error associated with dynamic field-testing of soil stiffness, an alternative data interpretation method, based on spectral analysis, concept of frequency response function, and single-degree-of-freedom mechanical analog is employed to extract the true static stiffness of the support (i.e. beam) from PRIMA 100 measurements. The results show a good agreement between the true static stiffness of the beam and its estimates determined using the modified data interpretation method.

Using an appropriate model for the soil, the same method is proposed for quality assurance applications. On the basis of laboratory experiments, a simplified, yet improved version of the commercial PFWD device also is proposed that improves the dynamic signature of the impact force and minimizes the detrimental effects of non-linear soil behavior in common field situations.

CHAPTER 1 - INTRODUCTION

1.1 Background

Although empirical methods are still widely used in pavement design, mechanistic-empirical design procedures are beginning to be implemented. Such methods are based upon the determination of the fundamental mechanical properties of pavement layers. The material properties typically used to characterize base and subgrade layers within the framework of mechanistic methods are the resilient modulus and Young's modulus. The former can be measured via laboratory tests (see the LTPP protocol P46 [1]), whereas the latter modulus, whose field measurement is the focus of this study, is typically estimated using nondestructive testing (NDT) techniques. The field techniques addressed in this report are limited to dynamic NDT methods. Other field methods that also are commonly employed to estimate Young's modulus include static NDT methods (bearing plate tests) and destructive methods (penetration tests). These methods do not fall within the scope of this study and will not be discussed.

In NDT of pavement profiles, the properties of soils, aggregate base and hot-mix asphalt (HMA) layers are commonly estimated from field measurements using backcalculation methods. The estimated property is often the stiffness of the NDT device's loading plate-pavement system. Due to their short test duration, the most promising devices are based upon a dynamic loading using vibratory or impulse sources. Such devices provide a fast and accurate tool that has important applications in construction quality assurance and pavement deterioration assessment. A good example would be the Falling Weight Deflectometer (FWD) devices. Indeed, the backcalculation of the elastic properties of pavement layers using FWD measurements is a well-recognized procedure in pavement assessment. The reader can find more about this topic in Lytton [2]. Among various testing devices for non-destructive in-situ assessment of soil properties, portable deflectometer-type devices have recently become the focus of increasing interest. These devices, being portable, are easier to use and require only one or two operators. These portable devices are based on the dynamic force and deflection measurements. They can be classified into three main categories: 1) vibratory devices, such as the Humboldt GEOGAUGE, 2) impact load devices based upon a transient type of loading, such as the Portable Falling Weight Deflectometers (PFWDs) PRIMA 100 and LOADMAN, and 3) devices based on the Spectral Analysis of Surface Waves (SASW), such as the Portable Seismic Pavement Analyzer (PSPA), and its revisions called "Dirt" SPA (D-SPA) and Olson SASW-2G. In contrast to SASW tools, vibratory and impact load devices are both based on the so-called deflectometer type analysis that will be the subject of this investigation. Among the latter, the most commonly used devices are the PFWDs and the GEOGAUGE.

1.2 Research issues and goals

This report addresses issues associated with portable NDT devices used by the Minnesota Department of Transportation (Mn/DOT), namely GEOGAUGE, PRIMA 100, and LOADMAN devices. The main concern is to assess whether or not the footing-on-soil stiffness (and soil modulus) estimates obtained from these devices are reliable. These devices all fall into the category of near-field testing devices, in the sense that the deflection measurements are made in the vicinity of the applied load. All of the above devices measure the stiffness of the footing-on-a-subgrade system and provide user with an estimation of the equivalent homogeneous elastic modulus of the granular base and subgrade materials. GEOGAUGE records the data in the frequency domain, whereas impact devices record the time history of dynamic measurements. PRIMA 100 measures both load and displacement time histories; GEOGAUGE records the dynamic stiffness transfer function, and LOADMAN acquires acceleration to estimate peak deflection and uses either an estimate of the load (original version) or a measured load (LOADMAN 2) to calculate the elastic modulus.

It is well-known that the modulus estimates obtained in the field are strongly dependant upon the applied stress and therefore upon the particular NDT device being used. For example, one can refer to comparative studies in Chen & al [3], Siekmeier and al. [4], Mc Kane [5] and Van Gorp and al. [6]. The inconsistency of stiffness estimates stemming from various portable devices is due to two main reasons: 1) the stress dependency of the soil and therefore the dependency upon the testing device 2) the correctness of stiffness estimates (i.e. the analysis) associated with a given device. The dependency upon the device renders comparison between modulus estimates obtained from several devices difficult. The treatment of the first issue is out of this report's scope. One way to overcome such disparity in the results is to investigate experimental correlations between devices or empirical relationships from laboratory results. Concerning the second issue, a rational approach needs to be developed to check and validate the stiffness estimates stemming from a given portable device, which is the focus of this study. The in-situ mechanical properties of soils and granular materials are generally unknown, especially owing to the stress dependency of the base and subgrade materials. To determine whether or not the stiffness estimates obtained from a given field-testing device are reliable, verification against a well-characterized foundation (or support) model is indispensable.

The main issue of this project is therefore to design a laboratory setup to verify on a routine basis the stiffness estimates resulting from portable deflectometer-type devices. A secondary issue is to investigate enhancing such devices. One particular portable device, PRIMA 100, has been chosen as a focus for this project. Among the devices available for this study, PRIMA device was the best example possible to set up the performance verification procedure, since both measurements of load and displacement can be checked. PRIMA testing is based upon measurement of the velocity due to impact load applied by a falling weight onto a plate resting on the surface of the tested layer. The primary concerns regarding verification of the performance of PRIMA device are 1) accuracy of the force and velocity sensors embedded in PRIMA, and 2) scrutiny of the

internal backcalculation procedure that produces stiffness estimates from peak values. The Beam Verification Tester (BVT) apparatus has been developed at the University of Minnesota for the Minnesota Department of Transportation (Mn/DOT). Using the BVT associated with a spectral analysis method, tests can be conducted to evaluate the performance of PRIMA stiffness estimation. Also, the BVT can be utilized to check whether the calibration factors of the sensors of PRIMA devices, as given by the manufacturer, are accurate or not, the objective being the detection of a potential occurrence of deterioration of the sensor's accuracy during the life of the devices.

1.3 Research approach

The interpretation of FWD and PFWD measurements is in practice based on a simplified waveform analysis, which focuses on the peak values of the force and displacement time histories. This *peak method* can be seen as an attempt to obtain static properties from tests that are dynamic in nature. A major drawback of this simplification is that the time offsets between peak values and the inertia effects are disregarded. The use of the traditional methods based on this peak method to provide an input to elastostatic backcalculation is known to lead to erroneous estimates of pavement layers properties. Using the entire waveforms as input to a dynamic backcalculation method would be associated with a high computational cost, which is currently not desirable for routine practice. As shown recently by Guzina and Osburn [7], the elastostatic backcalculations perform well when the peak method is advantageously replaced by a simple analysis involving the concept of Frequency Response Function (FRF).

Utilization of FRF-based method in quality assessment has not been implemented widely to date, although it has been revisited by several researchers. An example of FRF applied to pavement integrity evaluation is given in the 1994 paper by Lepert and al. [8]. Stolle [9] used a FRF associated with a Single Degree of Freedom System (SDOF) analog to estimate an equivalent homogeneous Young's modulus. Briaud [10] applied such method to the estimation of the static soil-under-a-spread-footing stiffness using an impact test.

The interpretation of PRIMA 100 measurements is based upon a peak values method associated with an elastostatic calculation algorithm. As a result, the verification of the performance of the device involves not only verification of the accuracy of the sensors, but also modification of the data interpretation method. An alternative methodology based upon a new data acquisition procedure and a determination of the static stiffness via FRF and spectral average concepts is one of the key contributions to this study.

1.4 Report organization

The remainder of this report is organized in six chapters. In Chapter 2, we will first examine the theoretical elastostatic framework embedded in the classical deflectometer-

type data interpretation and review useful notions such as SDOF systems, FRFs, and spectral analysis. In Chapter 3, we present the PRIMA device, explore how it operates, and how the measurements are interpreted in common practice. Chapter 4 describes the proposed verification setup and procedure that will be used to verify PRIMA stiffness estimates. The verification assembly, so-called Beam Verification Tester (BVT), based on a simply supported steel beam, will be introduced. Its mechanical stiffness will be examined theoretically and experimentally using a static calibration test. Results of verification tests on the BVT apparatus will be discussed. The consistency of the stiffness estimates obtained from PRIMA device as intended by the manufacturer is investigated with a focus on the data interpretation method. In Chapter 5, an alternative calculation approach is introduced and used to verify the performance the device. This approach involves both an enhancement of the device and a modification of the data acquisition and interpretation method. The proposed data interpretation method is based upon the full waveform analysis performed via measurement of an appropriated FRF, such as the mobility $M(\omega)$, from which the true static stiffness can be extracted. The BVT apparatus will be proposed as a tool to perform routine verification tests of the performance of PRIMA devices. Guidelines for extension of the BVT to other portable deflectometer devices will be presented. Finally, recommendations for the enhanced field performance of the PRIMA device and conclusions will be presented in Chapters 6 and 7, respectively.

CHAPTER 2 - THEORETICAL BACKGROUND

As stated in Chapter 1, the Young's modulus of base and subgrade layers is the parameter targeted by NDT methods. Typically, this modulus is inferred from field measurements of the device's-circular-footing-on-top-of-soil stiffness. However, there is a need to clarify what is a soil Young's modulus. Indeed, the Young's modulus of a soil is not unique and several definitions exist. The models used in practice to interpret field measurements generally assume linear elasticity and thus small deformations. The models developed to verify the field devices in this study also need to comply with these requirements. We will first clarify the modulus of interest. We will further examine the elastic forward model underlying the estimation of Young's modulus from force and deflection measurements, as intended by the manufacturers. We also will introduce some theoretical considerations concerning the Single Degree of Freedom (SDOF) model and the Frequency Response Functions (FRFs), anticipating their need in the subsequent chapters. Finally, the solution for the complex compliance of an elastic half-space model is introduced.

2.1 Soil modulus

Portable deflectometer devices are usually associated with data interpretation assuming a soil model that is semi-infinite, homogeneous, and elastic. In many cases, however, the field situation for pavement foundation testing can be more accurately described as a uniform layer on top of a half space, as sketched in Fig. 2.1. In this case, the modulus estimated using the device is a combination of the moduli of the base and subgrade layers. The resulting measured modulus is referred to as the *equivalent homogeneous modulus*.

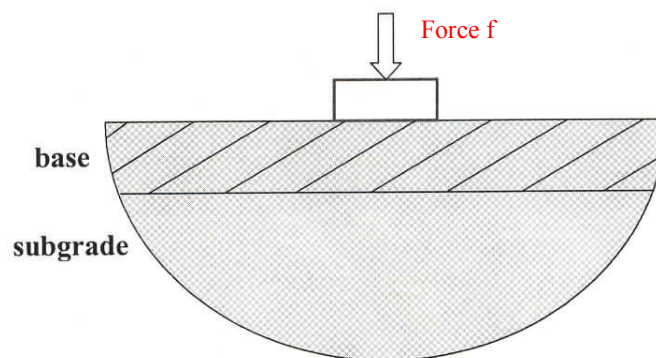


Fig. 2.1. Common in-situ test configuration

In the backcalculation of pavement profiles, the assumed forward models are commonly based on linear elasticity. However, the materials we are dealing with are highly non-linear. Indeed, soil properties are known to be highly dependent upon pressure and strain level, among other parameters (see Hardin and Drnevich 1972 [11]). Previous experimental work by Pak and Guzina [12] also illustrated the stiffness dependence of a soil-foundation system upon both the size of the foundation and the static pressure applied to the soil, on the basis of scaled centrifugal tests.

In the literature many definitions of soil moduli are utilized: secant modulus, tangent modulus, maximum modulus, resilient modulus. Let us examine the nonlinear constitutive stress-strain relation for cyclic shear test depicted in Fig. 2.2. This plot shows that the shear modulus $G(\gamma)$ is strain dependent: it decreases as the strain level increases.

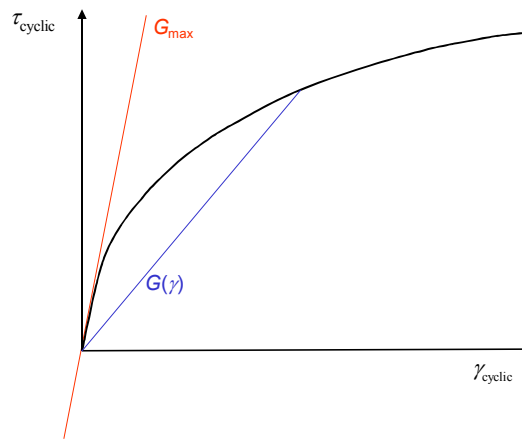


Fig. 2.2. Typical cyclic shear stress vs. cyclic shear strain curve (granular material)

Therefore, the measured equivalent homogeneous elastic modulus will depend upon the particular conditions associated with how each testing device applies the load. As a result, Young's modulus estimates from different devices or different testing setups inevitably will differ, and one has to be very careful when comparing different devices.

Fig. 2.2 also illustrates the fact that for small strains, $G(\gamma)$ becomes constant. In this case, the shear modulus is referred to as the maximum shear modulus G_{max} . The same concepts apply to Young's modulus E , and E_{max} is known as the *seismic modulus* or *small strain modulus*. E_{max} is also the slope of the initial unloading/reloading hysteresis loop for small deformations. As a matter of fact, it is accepted that at *low strain* level, (of the order of $10^{-4}\%$ for the cyclic shear strain), the soil exhibits an approximately elastic behavior (e.g. Kramer [13]; Richart et al. [14]; Seed et al. [15]). In other words, such strain level is not large enough to induce significant non-linear stress-strain behavior in the soil. Typically, E_{max} is estimated in the field using low strain level *nondestructive testing* (NDT) techniques.

For pavement construction quality assurance and deterioration monitoring purposes, the use of tests involving small deformations would bring more consistency in the sense that only one value of elastic modulus (namely E_{max} or G_{max}) would be

estimated. This would enable a direct comparison between various deflectometer devices. Such modulus estimates also could be directly compared to geophysics investigation methods. Furthermore, for a given dominant wavelength of the applied dynamic force, the use of testing methods transmitting a smaller energy level to the soil is associated with a smaller depth of penetration. This is appreciable in quality assurance of pavement construction where the modulus of the tested surface layer (e.g. base) needs to be checked only: The estimated equivalent homogeneous modulus would then correspond to the seismic modulus of the targeted layer.

2.2 Elastostatic model

For the sake of simplicity, it is generally assumed in portable NDT methods that the tested pavement foundation is elastic, isotropic, homogeneous and unbounded. The backcalculation problem is further simplified by considering the *static* load-displacement relationship. As illustrated in Fig. 2.3, the tested soil is modeled as an elastic semi-infinite half-space continuum, characterized by two elastic constants, Poisson's ratio ν and shear modulus G . Young's modulus E and shear modulus G are related by the well-known relationship from elasticity theory (for example, in Sokolnikoff [16])

$$E = 2 G (1 + \nu) \quad (1)$$

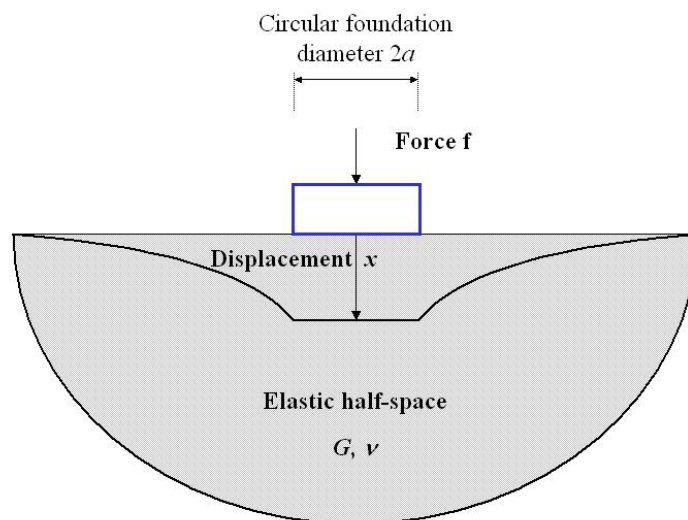


Fig. 2.3. Half-space loaded by a circular footing

As mentioned earlier, the devices under study are deflection-based. The measured quantities are load and displacement. From static measurements of load and displacement one can compute the static stiffness, defined for any linear system as

$$k = \frac{f}{x} \quad (2)$$

where x is the displacement of the surface due to the applied force f , measured at the center of the footing. As a result, the stiffness k is a parameter of fundamental interest in the operation of the portable deflectometer devices. During testing with PRIMA device, the load is applied to the soil support via a circular base plate of radius a (see Fig. 2.3). The resulting displacement is measured under the load, at the center of the plate.

The Boussinesq equation, classical elastic solution of the problem of a half-space subjected to a surface point load, can be used to derive the relationship between displacement and stresses for the case of a rigid or flexible foundation sitting on the half-space. Such relationships can be found, for example, in Craig [17]. In the particular case where the displacement under the center of circular footing of radius a resting on the surface of the elastic half-space is considered, the shear modulus G and Poisson's ratio ν are related to the static stiffness k according to

$$G = \frac{k(1-\nu)}{\eta a} \quad (3)$$

where η is a shape factor depending upon the stress distribution at the interface soil/footing. If the stress is uniformly distributed under the footing, which corresponds to a flexible footing, then $\eta = \pi$. At the extreme opposite, for the case rigid footing is modeled, the stress distribution is no longer uniform and $\eta = 4$.

To conclude, the elastostatic analysis provides a closed-form static solution from which, for a known or assumed value of the Poisson's ratio of the soil, the soil Young's modulus can be computed from measurements of the stiffness.

2.3 Review of the Single Degree of Freedom system

The section's purpose is to briefly review the main results of the motion of a Single Degree Of Freedom (SDOF) system. For more details, the reader should consult the specialized literature. Reference examples are a book of Meirovitch [18] for the fundamental aspects and a book of Inman [19] for more detailed engineering applications.

A SDOF system is defined as a system that contains only one significant rigid mass. The constitutive response of a SDOF system can be described in term of the mechanical Kelvin-Voigt analog. As depicted in Fig. 2.4, the SDOF system is comprised of a mass m , a massless dashpot with damping coefficient c , and a massless spring of constant k . The spring represents the elastic part (stiffness) of the system whereas the dashpot represents the viscous damping. In this example the SDOF system is attached at its base to a rigid support and subjected to a top excitation time varying force $f = f(t)$.

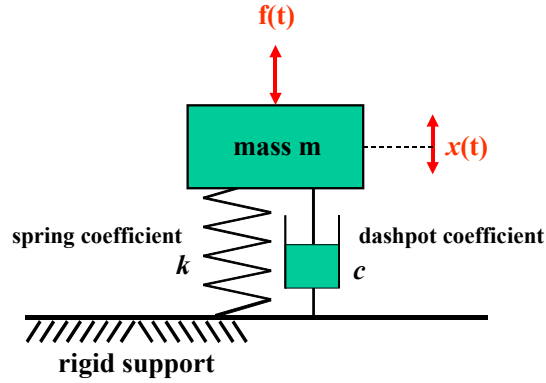


Fig. 2.4. SDOF system - top force excitation

With reference to Fig. 2.4, the SDOF system responds with a displacement $x = x(t)$ induced by the applied force $f = f(t)$. The corresponding equation of motion is

$$m \ddot{x} + c \dot{x} + k x = f \quad (4)$$

The notation \dot{x} represents the velocity dx/dt and \ddot{x} stands for the acceleration d^2x/dt^2 . Using the definition of the undamped natural frequency ω_n and the damping ratio ξ , i.e.

$$\omega_n = \sqrt{\frac{k}{m}} \quad (5)$$

$$\text{and} \quad \xi = \frac{c}{2 m \omega_n} \quad (6)$$

the equation of motion can be rewritten as

$$\ddot{x} + 2 \xi \omega_n \dot{x} + \omega_n^2 x = \frac{f}{m} \quad (7)$$

The solution to this ordinary differential equation (ODE) can be derived via the time domain analysis or via the frequency domain analysis. The solution of the ODE can be written as the sum of a general or homogeneous solution corresponding to the case $f = 0$, and of a particular solution that takes into account the applied force. The total motion of the SDOF is correspondingly decomposed into a free vibration part (homogeneous solution) and a forced vibration part (particular solution). For the free vibration case, enforcing a solution of the type $x(t) = A e^{\lambda t}$, it can be shown that

$$x = A_1 e^{\lambda_1 t} + A_2 e^{\lambda_2 t} \quad (8)$$

where A_1 and A_2 are constants to be determined from the initial conditions and where λ_1 and λ_2 are the roots of the characteristic equation

$$\lambda^2 + 2 \xi \omega_n \lambda + \omega_n^2 = 0 \quad (9)$$

Depending upon the value of the damping coefficient ξ , several cases can be distinguished: the undamped case ($\xi = 0$), the overdamped case ($\xi > 1$), the critically damped case ($\xi = 1$), and the underdamped case ($\xi < 1$). The roots of the characteristic equation are synthesized in Table 2.1.

	undamped case	overdamped case	critically damped case	underdamped case
roots of the characteristic equation $\lambda_{1,2}$	$\pm \omega_n i$	$-\xi \omega_n \pm \omega_n \sqrt{\xi^2 - 1}$	$-\omega_n$	$-\xi \omega_n \pm i \omega_n \sqrt{1 - \xi^2}$
solution $x(t)$	$A \sin(\omega_n t + \phi_A)$	$B_1 e^{- \lambda_1 t} + B_2 e^{- \lambda_2 t}$	$e^{\omega_n t} (C_1 + C_2 t)$	$e^{-\xi \omega_n t} D \sin(\omega_d t + \phi_D)$
associated definitions	$A = \sqrt{A_1^2 + A_2^2}$ $\phi_A = \text{atan}\left(\frac{A_1}{A_2}\right)$	-	-	$D = \sqrt{D_1^2 + D_2^2}$ $\phi_D = \text{atan}\left(\frac{D_1}{D_2}\right)$ $\omega_d = \omega_n \sqrt{1 - \xi^2}$

Table 2.1. SDOF free vibration solutions

The constants A_1 , A_2 , B_1 , B_2 , C_1 , C_2 , D_1 and D_2 must be determined from the initial conditions. They represent the amplitude of vibration. The parameter ω_d is called the damped natural frequency. Both ϕ_A and ϕ_D are referred to as the phase angle. The free vibration characteristics of the SDOF system depend only upon the properties of the SDOF and the initial conditions of motion.

Concerning the forced vibration, the most general case is the one of an arbitrary time varying applied force. The particular solution can be recovered using the Duhamel or convolution integral. For example, in the case of an underdamped SDOF system subjected to a force f applied from $t = 0$ to $t = T$, the particular solution can be written in terms of Duhamel integral as

$$x(t) = \frac{1}{m \omega_d} \int_0^t e^{-\xi \omega_n (t-\tau)} \sin(\omega_d (t-\tau)) f(\tau) d\tau \quad (10)$$

The Duhamel integral can be determined in a closed-form manner only for a few cases where f is simple enough and known analytically. In general, integral (10) has to be evaluated numerically.

An alternative and yet very common way to evaluate the system motion is to perform a direct numerical integration of the equation of motion. Among the various existing methods, one can refer to the linear acceleration method in Wilson and Clough [20]. This step-by-step method is easy to implement and gives accurate results.

A particular case of forced vibration is the steady-state case, in which the transient part is disregarded. In this case the analysis is simplified. Assuming a harmonic applied force, for example a sine force described by

$$f = F_0 \sin(\omega t) \quad (11)$$

one can show that the motion is given by

$$x = X_0 \sin(\omega t - \phi) \quad (12)$$

where X_0 is defined as

$$X_0 = \frac{F_0}{m \sqrt{(\omega_n^2 - \omega^2)^2 + (2\xi \omega \omega_n)^2}} = \frac{F_0}{k} \frac{1}{\sqrt{(1 - \beta^2)^2 + (2\xi \beta)^2}} \quad (13)$$

and ϕ is

$$\phi = \text{atan}\left(\frac{2\xi \omega \omega_n}{\omega_n^2 - \omega^2}\right) = \text{atan}\left(\frac{2\xi \beta}{1 - \beta^2}\right) \quad (14)$$

In these equations, ω is the driving frequency, f_0/k corresponds to the static displacement x_{static} and β is the tuning ratio defined as

$$\beta = \frac{\omega}{\omega_n} \quad (15)$$

A useful quantity is the amplification or *magnification factor* of the SDOF model, defined as

$$\frac{X_0}{x_{static}} = \frac{1}{\sqrt{(1 - \beta^2)^2 + (2\xi \beta)^2}} \quad (16)$$

Note that all the equations are written using the circular frequency ω , given in terms of the linear frequency f by

$$\omega = 2 \pi f \quad (17)$$

2.4 Motion transducers

In the existing portable deflectometer devices, measurement of dynamic displacement is performed using motion transducers operating without a fixed frame of reference, namely geophones (velocity transducers) or accelerometers (acceleration sensors). The associated backcalculation process also utilizes these transducers, and it is important to introduce some of the basic concepts used for the measurement of displacement.

Geophones are sensors whose output is proportional to velocity, whereas the output of accelerometers is proportional to acceleration. The displacement time history can be obtained by integration of the velocity time history or by double integration of the acceleration time history. Regular geophones and accelerometers are both referred to as seismic transducers, designed using SDOF system theory. Also common are the piezoelectric transducers, for which acceleration is sensed. However, the output of piezoelectric sensors also can be proportional to velocity by integration of the acceleration. Geophones are sensors designed with a low natural frequency (typically of the order of 3 to 20 Hz) whereas accelerometers are designed with very high natural frequency (typically several kHz).

The operating frequency range of geophones is typically located above their natural frequency, whereas accelerometers are theoretically accurate for frequencies lower than their natural frequencies. Poor noise/signal ratios, however, reduce the reliability measurements from accelerometers at very low frequencies. As a result, the output of both types of sensors at very low frequencies (of the order of 3-15 Hz) is disregarded in practice.

To illustrate the operation of common seismic transducers, the theoretical response of a geophone, for which the output voltage is proportional to the velocity of the mass, is examined. The output voltage of an SDOF-type velocity transducer is generated by a coil of mass m moving through a magnetic field. Moreover, the output voltage is directly proportional to the relative velocity between the coil and the magnet (Faraday's law). Consider a SDOF system subjected to a steady-state sine displacement $u = u(t)$ at its base (see Fig. 2.5) where

$$u = U_0 \sin(\omega t) \quad (18)$$

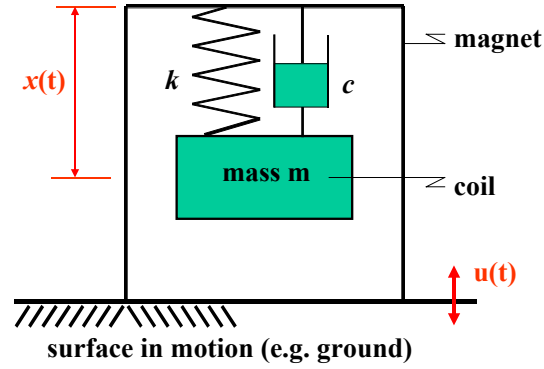


Fig. 2.5. SDOF system - base motion excitation

With regards to Fig. 2.5, the magnet is made part of the transducer's frame, which experiences the same motion as the attached surface. In such scenarios, the output voltage is, therefore, directly proportional to the relative velocity between the coil and the surface in motion. Similarly to the case presented in the previous section, it can be shown that the motion $x = x(t)$ of the transducer relative to its support is

$$x = X_0 \sin(\omega t - \phi) \quad (19)$$

and that the magnification factor is

$$\frac{X_0}{U_0} = \frac{\dot{X}_0}{\dot{U}_0} = \frac{\beta^2}{\sqrt{(1 - \beta^2)^2 + (2\xi\beta)^2}} \quad (20)$$

Based on equation (20), it can be readily proved that for $\beta \gg 1$, i.e. for frequencies higher than the natural frequency of the geophone, the magnification factor tends towards a unit value. That is, the geophone experiences the same motion as its support for $\beta \gg 1$.

The complete plot of the magnification factor versus tuning ratio is presented in Fig. 2.6 for three different values of damping ratio ξ . From Fig. 2.6 we observe that for $\beta > 2$ to 3, the magnification factor of a geophone can be considered as constant and equal to 1. On the contrary, for $\beta < 2$ to 3, the magnification factor, and therefore the geophone output, is highly non-linear. With reference to Fig. 2.6, the amplification factor is constant on a larger frequency range for a damping ratio close to 70% than for smaller damping ratios. Indeed, 70% of damping is very often the value chosen in the design of seismic sensors when the goal is to obtain a maximum operational range for the amplitude of the measured signal.

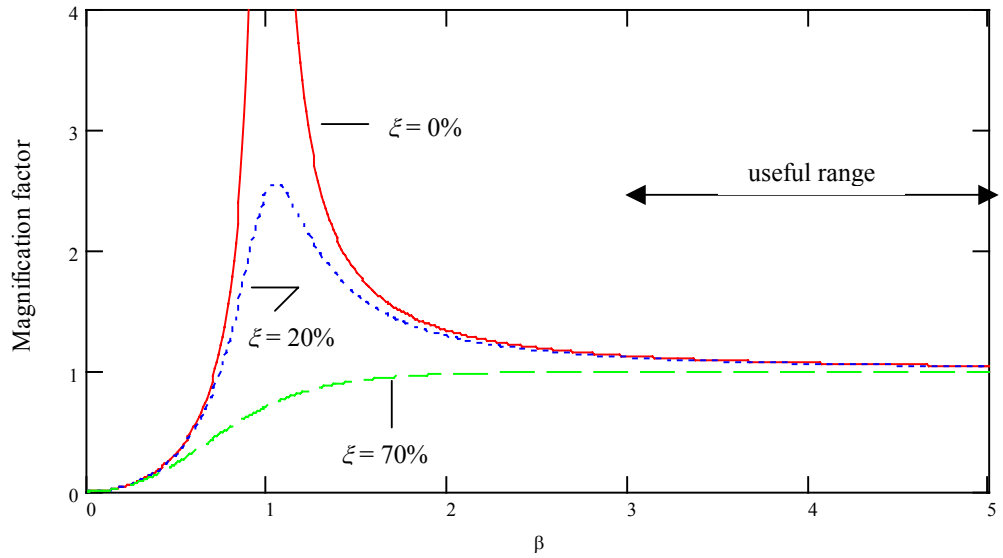


Fig. 2.6. Plot of the magnification factor for a SDOF system - base motion excitation

The main consequence resulting from the featured magnification factor is that the output of an SDOF-type geophone should be disregarded at very low frequencies. To provide for engineering applications, let us consider the common case of a geophone with a natural frequency of the order of 5 Hz. As a guideline, the output of such a transducer should not be taken into account for frequencies below 10 – 20 Hz.

2.5 Frequency Response Function (FRF) for a SDOF system

Let us consider the ideal linear system depicted in Fig. 2.7. The system is subjected to an input $\theta(t)$ and responds with an output $y(t)$. Let $\Theta(\omega)$ and $Y(\omega)$ be the Fourier transforms of $\theta(t)$ and $z(t)$. Frequency response functions $\text{FRF} = \text{FRF}(\omega)$ of the linear system are defined in frequency domain as the ratio between output $Y(\omega)$ and input $\Theta(\omega)$

$$\text{FRF}(\omega) = \frac{\Psi(\omega)}{\Theta(\omega)} \quad (21)$$

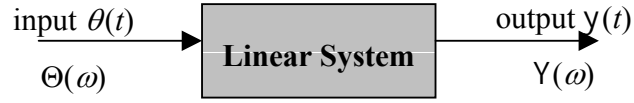


Fig. 2.7. Ideal single input/single output linear system

FRFs constitute a particular case of the so-called transfer functions, which are defined in the Laplace domain rather than in Fourier domain. Several types of frequency response functions can be defined, depending upon the quantities of interest taken as system input and output. The most commonly used type of FRF describes the relation between a force input and the system's kinematic output, which can be displacement, velocity, or acceleration. This type of FRF will be the only one discussed here. Table 2.2 presents a general nomenclature based on the output's type.

FRF definition	$\frac{\text{Displacement}}{\text{Force}}$	$\frac{\text{Velocity}}{\text{Force}}$	$\frac{\text{Acceleration}}{\text{Force}}$	$\frac{\text{Force}}{\text{Displacement}}$	$\frac{\text{Force}}{\text{Velocity}}$	$\frac{\text{Force}}{\text{Acceleration}}$
FRF name adopted in the study	<i>Compliance</i> $C(\omega) = \frac{1}{K(\omega)}$	<i>Mobility</i> $M(\omega) = \frac{1}{I(\omega)}$	<i>Accelerance</i> $A(\omega) = \frac{1}{AP(\omega)}$	<i>Dynamic stiffness</i> $K(\omega) = \frac{F(\omega)}{X(\omega)}$	<i>Impedance</i> $I(\omega) = \frac{F(\omega)}{\dot{X}(\omega)}$	<i>Apparent mass</i> $AP(\omega) = \frac{F(\omega)}{\ddot{X}(\omega)}$
Other names encountered in the literature	<i>Dynamic compliance</i> <i>Admittance</i> <i>Receptance</i>	-	<i>Inertance</i>	<i>Impedance</i>	<i>Mechanical impedance</i>	<i>Effective mass</i>

Table 2.2. Nomenclature for FRF

The two FRFs used in this study, the mobility and the dynamic stiffness, will be presented in more details in the coming sections.

2.5.1 Fourier transform

Let us consider a continuous temporal signal $z(t)$ and recall the definition of its forward Fourier transform $Z(\omega)$

$$Z(\omega) = \int_{-\infty}^{\infty} z(t) e^{-i\omega t} dt \quad (22)$$

where i is the imaginary number defined by $i = \sqrt{-1}$. The inverse transformation can be written as

$$z(t) = \frac{1}{2\pi} \int_{-\infty}^{\infty} Z(\omega) e^{i\omega t} d\omega \quad (23)$$

By convention, in this report, the capital letters represent the Fourier transform of the quantities in the corresponding lower case letters. The above equations are valid for continuous signals of infinite duration. Measurements, however, are made using digitized records of finite duration, and, therefore, these equations cannot be applied. In this case, it is convenient to use the Discrete Fourier Transform (DFT). If we consider $z(t)$, temporal signal of finite duration T_z , and $z(t_k)$, discrete record issued from $z(t)$ sampled at $t_q = q \Delta t$ (with $q = 0, 1, 2, \dots, N_z-1$), where Δt is the sampling period, the DFT pair is

$$Z(\omega_j) = \Delta t \sum_{q=0}^{N_z-1} z(t_q) e^{-i\omega_j t_q} \quad (24)$$

$$z(t_q) = \frac{\Delta\omega}{2\pi} \sum_{j=0}^{N_z-1} Z(\omega_j) e^{i\omega_j t_q} \quad (25)$$

where $N_z = T_z / \Delta t$ is the length of the records (number of points) and $\omega_j = j \Delta\omega = \pi j / T_z$. The frequency resolution is given by $\Delta\omega = 2 \pi / T_z$. The DFT is usually implemented on computers using Fast Fourier Transform (FFT) algorithms, which provide significant computational time savings and render DFT calculations efficient on personal computers.

2.5.2 Mobility function $M(\omega)$

Applying the forward Fourier transform, equation (22), to both sides of the equation of motion, and using

$$\ddot{X} = i\omega \dot{X} = -\omega^2 X \quad (26)$$

where $\ddot{X} = \ddot{X}(\omega)$ and $X = X(\omega)$, one obtains

$$\dot{X} \left[i\omega + 2 \xi \omega_n + \frac{\omega_n^2}{i\omega} \right] = \frac{F}{m} \quad (27)$$

This equation can be rearranged to yield

$$M(\omega) = \frac{\dot{X}(\omega)}{F(\omega)} \quad (28)$$

The mobility function $M = M(\omega)$ is therefore given by

$$M = \frac{1}{k} \frac{i\omega}{(1 - \beta^2) + (2 i \xi \beta)} \quad (29)$$

The mobility function of a SDOF system is complex valued and can be decomposed into real and imaginary parts. It can be readily shown that

$$\text{Re}\{M(\omega)\} = \frac{1}{k} \frac{2 \xi \beta \omega}{(1 - \beta^2)^2 + (2 \xi \beta)^2} \quad (30)$$

$$\text{Im}\{M(\omega)\} = \frac{1}{k} \frac{1}{\omega_n} \frac{\omega \omega_n - \beta^3}{(1 - \beta^2)^2 + (2 \xi \beta)^2} \quad (31)$$

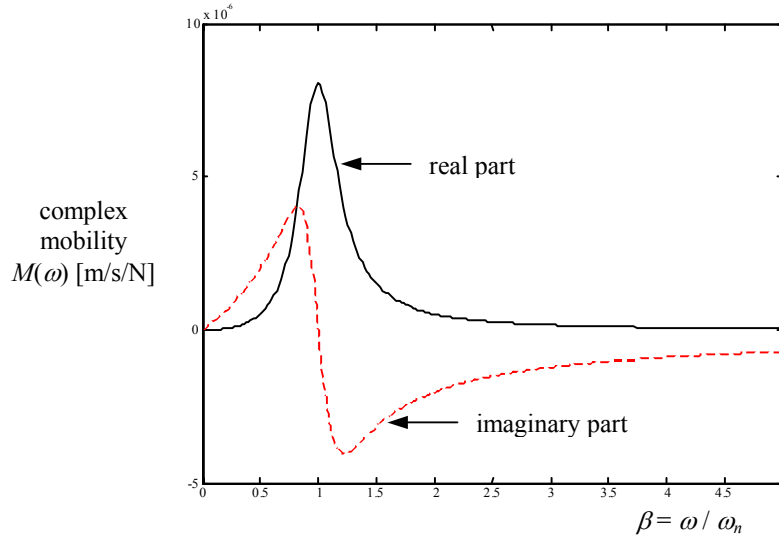


Fig. 2.8. Plot of the mobility function – theoretical example for a SDOF system

Fig. 2.8 presents the mobility function, for a tuning ratio β ranging from 0 to 5. The order of magnitude for the amplitudes reflects only the particular values chosen for the properties of the SDOF system represented ($m = 24 \times 10^3$ kg, $\xi = 20\%$ and $k = 4$ MN/m).

2.5.3 Dynamic stiffness function $K(\omega)$

The dynamic stiffness function is defined as $K = K(\omega)$

$$K(\omega) = \frac{F(\omega)}{X(\omega)} \quad (32)$$

Following the same pattern than for the mobility function, it can be shown from that

$$K = k \left[(1 - \beta^2) + (2 i \xi \beta)^2 \right] \quad (33)$$

For a SDOF system, real and imaginary parts are

$$\text{Re}\{K(\omega)\} = k(1 - \beta^2) \quad (34)$$

$$\text{Im}\{K(\omega)\} = 2k\xi\beta \quad (35)$$

Using equation (5), equation (6) can be rewritten as

$$c = 2m\xi\omega_n = 2\xi\sqrt{km} = 2\xi\frac{k}{\omega_n} \quad (36)$$

Plugging equation (36) into equation (35) yields

$$\text{Im}\{K(\omega)\} = c\omega \quad (37)$$

Examination of equation (34) implies that, for a SDOF system, the real part of the dynamic stiffness (i) is a parabola and (ii) does not depend on the damping. Similarly, equation (37) corresponds to a line of slope c . In Fig. 2.9, the dynamic stiffness function is presented for β ranging from 0 to 5. The same comment on the meaning of the amplitude values than for Fig. 2.8 applies.

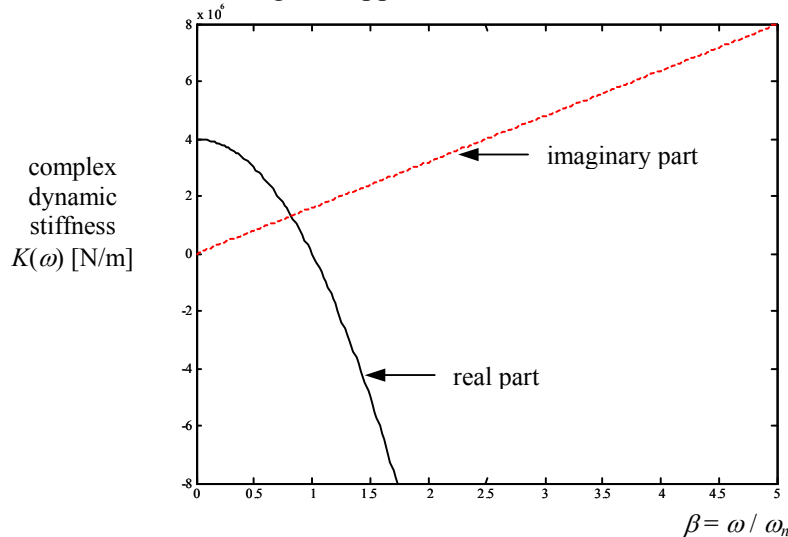


Fig. 2.9. Plot of the dynamic stiffness function – theoretical example for a SDOF system

2.5.4 Practical considerations

Relationships between FRFs can be constructed on the basis of integration and differentiation in the frequency domain. Recalling equation (26), integration in time domain corresponds to a division in frequency domain by $(i\omega)$, whereas a differentiation in time domain is equivalent to a multiplication by $(i\omega)$ in frequency domain. Similarly, double integrating in time domain corresponds to division by $(-\omega^2)$ in frequency domain and differentiating twice to multiplying by $(-\omega^2)$, respectively. On that basis, one can obtain the relationships presented in Fig. 2.10.

If the data acquisition involves only one type of motion transducer, only one type of FRF can be directly measured. However, advantage can be taken of the relationships in Fig. 2.10 to obtain all remaining FRFs. For example, using a geophone, one can measure directly $M(\omega)$ or $I(\omega)$ and obtain by simple multiplication or division the other response functions. The FRF are commonly used in problems involving structural vibrations, such as modal testing and system identification. Experimental FRFs are used to extract the properties of the equivalent SDOF or MDOF (Multiple Degree of Freedom) analogs of the system under testing, such as natural frequency, mass, damping, and stiffness.

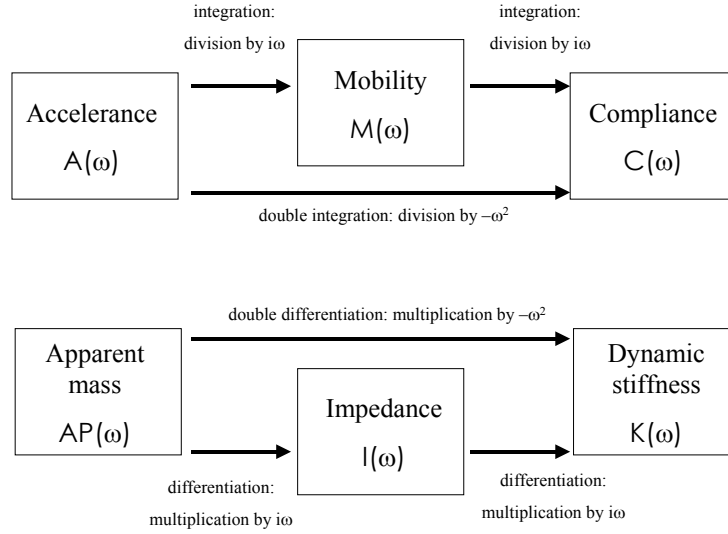


Fig. 2.10. Relationships among FRFs

2.5.5 Estimation of FRF

Let us consider the single input/single output, constant parameter linear system of Fig. 2.7. Measurement of the FRF = FRF (ω) defined by

$$\text{FRF}(\omega) = \frac{\Psi(\omega)}{\Theta(\omega)} \quad (21)$$

can be conducted using 1) measurements of both input and output signals, and 2) a direct division of the signals in the frequency domain. Data can be acquired either directly in frequency domain, either in time domain. In the case of time histories data, a FFT algorithm is employed to obtain the corresponding frequency histories. This method is not very robust to noise perturbations and experimental variability. As shown in Bendat and Piersol [21], spectral average is a tool indispensable to minimize the effect of random noise and measurement errors on the FRF estimates. It is shown in [21], for records from stationary random processes with zero mean value, that the so-called input/output cross-spectrum relation is

$$\text{FRF}(\omega) = \frac{G_{\theta\psi}(\omega)}{G_{\theta\theta}(\omega)} \quad (38)$$

where $G_{\theta\theta}$ is the one-sided auto-spectral density function and $G_{\theta\psi}$ is the one-sided cross-spectral density function. Switching notations to use frequencies in Hertz leads to

$$\text{FRF}(f) = \frac{G_{\theta\psi}(f)}{G_{\theta\theta}(f)} \quad (39)$$

These relations apply for ideal situations where no extraneous noise and no time varying or nonlinear characteristics are present. In practice, when dealing with

N_T ($n = 1, 2, \dots, N_T$) digital records of length N_ψ each, the averaged DFT of θ and ψ are given respectively by

$$[\Theta(f_j)]_n = \Delta t \sum_{q=0}^{N_\psi-1} [\theta(t_q)]_n e^{-2\pi i t_q f_j}, \quad j = 0, 1, 2, \dots, N-1 \quad (40)$$

$$[\Psi(f_j)]_n = \Delta t \sum_{q=0}^{N_\psi-1} [\psi(t_q)]_n e^{-2\pi i t_q f_j}, \quad j = 0, 1, 2, \dots, N-1 \quad (41)$$

where $f_j = \frac{\omega_j}{2\pi} = \frac{j}{N_\psi \Delta t}$ and $t_q = q \Delta t$. With equations (40) and (41), the one-sided spectral density functions are given by

$$G_{\theta\psi}(f_j) = \frac{1}{N_T} \sum_{n=1}^{N_T} [\Theta(f_j)]_n^* [\Psi(f_j)]_n \quad (42)$$

$$G_{\theta\theta}(f_j) = \frac{1}{N_T} \sum_{n=1}^{N_T} [\Theta(f_j)]_n^* [\Theta(f_j)]_n \quad (43)$$

where “*” denotes the complex conjugation. To reduce the effects of side leakage during the FFT evaluation, the acquisition process can use various types of time window function $\Lambda(t)$, such as boxcar, Hanning or triangular windows. When using a window, the DFT of the n^{th} measurement ($n = 1, 2, \dots, N_T$) of a temporal record $z(t)$ of length N_z becomes

$$[Z(\omega_j)]_n = \Delta t \sum_{q=0}^{N_z-1} \Lambda(t_q) [z(t_q)]_n e^{-i\omega_j t_q} \quad (44)$$

The spectral average approach also provides the user with a tool to estimate the quality of the measurements via the coherence function $\gamma^2 = \gamma^2(\omega)$

$$\gamma^2(\omega) = \frac{|G_{\theta\psi}(\omega)|^2}{G_{\theta\theta}(\omega)G_{\psi\psi}(\omega)} \quad (45)$$

It can be shown that

$$0 \leq \gamma^2(\omega) \leq 1 \quad (46)$$

The case $\gamma^2 = 1$ corresponds to a perfect constant parameters linear system associated with zero noise in the measurements. The case $\gamma^2 = 0$ is encountered when there is no correlation at all between input and output. All intermediate cases can be due to the presence of extraneous noise in the measurements, of non-linearity in the system, or to the contribution of additional inputs.

Spectral average techniques, assorted with windowing options are implemented in modern data acquisition systems such as the SigLab spectrum analyzer used for this study. A description of the methods used to determine FRFs with SigLab can be found in the manufacturer’s technical documentation [22].

2.6 FRF for a homogeneous elastic half-space model

On the one hand, assuming that the soil-foundation system depicted in Fig. 2.3 behaves as a linear system, one can measure experimentally any FRF listed in Table 2.2 using the tools presented in previous sections. On the other hand, theoretical formulations of these FRFs describing dynamic Soil-Foundation Interaction (SFI) for an elastic half-space are also available.

2.6.1 Exact solution for the vertical compliance of a massless footing

The theoretical solution for the vertical dynamic interfacial compliance C_{vv} for the case of a massless rigid disk resting on the surface of a semi-infinite homogeneous and linearly elastic continuum is presented in Luco and Westman [23] and Pak and Gobert [24]. This solution, developed for the case of a vertical steady-state force, can be written as

$$C_{vv}(\omega) = C_{vv}(0)[\bar{C}_{vv}(\omega)] \quad (47)$$

The dimensionless vertical compliance function $\bar{C}_{vv}(\omega)$ is essentially independent of Poisson's ratio ν . The static vertical compliance $C_{vv}(0)$ of a circular rigid footing of radius a is given by

$$C_{vv}(0) = \frac{1-\nu}{4Ga} \quad (48)$$

where G and ν represent the equivalent homogeneous shear modulus and Poisson's ratio of the half-space. The dimensionless vertical compliance \bar{C}_{vv} is a complex function that can be represented as the sum of the dimensionless frequency functions F_1 and F_2

$$\bar{C}_{vv}(\bar{\omega}) = F_1(\bar{\omega}) + iF_2(\bar{\omega}) \quad (49)$$

where F_1 and F_2 are respectively the real and imaginary parts of \bar{C}_{vv} and where the dimensionless frequency $\bar{\omega}$ defined as

$$\bar{\omega} = \frac{\omega a}{c_s} \quad (50)$$

In equation (50), c_s is the velocity of the shear wave propagating in the continuum with mass density ρ and is defined as

$$c_s = \sqrt{\frac{G}{\rho}} \quad (51)$$

A plot of \bar{C}_{vv} versus $\bar{\omega}$, constructed using the values of F_1 and F_2 tabulated in the paper by Pak and Guzina [12], is presented in Fig. 2.11.

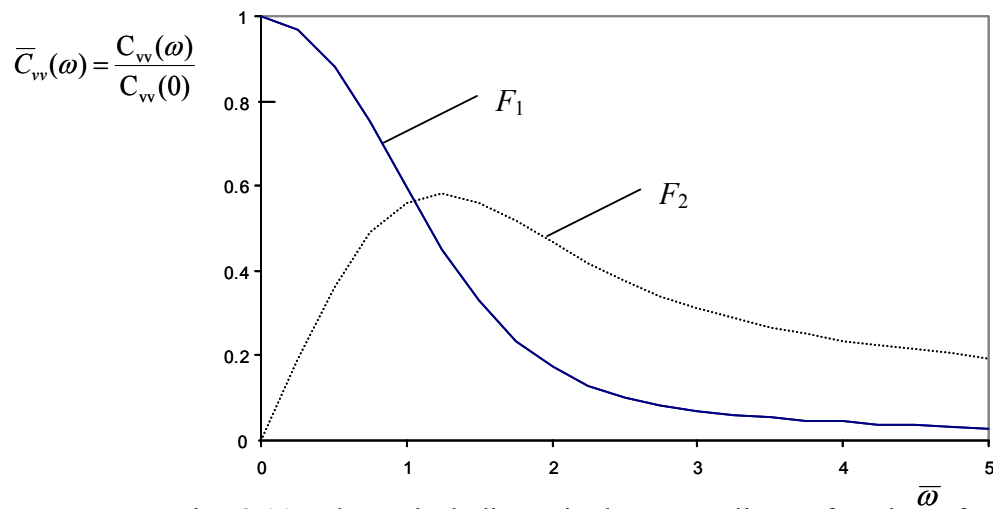


Fig. 2.11. Theoretical dimensionless compliance functions for the vertical mode of vibration of a massless rigid disk resting on an elastic half-space

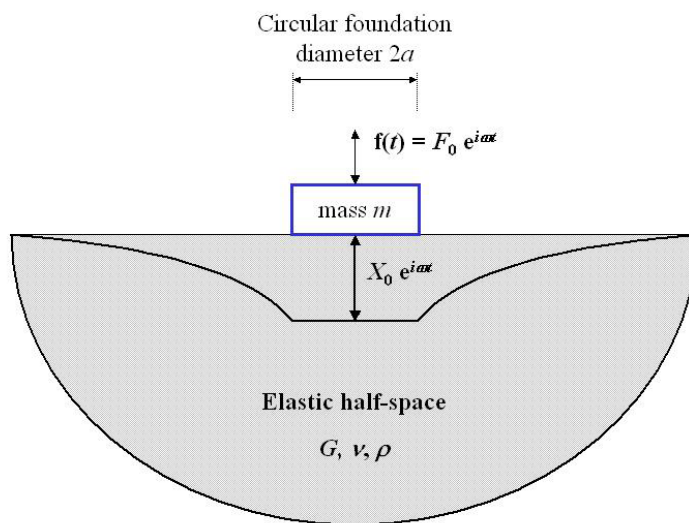


Fig. 2.12. Steady-state forcing of the elastic half-space - massive rigid footing

2.6.2 Vertical compliance of a massive footing

The solution presented in the previous section relates to the case of a rigid massless footing resting on the top of an elastic half-space and subjected to a vertical steady-state force. However, the mass of the footing needs to be taken into account in order to describe completely the soil-foundation interaction. When the massive footing is subjected to a steady-state force $f(t) = F_0 e^{i\omega t}$, as depicted in Fig. 2.12, it can be shown that the steady-state displacement X_0 is given by

$$X_0 = \frac{F_0}{\frac{1}{C_v(\omega)} - m\omega^2} \quad (52)$$

where m is the mass of the footing, ω the driving frequency, C_v the massless compliance function and $(m\omega^2)$ the footing's transfer function. Therefore, the displacement can be computed, for a given driving frequency and a given foundation's mass, on the basis of equations (50) and (52), by using the curves presented in Fig. 2.11. Also, the vertical compliance for the massive foundation, C_v^m , is readily obtained from equation (52) as

$$C_v^m(\omega) = \frac{X_0}{F_0} = \frac{1}{\frac{1}{C_v(\omega)} - m\omega^2} \quad (53)$$

CHAPTER 3 - PFWD PRIMA 100 DEVICE

The PRIMA 100 is a portable FWD device. The device used in this study was purchased from Carl Bro Paving Consultants, a Danish company. During the study, Carl Bro Pavement Consultants, and Keros Technology, Denmark, provided technical assistance regarding the hardware and software. In the operation of this device, the elastic (equivalent homogeneous) Young's modulus of an unbounded pavement foundation is estimated from the measurement of the surface deflection due to transient (impact) loading applied to the foundation through a circular loading plate. The device is commercialized with a software program for data acquisition and interpretation from a laptop computer. The software, developed for a Microsoft Windows environment, enables user to choose the test setup, and visualize and save the test results. Displayed results include time histories and peak values of load and displacement, as well as an estimated value of the Young's modulus. Maximum applied stress and load pulse duration also are displayed.

3.1 Experimental setup

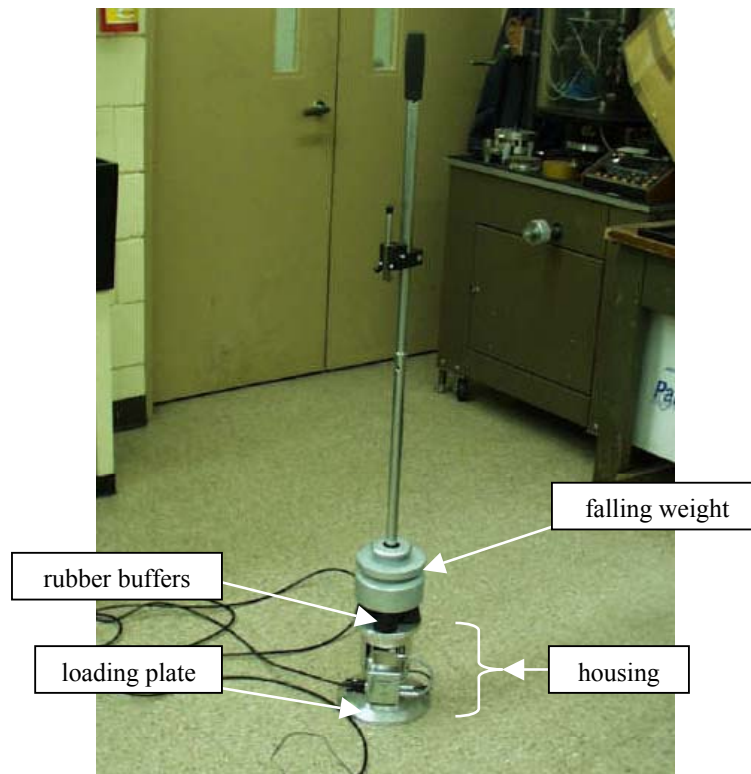


Fig. 3.1. General illustration of PRIMA 100 device

The experimental PRIMA setup is shown in Fig. 3.1. The device itself is composed of three main parts: 1) sensors with the associated electronics, 2) housing protecting the sensors, and 3) falling weight (sliding hammer).

The device incorporates two sensors: a load cell and a central geophone, shown in Fig. 3.2. The load cell is a force transducer that measures static and dynamic compressive forces, with a nominal range 0 - 2 kN. Its measuring body is a steel spring with 8 strain gages attached. The geophone is a velocity transducer, i.e. a sensor with output proportional to the velocity. Two additional geophones also can be added to obtain the deflection away from the loading point, but only the version with one central geophone will be studied here. This geophone is spring-mounted inside the base part of the housing, so that it can measure the motion at the center of the loading area. Both sensors are connected to an electronic box comprising the data acquisition system that stores the data before sending them to the portable computer.

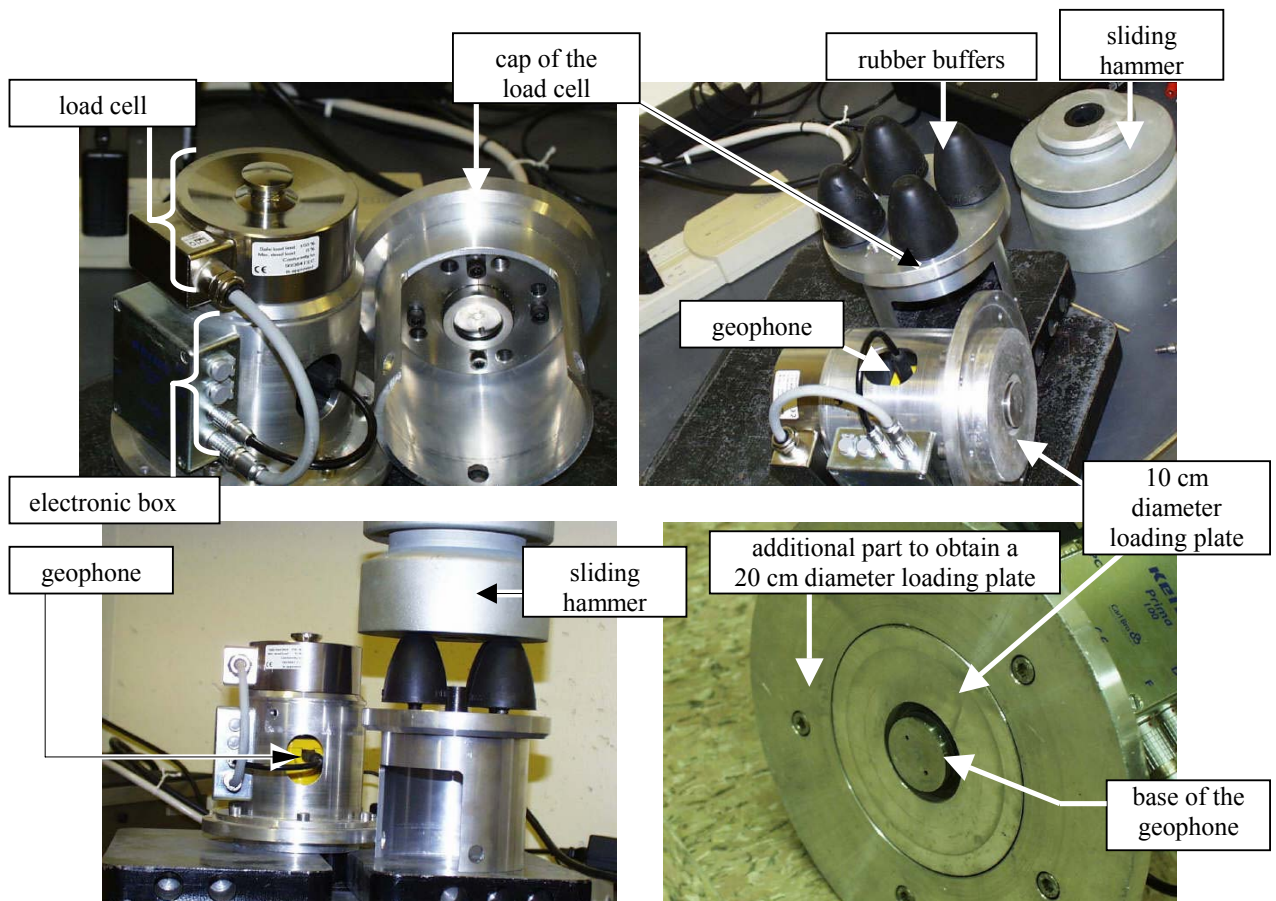


Fig. 3.2. Detailed illustration of PRIMA 100 device

The steel housing can be decomposed into a base that houses the sensors and a movable upper part, the load cell cap, which supports four rubber buffers and a central movable

guidance rod. The rod consists of two rods screwed together. It supports a movable hanger for the falling mass and ends with a rubber handle.

The load cell cap is a movable part that seats directly onto the load cell located at the upper part of the base. The contact area between the load cell and cap resembles a point contact and is the unique point of contact between them. This design responds to the necessity to obtain a centered and integrally transmitted force.

The intermediate part of the base, under the load cell, consists of a hollow cylinder that houses the central geophone. The load is transmitted from the load cell via the walls of the cylinder. The base's bottom part, where the load is finally transmitted to the tested support, is a 10 cm diameter circular plate. It can be seen from Fig. 3.2 that the device is designed such that the geophone is in direct contact with the soil. The geophone is mounted on a spring to ensure a good contact. Optional additional rings can be attached onto the loading plate to obtain either a 20 cm either a 30 cm diameter loading surface, to accommodate different types of soil and contact pressures. For a given load applied, the use of larger plates produces smaller stresses and surface deflections.

The falling weight is a nominal 10 kg sliding hammer that can be released from variable heights onto the set of rubber buffers on top of the housing. The maximum drop height is about 0.85 m. The manufacturer also supplies two additional masses of 5 kg each.

The duration of the recorded force and velocity signals can be chosen by the user in the range from 10 ms to 120 ms. With such short time windows, only the force and velocity time histories corresponding to the first impact are captured by the data acquisition system. Further impacts of the falling weight (due to bouncing) after rebound are not taken into account. The load pulse shape resembles a half-sine form. Using various drop heights and masses enables the user to obtain different loading characteristics. According to the manufacturer, the load pulse duration can approximately range from 15 ms to 20 ms, and the maximum force that the device can experience is 15 kN. The corresponding maximum stress underneath the bearing plate is about 210 kPa for the 30 cm diameter plate and about 1.9 MPa for the 10 cm diameter plate.

The manufacturer recommends choosing plate diameter, mass of the sliding hammer and drop heights such that the measured deflection does not exceed 2 mm. Also, they limit the use of the 30 cm and 20 cm plates to a calculated Young's modulus below 125 MPa and 170 MPa, respectively.

3.2 Measurement principle

The software provided with PRIMA device uses the time histories of both the force signal obtained from the load cell and the velocity signal obtained from the geophone. The displacement time history is obtained by integrating the velocity record. The user does not have access to the primary velocity record, only to the displacement record. After the test is completed, the displacement and load time histories are displayed on the computer screen. The results can be saved in specific files, with extension “.pkv” and “.crv”. The

files produced by PRIMA's software can be opened afterwards using a text editor, a spreadsheet program, or another tool such as Matlab.

Fig. 3.3 shows a plot constructed using Microsoft Excel from the software's output. The plot corresponds to a test on the laboratory's concrete floor, but its characteristics are comparable to ones that would be obtained from field tests. The displacement time history reflects the convention that downwards displacements are negative. The output also gives the maximum (in absolute values) deflection x_{peak} and load f_{peak} , in this case 43 μm and 6.16 kN respectively, as well as the load pulse duration, 14.8 ms.

The key characteristics featured on Fig. 3.3 are: The peak value of the deflection signal lags the peak value of the force signal, and the general trend is that the deflection signal amplitude decays after the peak of the first oscillation. Indeed, the expected behavior for the deflection time history would be to die off rapidly due to the effects of radiation damping in the support. The *time lag* between the peak values is due to the effects of *inertia*. The *amplitude decay* is due to *damping* (energy dissipation). In details, the deflection signal in Fig. 3.3 shows after the end of the load pulse oscillations that do not decay towards a zero value, and that incorporate some "ringing". This can be explained by several factors: a non-perfect contact between the device and the support, a non-constant stress distribution across the contact area (due to eccentricity) applied by the operator, and the numerical integration of (measured) velocity to obtain the deflection. These effects are particularly significant in this case where the tested system is very stiff.

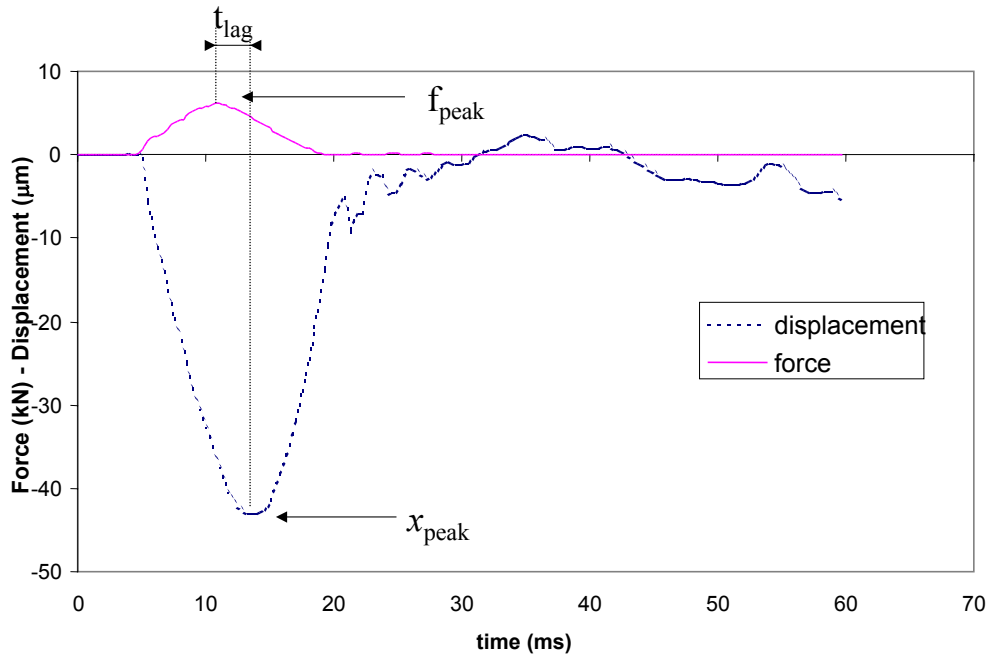


Fig. 3.3. Plot of PRIMA's software output

In accordance with the common practice in FWD testing [2], an estimation of the stiffness footing-over-a-support-system is based upon the peak values of the load and displacement time histories, i.e.

$$k_{est} = \frac{f_{peak}}{x_{peak}} \quad (54)$$

As a result, the quantity directly estimated from the measurements is the stiffness of the system footing-on-a-support. With the tested version of PRIMA 100, the estimated Young's modulus is computed in the manufacturer's software using the elastic half-space solution, equation (3), for the case of a flexible circular foundation, and under the assumption that $\nu = 0.35$

$$E_{est} = 2 \frac{1 - \nu^2}{\pi a} \frac{f_{peak}}{x_{peak}} \quad (55)$$

Both the manufacturer and a few experimental verifications confirmed that equation (55) was indeed the one being used. Applying equations (54) and (55), to the particular case illustrated in Fig. 3.3, for example, yields $K_{est} = 143 \text{ MN/m}$ and $E_{est} = 1.6 \text{ GPa}$.

3.3 Issues regarding the current PRIMA device

During FWD data interpretation, it is convenient to assume a uniform stress distribution under the load. To simulate this condition, some full-scale FWD devices are equipped with a rubber membrane added between the loading plate and the soil. Even though PRIMA device does not use a rubber membrane, this simplifying assumption is embedded into the data interpretation framework of the PRIMA device. However, according to the manufacturer, a new release of the software is now available. In this new version, more control is given to the user. For example, the value of Poisson's ratio in equation (55) can be changed, and the influence of the contact pressure distribution can be taken into account. The difference in estimates of Young's modulus resulting from fully flexible compared to fully rigid contact is of the order of 20 percent.

Another convenient simplification is to assume that the loading area is a disk. However, examination of the loading plate in Fig.3.3 shows that this is not the case. The loading plate itself corresponds to an annulus of outer diameter 10 cm and inner diameter 4 cm. However, the center geophone (3 cm diameter) also contributes to the loading area. The exact loading area is therefore a composite area, approximated in the featured data interpretation as a disk. Also, PRIMA device is designed such that the center geophone measures the ground deflection. This implies that ground and footing are assumed to experience the same motion. The analysis presented in this report is based on these two assumptions (circular footing and equality of displacements). Rigorous examination of the influence of these assumptions on the performance of PRIMA device on the estimation of the (elastic equivalent homogeneous) Young's modulus falls out of the scope of this study, which focuses on stiffness estimation.

With reference to Fig. 3.3, the recorded time histories can reflect measurements that do not depend only upon the soil's characteristics. The quality of the measurements

depends upon the operator (i.e. how the device is manipulated) as well as upon the seating conditions of the device. Given the type of testing, where dynamic loads are applied, obtaining reliable measurements at times greater than the load pulse period is difficult, especially on stiff supports. Also, the displacement is computed via numerical integration of the velocity, and numerical integration is generally associated with increasing errors with increasing computation time (that is, the computed displacement at the end of the time history may be erroneous). The advantage of estimating the stiffness from the peak values measurements is that the peak values are less likely affected by these factors.

The response of the PRIMA geophone is similar to the curve presented in Fig. 2.6 for 70 percent of damping. For such sensors, the response is not linear (and thus does not reflect the true ground motion) at very low frequencies. According to the calibration guidelines from Carl Bro Pavement Consultants (CBPC) [25], the response of the geophone equipping PRIMA device is not linear in the range 0 – 7 Hz. To partially compensate for this non-linearity and obtain a flat response over the range 0 – 300 Hz, a digital filter is added to modify the signal from the geophone. The filter has been calibrated and implemented in PRIMA by the manufacturer.

3.4 Enhancement of PRIMA device

PRIMA 100 is a PFWD designed following the principles of standard full-scale FWD devices. It is commonly believed that, in assessing the characteristics of a pavement structure, using a dynamic impulse that simulates a moving wheel load gives reliable results from FWD measurements. The device is designed to produce typical stress levels, as they would exist beneath paved roadways. For this reason the record duration of FWD is typically in the range 15 to 60 ms, and the record duration of PRIMA 100 does not exceed 120 ms. Also, the maximum load of 15 kN to 20 kN developed during impact simulates real traffic situations on paved roadways. This approach, however, does not take into account the traffic conditions during construction, which are often more detrimental than the loads taken into account for the long-term design.

It is important to point out that in the quality assurance of pavement construction, the targeted property is the small strain Young's elastic modulus or E_{max} . In this case, the conditions of the test must produce small deformations. Under small strains, the true value of the tested material elastic modulus is unique (E_{max}) and should not depend upon the characteristics of the applied load (e.g. the pulse shape). Based on this argument, simulating traffic conditions is not relevant. As mentioned in Section 2.1, it would be advantageous for quality assurance purposes to use a device that produces small strains in the soil mass.

It will be shown in Chapters 5 and 6 that the proposed alternative determination of the static footing-on-support stiffness k_s using FRF techniques does not depend upon the applied force, as long as the behavior of the tested material remains approximately linear. An enhanced experimental setup, as shown in Fig. 3.4, can be proposed for FRF measurement purposes. As illustrated in Fig. 3.2, the load cell's cap can be removed. This

allows for tests where the load can be applied directly to the load cell, using, for example, a rubber hammer instead of the sliding hammer. By using this alternative technique, the applied load is low enough to ensure small deformations that can be used to characterize accurately the seismic modulus E_{max} beneath a paved road.

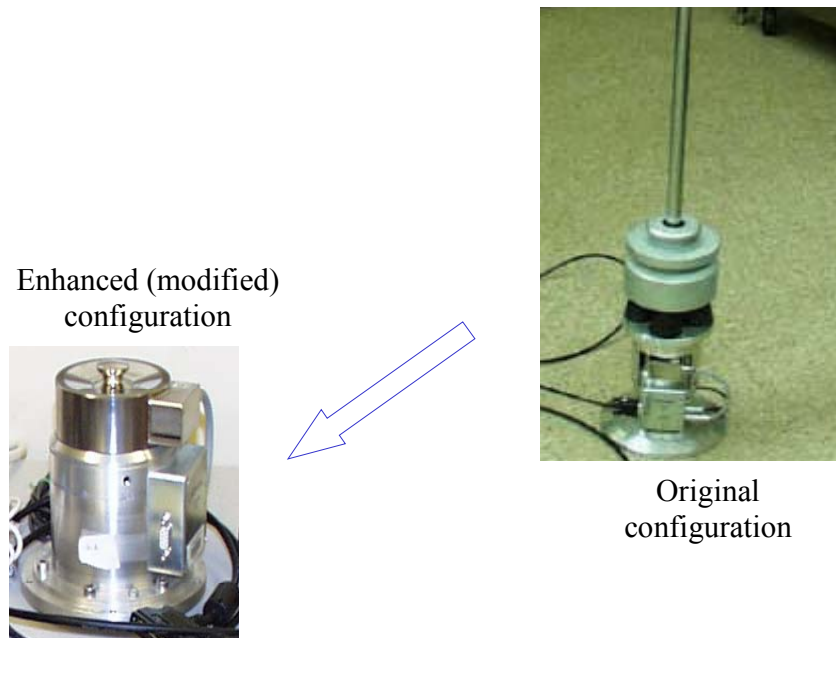


Fig. 3.4. Modification of the setup of PRIMA device

This enhanced setup, which limits the amplitude of vibrations due to applied impact force, is also very advantageous during the verification tests conducted on a simply supported steel beam (reduced “ringing”). For field-testing, this setup could replace the original setup to reduce the weight of the device (more portable), provide a small deformation test (corresponding to Young’s modulus), and offer an even more easy-to-use apparatus (less awkward and fewer parts). The repeatability of the tests would be improved and the data interpretation, based upon E_{max} , greatly simplified.

CHAPTER 4 - BEAM VERIFICATION TESTER: TRUE STIFFNESS OF THE BEAM VS. PRIMA ESTIMATES

The Beam Verification Tester (BVT) for PFWD utilizes a simply supported steel beam. The true static stiffness k_s of the beam is measured using two independent static calibration tests. With such information, the performance of the PRIMA device is examined using the BVT, and the stiffness estimate k_{est} from PRIMA is compared to k_s . The reasons of the observed poor correlation between k_{est} and k_s are investigated, and an alternative data interpretation method is proposed that eliminates the observed discrepancy.

4.1 Setup for the BVT

4.1.1 Choice of the setup

In order to examine the performance of PRIMA device, PFWD tests need to be conducted on a supporting structure with known stiffness. Also, it is advantageous to perform these verification tests on a supporting structure whose stiffness can be adjusted over a range of values. Furthermore, the structure has to offer the ability to be easily modeled not only statically but also dynamically. Finally, the structure should be instrumented to allow for direct measurements of support deflection and load applied to the structure. The use of a simply supported steel beam matches those objectives.

The idea is to use an instrumented simply supported beam as a support with known stiffness k_s for the PRIMA device, and then to compare PRIMA output to k_s . It is understood that soils and steel beams have little in common. However, owing to its primary role as a tool for measuring the foundation (i.e. support) stiffness, the PFWD device also should be suitable for determining the footing-on-top-of-a-supporting-beam stiffness. To approximate in-situ conditions, characteristics of the beam are chosen to match the realistic range of in-situ footing-on-base and footing-on-subgrade stiffnesses. For comparison, the static stiffness of the PRIMA's footing (10 cm to 30 cm diameter) resting on typical construction soils ranges from 6 MN/m to 24 MN/m.

4.1.2 Beam setup description

During the verification test, the PRIMA device stands centrally on a straight homogeneous beam with a solid rectangular cross-section as illustrated in Fig. 4.1 and 4.2. As mentioned earlier, the verification setup uses only the bottom portion of the PRIMA device together with a rubber hammer as a means to apply the impact load. In addition to the issues discussed in Chapter 3, this setup offers several practical

advantages. Owing to the low amplitude of vibration after impact, this modified PFWD configuration is preferred over the manufacturer’s setup to obtain quality measurements and to guarantee repeatability. These two latter requirements are not necessarily satisfied when the beam is impacted by the falling mass, because of uncontrolled “ringing” of the entire apparatus.

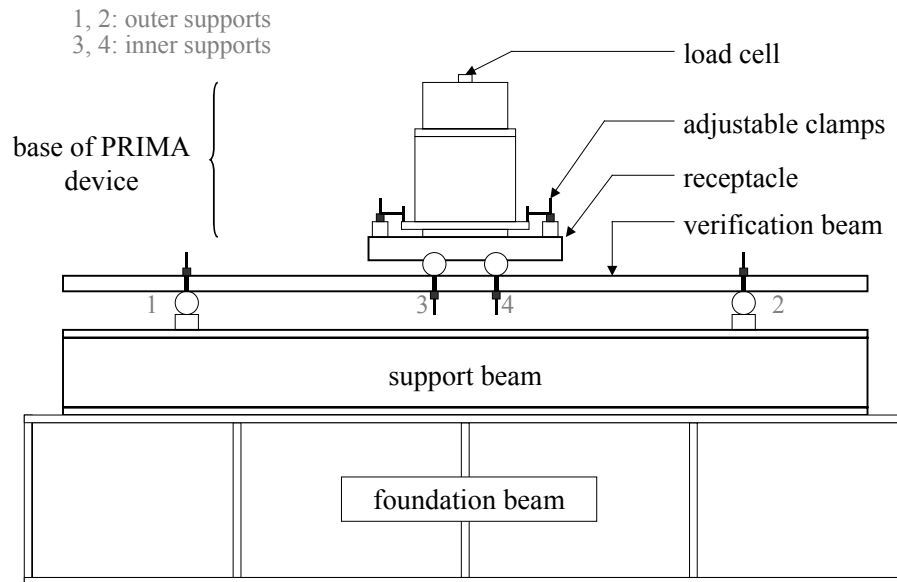


Fig. 4.1. Sketch of the verification setup

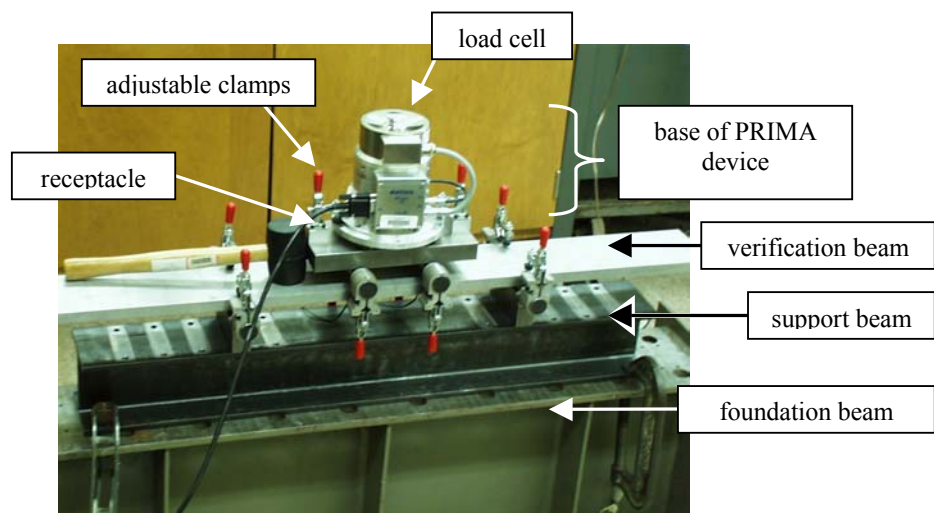


Fig. 4.2. Verification setup

Fig. 4.1 and 4.2 show the BVT setup for verification testing. The BVT assembly comprises (i) a 10.16 cm (4”) wide and 1.59 cm (5/8”) deep ‘O-1 tool’ type steel beam sitting on two adjustable supports (denoted 1 and 2 in Fig.4.1), (ii) a support beam

attached to the foundation beam, and (iii) a receptacle for PRIMA device. The supports for the verification beam (1 and 2 in Fig. 4.1) and the supports of the receptacle (3 and 4 in Fig.4.1) are made of a 2.54 cm (1”) diameter hardened steel rod.

The verification setup resembles a four-point bending test, with beam effective span L (in-between the outer supports 1 and 2) and a so-called loading span d (in-between the inner supports 3 and 4). There are two main advantages to use such configuration, as opposed to using a single support at mid-span or to sitting the device directly on the beam: The tested device is stable on the supports, and any contact between the loading plate edges and the beam during bending is avoided.

As shown in Fig. 4.1 and 4.2, the PRIMA device is rigidly clamped to the BVT receptacle using movable clamps mounted on the receptacle. The clamping force of these clamps is roughly adjustable via a screw system. The same type of clamp also is used to insure constant contact between the verification beam and its supports during impact testing. In the latter case, the clamping force is set to a moderate value to reduce the clamps’ influence on beam bending.

Five pairs of slots are machined on the top of the support beam to receive the movable supports for the tested beam (outer supports 1 and 2). This allows for verification tests using five different spans ranging from 0.3 m to 0.7 m with an interval of 0.10 m. The support beam is rigidly clamped to a heavy ‘S’ type steel foundation beam. Its stiffness has been found to be high enough, at least for the longer beam spans tested, for the support to be considered rigid. Also, measurements from accelerometers located on the foundation beam showed that the amplitude of its motion during testing is negligible when compared to the receptacle motion. The use of the foundation beam was advantageous for preliminary testing. For definitive use in Mn/DOT facilities, we recommend that the support beam be attached to a heavy foundation or cast into concrete. The advantages would be to obtain a heavier support with more damping, which results in increasing stability and stiffness of the support and decreasing ringing in the support.

The receptacle is a short 10.16 cm (4”) wide and 1.59 cm (5/8”) deep steel beam. Its span when placed on the supports (i.e. loading span) is $d = 0.1$ m. The receptacle is considered rigid when compared to the beam. It has been verified that the receptacle stiffness exceeds the tested beam stiffness by a factor of over 100. Consequently, the receptacle experiences the same rigid body motion as the PFW device attached to it.

4.2 Static stiffness of the beam

4.2.1 Theoretical static stiffness of the beam

The theoretical model describing the actual verification setup is developed using the engineering beam theory or Euler-Bernoulli beam model. The assumptions or approximations embedded in this model are that: 1) the beam is made of an isotropic linear elastic material undergoing small strains; 2) planar cross-sections of the beam remain planar during deformation, which implies that the length of the beam needs to be significantly greater than its width, and 3) the beam is thin. Further, the verification beam

will be considered to have a constant rectangular cross-section and to be simply supported, even though the beam is slightly clamped on its support. Finally, all the contacts between clamps, supports, beam and receptacle will be approximated as point-contacts that provide no moment restraint.

The BVT setup presented in Fig. 4.1 and 4.2 can be idealized for the purpose of the theoretical analysis as sketched in Fig. 4.3, for a beam of width b , thickness h and effective span L . In the foregoing static analysis, the overhanging part S of the beam is disregarded. The load f applied at mid-span by the PFWD device sitting on the receptacle is split into two equal forces p located at $\pm (d/2)$ apart from the mid-span, d being the distance separating the supports of the receptacle (inner supports 3 and 4 in Fig.4.3).

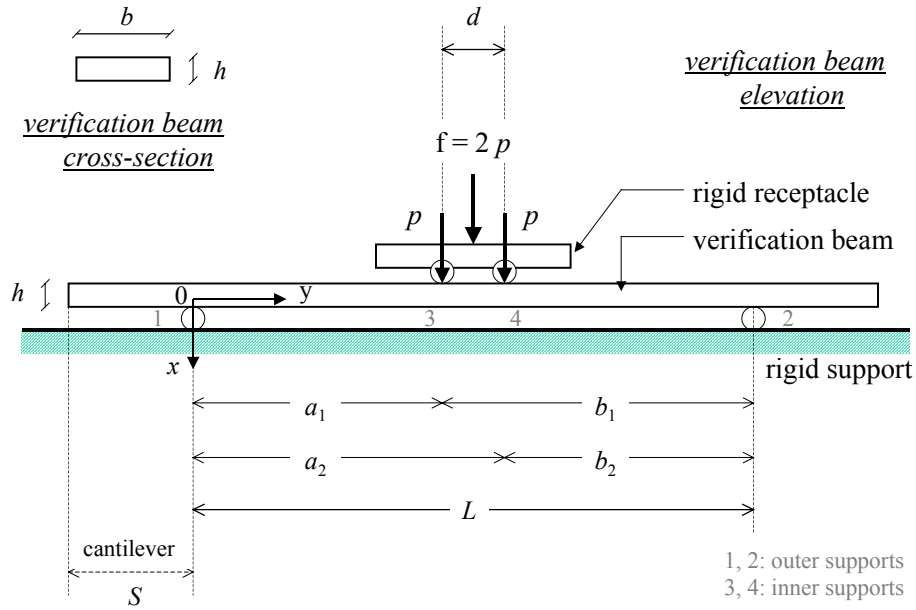


Fig. 4.3. Idealized verification beam layout

The classical solution for the static deflection of a simply supported beam under a single point load p applied at $y = a_1$ can be found in many publications, for example in Lardner and Archer [26]. Using this solution and the principle of superposition, one can construct the solution for the displacement function of the simply supported beam subjected to two point loads as depicted in Fig. 4.3. For this loading configuration, it can be readily shown that the stiffness k_s evaluated under either of the receptacle's supports (i.e. support 3 or 4) is given by

$$k_s = \frac{f}{x(a_1)} = \frac{f}{x(a_1 + d)} = \frac{12EI}{3a_1^2L - 4a_1^3} \quad (56)$$

where $x(a_1)$ is the deflection at $y = a_1$ and, for the rectangular cross-section, the cross-sectional moment of inertia I of the beam is given by

$$I = \frac{bh^3}{12} \quad (57)$$

4.2.2 Experimental Young's modulus of the steel

An accurate value for the Young's modulus of the steel E_{true} is necessary because it can be used to determine the beam true stiffness k_s . The four-points bending beam test is a well-recognized method of determination of Young's modulus, using measurements of load and strain. In this method, one or several strain gages are mounted, in-between the innermost loads, on the surface of the beam specimen, to measure the strain experienced by the specimen subjected to a known applied force.

From the engineering beam theory [26], the maximum tensile stress σ at any cross-section y on the surface of the beam of Fig. 4.3 can be computed from

$$\sigma(y) = M_b(y) \frac{h}{2I} \quad (58)$$

From solid mechanics [26], the bending moment M_b in a four-point configuration is constant between the innermost loads (pure bending) and linearly proportional to y otherwise. Given the symmetry of the problem, the analysis can be restricted to the left half-beam for which

$$\begin{aligned} M_b(y) &= p y \quad \text{for } 0 \leq y \leq a_1 \\ M_b &= p a_1 = \frac{f}{2} a_1 \quad \text{for } a_1 \leq y \leq \frac{L}{2} \end{aligned} \quad (59)$$

Combining equations (57), (58) and (59) yields the expression for the maximum tensile stress (occurring at the beam's bottom fiber) in terms of the applied load

$$\sigma = \frac{3f a_1}{b h^2}, \quad a_1 \leq y \leq a_1 + \frac{d}{2} \quad (60)$$

Assuming a linear relationship between stress σ and strain ε , and also a uniaxial state of stress (narrow beam approximation), Hooke's law can be used

$$\sigma(y) = E \varepsilon(y) \quad (61)$$

Equation (61) is the basis of the experimental determination of the steel's Young's modulus $E = E_{true}$ using the four-point bending test, E_{true} being the slope of the curve σ vs. ε . Using a strain gage located at mid-span on the beam enables to take advantage of equation (60), in which the measured strain does not depend on the exact location of the gage. The orientation of the gage, however, is still a potential source of error on the strain measurement. The gage must be aligned in the axial direction of the beam, which is the major principal direction of the stress state.

Experiments have been conducted on the beam using a MTS load frame located in the Rock Mechanics Laboratory of the civil engineering department. Fig. 4.4 shows the testing setup. The load was recorded using the internal load cell of the testing machine; the displacement of the receptacle was measured using a Linear Variable Differential Transformer (LVDT), and the strain was read out of the Vishay P-3500 strain indicator. A Micro-Measurements 350 Ω strain gage was mounted at mid-span on the top surface of the beam.

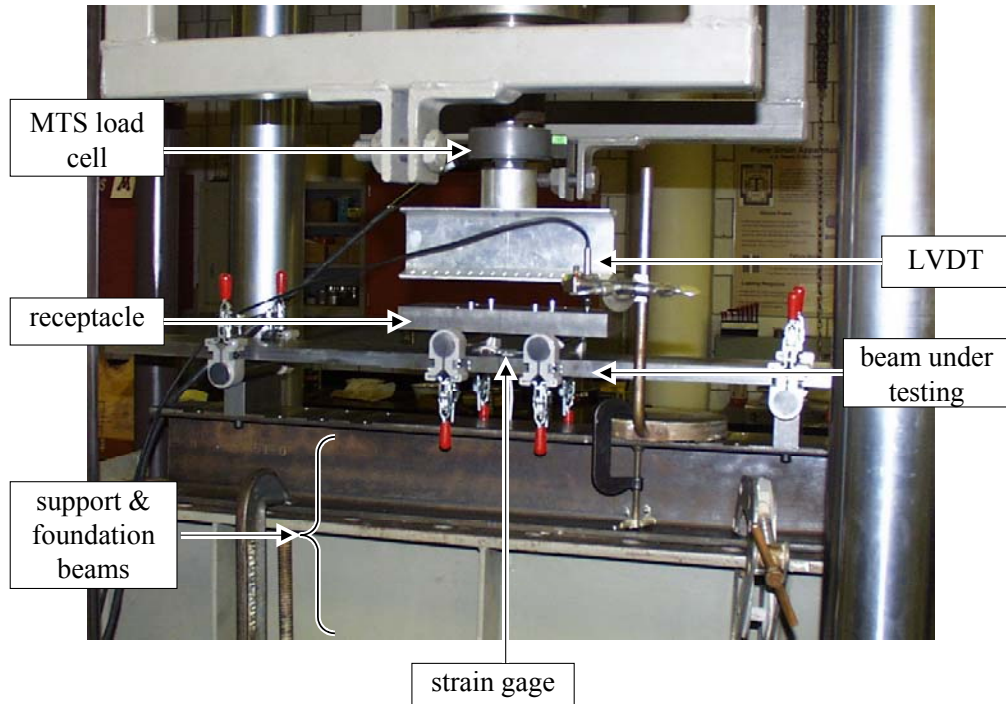


Fig. 4.4. Four-point bending and static stiffness tests setup

To estimate the influence of the length of the loading span d (distance between innermost supports 3 and 4) when compared to the length of the supported beam L (i.e. effective span, distance between outermost supports 1 and 2), several beam configurations were used. Some tests have been performed with spans $L = 0.6$ m and $L = 0.7$ m associated with a loading span $d = 0.10$ m, and others with $L = 81.28$ cm (32") associated with loading spans $d = 30.48$ cm (12") and $d = 40.64$ cm (16"). On the basis of equations (60) and (61), the measured force and strain yields an experimental value of $E = E_{true}$ for each of the tested configurations. The strain measurements were corrected from the gage transverse effects using the standard procedure (e.g. Dally and Riley [27]; manufacturer technical documentation [28]). Averaging the results obtained from the various configurations leads to the experimental value that will be used later. This value is $E_{true} = 212.3 \pm 0.7$ GPa. The values of k_s computed from E_{true} and equation (56), labeled as "beam theory," are presented in Table 4.1.

4.2.3 Experimental static stiffness of the beam

The beam's static stiffness k_s is the reference for the PFWD device performance verification. Therefore, rather than calculating the static stiffness from the beam theory using an estimated value of the Young's modulus, it is highly preferable to directly measure the stiffness of the beam for different spans.

As an alternative to the "beam theory" approach outlined in Section 4.2.2, experimental values of the beam static stiffness k_s also were directly measured using a

series of load-deflection tests performed with the MTS loading frame. As observed in Fig. 4.4, the entire beam assembly, i.e. the tested beam itself mounted on its foundation beam, has been employed for this calibration. The force was recorded from the load cell of the MTS machine, and the displacement of the receptacle on the beam was evaluated using a Linear Variable Differential Transformer (LVDT). The support of the LVDT was secured on the foundation beam's top, so that only the deflection of the verification beam tested was measured. For each test, the stiffness is determined by fitting a straight line, in the least-square sense, to the force vs. displacement experimental data. Table 4.1 summarizes the results of the static tests.

Beam span [m]		0.3	0.4	0.5	0.6	0.7
k_s [MN/m]	Direct measurement	17.44	6.28	3.08	1.71	1.06
	Beam theory	17.26	6.39	3.08	1.73	1.07

Table 4.1. Values of k_s using direct measurement and beam theory

Table 4.1 shows that there is a good agreement between the theoretical values of static stiffness derived from beam theory and from direct measurements. The difference between averages does not exceed $\pm 1.7\%$ for the smallest spans (0.3 and 0.4 m) and $\pm 0.8\%$ for the longest spans. Therefore, the static stiffness directly measured is designated as k_s .

4.3 Estimated beam stiffness k_{est} from PRIMA vs. k_s

Performance of the PRIMA device is verified by placing it on the BVT with known stiffness, k_s . In these tests, PRIMA's stiffness estimates k_{est} are computed following equation (54), i.e. as the ratio of the measured peak force and the peak displacement, as intended by the manufacturer. Several types of tests were conducted, using either the base of PRIMA device and a rubber hammer, or the entire device with the sliding hammer. For each test, peak force, peak displacement, k_{est} and duration of the force pulse were read directly from PRIMA software display. k_{est} was then compared to the known beam stiffness k_s (see Table 4.1) associated with each tested beam span. Table 4.2 summarizes the average results of these tests.

The tests have been conducted with the original PRIMA setup as well as with the enhanced setup (i.e. PRIMA base + rubber hammer), because the original setup had to be tested to establish a comparison. Nevertheless, the original falling weight is dropped only from small heights (approximately 10 cm) to limit the beam's vibration level and the beam "ringing," and to avoid beam rebound on its supports. Also, the falling mass is carefully manually held during the rebound following the impact, to avoid further impacts. These precautions are necessary for meaningful measurements. It is important to note that such precautions cannot be realized if the LOADMAN device is used, because

the falling mass is internal to the device. As a result, the BVT cannot be used as a tester for this device without further modifications.

Beam span [m]		0.3	0.4	0.5	0.6	0.7
k_s [MN/m]		17.44	6.28	3.08	1.71	1.06
k_{est} [MN/m]	Original	0.51	0.55	0.91	1.23	1.39
	Enhanced	1.00	1.74	2.17	2.67	3.4
k_{est} / k_s	Original	0.03	0.09	0.30	0.72	1.31
	Enhanced	0.06	0.28	0.70	1.56	3.21

Table 4.2. Average k_{est} from PRIMA's: original (with small height drops) and enhanced configurations vs. k_s

The length of the force pulse depends upon the mass of the falling weight (or hammer), the buffer characteristics, and the stiffness of the support. When using the original loading configuration, the measured period of the load pulse is about 15 ms, with peak values reaching approximately 1 kN. Using the enhanced configuration, the measured period of the load pulse ranges approximately between 4 and 10 ms, with peak values being consistently below 1 kN. Typical force and deflection records from PRIMA's software for the case when PRIMA is placed on the BVT are presented in Fig. 4.5.

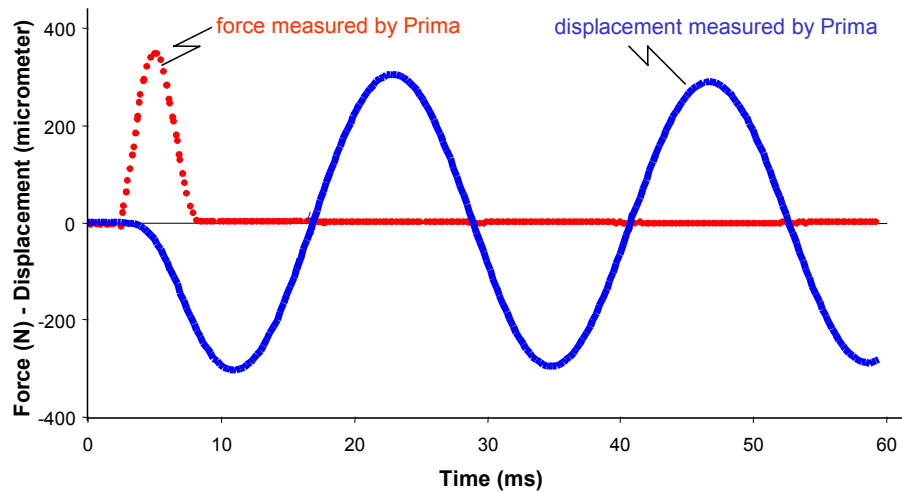


Fig. 4.5. PRIMA measurements on the 70 cm span beam, using a rubber hammer

When comparing the record in Fig.4.5 with the one on Fig. 3.3, the displacement signal associated with the beam deflection does not die off at the end of the 60 ms acquisition window. This is due to the fact that the beam has very little damping, while

soils have much higher damping characteristics, which would result in a displacement time history with smaller duration.

From Table 4.2, one can observe a severe discrepancy between the true BVT stiffness, k_s , and its estimates from the PRIMA device, k_{est} . The two sets of measurements involving alternative PRIMA setups (original and modified) give different results, but neither shows a good agreement with the true values. The general trend shown in Table 4.2 is a very great underestimation of the stiffness for short spans, and a significant overestimation of the stiffness for longer spans. Further, the ratio k_{est}/k_s ranges between 0.72 and 3.21, even for the longer spans, which corresponds to an error on the estimation of k_s ranging from 30 percent to 220 percent.

4.4 Possible causes of the misfit between k_{est} and k_s

As shown in the previous section, the estimates from PRIMA device, k_{est} , do not match the true value of the beam stiffness k_s . Two possible reasons could contribute to this misfit: a major problem with PRIMA's sensors, or the fact that the method of stiffness calculation (peak method), based on equation (54) is not appropriate. To distinguish between these two possible causes, it is instructive to examine first the sensor accuracy. To examine the second possibility, we will test the peak method using a theoretical Single Degree of Freedom (SDOF) model.

4.4.1 PRIMA sensor accuracy

a) Load cell

The load cell direct output has been calibrated under static loading provided by dead loads. This calibration proved a good agreement between the measured load cell sensitivity and the calibration factor indicated by the load cell manufacturer (which is 0.1 mV/kN per unit input voltage).

b) Geophone

The beam was instrumented using accelerometers and a geophone placed directly on the receptacle. PRIMA's geophone output has been verified against the output of the accelerometers (comparison of integrated/differentiated signals) and of the geophone (direct comparison) during impact testing.

The added sensors used for comparison were mounted either on the top surface of the receptacle (geophone) or on the bottom surface of the verification beam, under the exact location of the receptacle's supports (accelerometers). Fig. 4.6 presents an example of the comparison between the velocity record from PRIMA (as recovered by numerical differentiation of the displacement signal stored by PRIMA's software), and the velocity obtained by numerical integration of the acceleration measured by an accelerometer.

Comparisons in time domain such as the one presented in Fig. 4.6 show that the accuracy of the geophone's output is satisfactory. Note that such comparisons not only

check the geophone accuracy itself but also the numerical error associated with the integration from velocity to displacement performed by PRIMA.

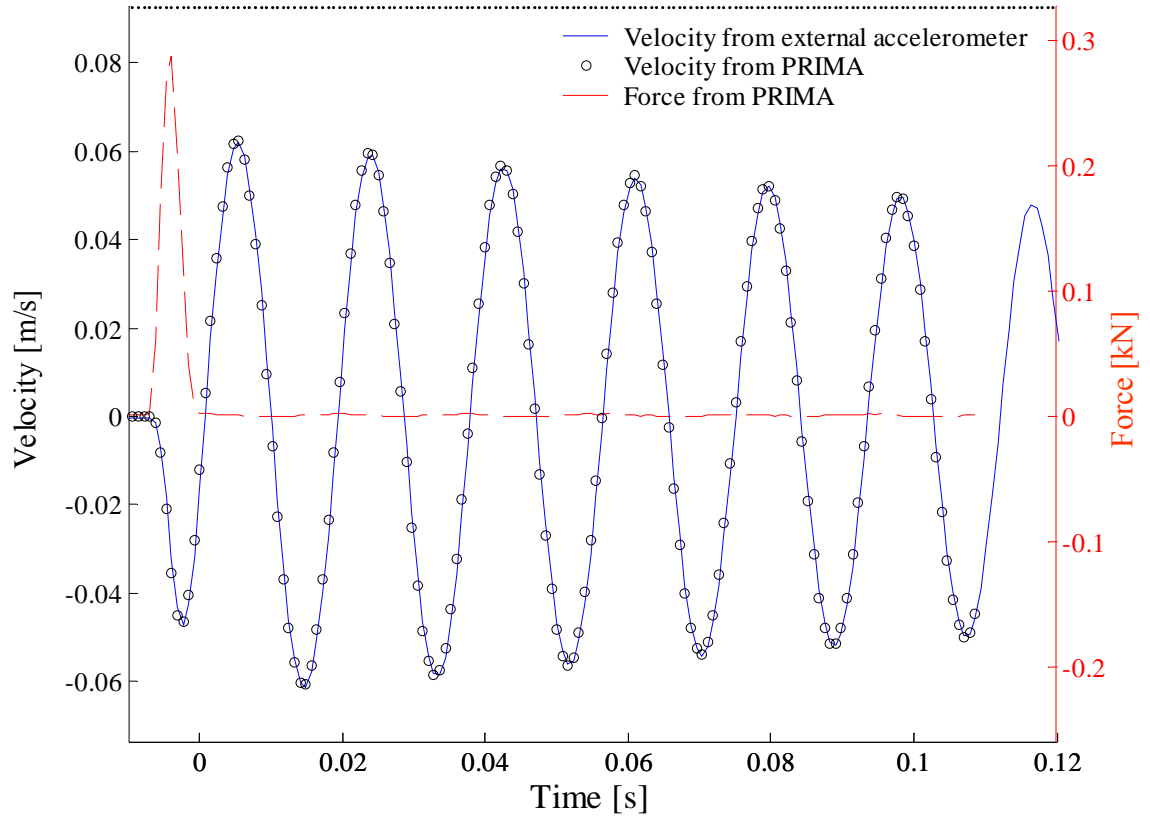


Fig. 4.6. Verification of PRIMA’s geophone output against an accelerometer

The accelerometers used for this study are high sensitivity PCB Piezotronic ICP[®] accelerometers. The geophone used is an IMI Sensors (a PCB Piezotronic division) industrial ICP[®] accelerometer. This sensor is actually an accelerometer with a velocity output (integration performed within the sensor). The conditioner/power supply for the accelerometers and the geophone is a PCB Signal Conditioner. The analog/digital (A/D) converter and spectrum analyzer, used for data acquisition, comprises two DSP SigLab units of two channels each. The conditioners are used to both power the sensors and send the signals from the sensors to the SigLab analyzers. The SigLab units collect the signals from the conditioners and are directly connected to a laptop where the data can be visualized, stored and post-processed.

Based on the above results obtained for both PRIMA geophone and its load cell, the accuracy of PRIMA’s sensors is satisfactory and cannot explain the observed misfit between k_{est} and k_s in Table 4.2.

4.4.2 Theoretical comparison of peak-based k_{est} vs. k_s

Since the accuracy of PRIMA sensors has been checked, the observed stiffness prediction error in Table 4.2 must be attributed to the peak-based data interpretation method used for PRIMA's stiffness estimation. To explain the discrepancies between PRIMA's estimates and true values of the static stiffness of the beam, we can examine the peak method using a simple theoretical model, with known k_s , for which we can compute k_{est} using the peak method. A simple Single Degree of Freedom (SDOF) system is chosen for this purpose. As will be seen later, such system can be chosen as an analog for the vibrating beam. With such a system, the features observed in the field and with beam measurements can be reproduced: the mass m introduces inertial effects (time lag between force and displacement time histories), the spring constant k is the elastic stiffness ($k = k_s$) and the viscous damping coefficient c is responsible for the vibration decay.

With reference to the SDOF system presented in Section 2.3, the displacement time history of a SDOF system due to external loading is shown via the Duhamel integral, equation (10), to depend upon the entire loading history. On this basis, different load pulse shapes and durations will produce different time histories. Unfortunately, the peak-based method takes into account only one point of the entire load pulse and therefore cannot produce an accurate prediction of the SDOF stiffness in general. To illustrate the systematic error in stiffness estimation that arises from the use of the peak method, the effect of varying load pulse durations T on the estimated stiffness of a SDOF system is examined. The response, in terms of displacement, of a SDOF system subjected to a half-sine force pulse applied at its top can be computed either via the linear acceleration method (Wilson and Clough [20]), or using an analytical solution derived from the Duhamel integral. The true stiffness of the SDOF system (i.e. the spring constant, k_s) is an input to the displacement computation, along with the damping ratio ξ and the (undamped) natural period of vibration T_n of the SDOF system. Let us recall that $T_n = 1/f_n$ where f_n is the (undamped) natural frequency of the SDOF system, which itself depends on both k_s and the mass of the SDOF system, as shown in equations (5) and (17).

In this exercise, the peak values are extracted from the (prescribed) load and (computed) displacement time histories as shown in Fig. 4.7. The plot presented in Fig. 4.7 was constructed from a by prescribed half-sine force (sine period $2.T$) by means of the linear acceleration method. The estimated static stiffness k_{est} is then obtained from equation (54) and can be compared to its true value k_s .

When repeating this procedure for various durations of the load pulse, one can construct the comparison presented in Fig. 4.8. This plot shows, for different amounts of damping ξ , the effect of the load pulse duration T on the goodness of the peak-based estimation of the SDOF system stiffness k_s . The best agreement between peak method estimates and true stiffness value is given by the horizontal line $k_{est}/k_s = 1$. The diagram in Fig. 4.8 shows that using the peak method to estimate the SDOF stiffness, k_s , results in a significant systematic error. This error can be either an overestimation or an

underestimation, depending partly upon the damping ratio of the SDOF and mainly upon the impact duration relative to the natural period T_n of the SDOF.

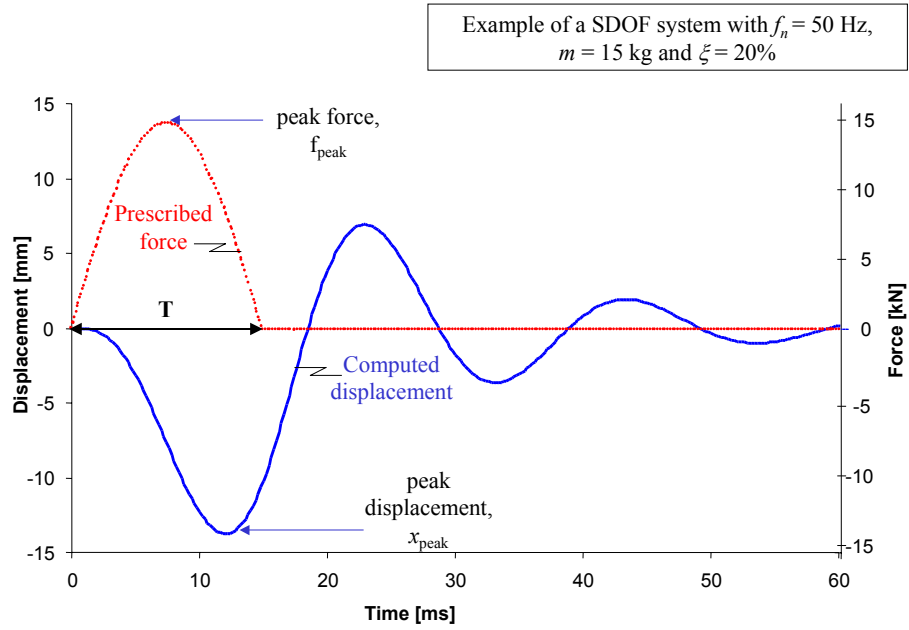


Fig. 4.7. Peak method applied to a theoretical SDOF system

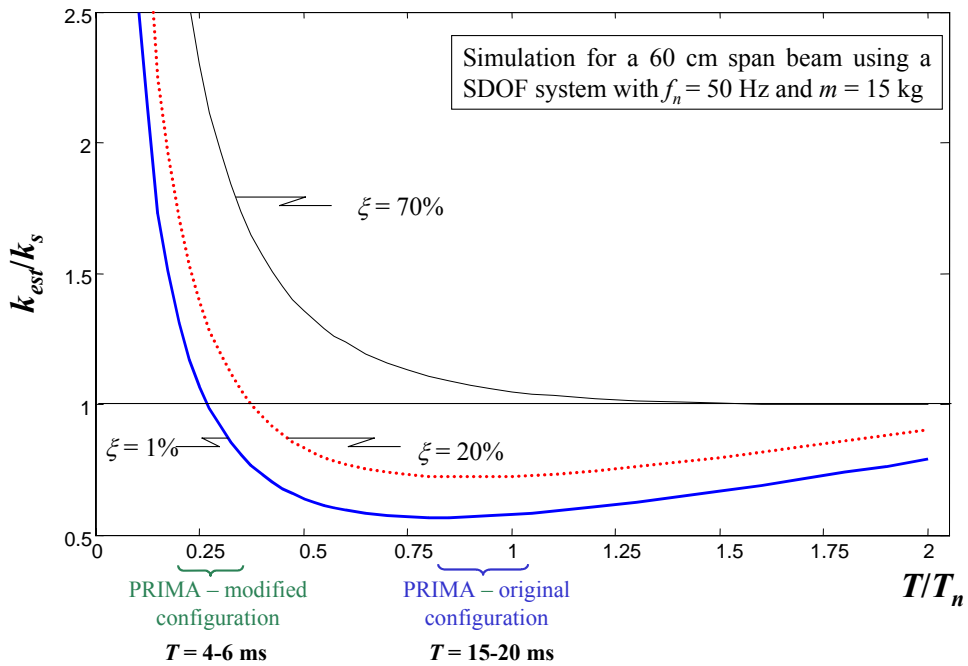


Fig. 4.8. Influence of the pulse duration on peak-based stiffness estimation goodness - theoretical SDOF system

For engineering applications, approximate ratios T/T_n range for PRIMA tests on a particular beam are indicated in Fig. 4.8. The stiffness of the SDOF system has been chosen to approximate the characteristics of the verification beam for a 60 cm span, which stiffness may be comparable the in-situ stiffness for a soft soil ($k_s = 1.71$ MN/m): SDOF parameters that resemble this particular span are $f_n = 50$ Hz, or $T_n = 20$ ms. In this case the experimental results shown in Table 4.2 and the trend observed in Fig. 4.8 (for light damping) lead to the same conclusion that the true stiffness of the 60 cm span beam, approximated by a SDOF system, is overestimated by the enhanced setup and underestimated by the original configuration of PRIMA device.

The above theoretical analysis simulates an impact test performed on a SDOF system. It demonstrates the strong influence of the loading time history (pulse duration) on the results of the peak method. It also shows that significant systematic errors are associated with the peak method when applied to a SDOF system. Based upon the analogy between the SDOF system and simply supported vibrating beam, the same trend can be expected when applying the peak method to the case of the Beam Verification Tester (BVT).

CHAPTER 5 - ENHANCEMENT OF BEAM STIFFNESS

ESTIMATION USING PRIMA DEVICE

The PFWD Beam Verification Tester (BVT), has shown that the stiffness estimates k_{est} from PRIMA device do not match the true stiffness k_s of the beam. Upon verifying the accuracy of PRIMA's sensors, it was concluded that the mismatch was primarily due to the peak method used to estimate the support stiffness from dynamic force and deflection measurements. It was demonstrated theoretically using the SDOF analog that the peak method leads to significant systematic errors in the determination of the support stiffness.

This chapter examines a consistent method to determine the static stiffness of the support from dynamic measurements, based upon a spectral analysis of the recorded data. The key point underlying this method is that the static stiffness can be extracted from dynamic measurements to estimate the stiffness at zero frequency, as shown for example in Guzina and Osburn [7] and Briaud and Lepert [10]. Therefore, the method proposed here focuses on the low frequency range measurements.

The physical setup of PRIMA device used on BVT apparatus corresponds to the enhanced setup as described in Chapters 3 and 4.

5.1 Consistent data interpretation

In the peak method, the static stiffness is incorrectly estimated from dynamic force and displacement time histories as the ratio of peak force over peak displacement. Indeed, the dynamic peak values do not occur at the same time and do not correspond to the static values. Strictly speaking, the static force and displacement correspond respectively to the values of force and displacement at zero frequency in the frequency spectra computed from time histories. Therefore, the correct method to estimate the true static stiffness of the beam is to use the ratio of force over displacement at zero (or near-zero) frequency.

In this study, the frequency spectra are obtained from respective time measurements using Fast Fourier Transform algorithms. Recalling the definitions of the Fourier Transform presented in Section 2.5.1, the main practical requirement to perform a correct transformation into frequency domain is that entire transient signals must be sampled. Recording the entire time histories is therefore a key step. Due to PRIMA's hardware limitations (maximum record duration of 120 ms), however, it was not possible to obtain the entire time histories for the beam tests (duration of motion up to a few seconds) directly from PRIMA device. As a result, an external data acquisition system is used. Furthermore, rather than using the manufacturer's software to extract the measurements, an in-house program is developed to record the time histories and interpret the data.

In addition to the force and velocity sensors, the data acquisition system is composed of the conditioner/amplifier for an independent monitoring of PRIMA's load cell, a conditioner/power supply for the accelerometers and the geophone, the DSP SigLab spectrum analyzer, and a portable computer. All these elements have been already described in Section 4.4.1, except the signal conditioner/ amplifier used for PRIMA's load cell. This signal conditioner is a Vishay strain gage conditioner model 2120 coupled with a model 2110A power supply. The data acquisition layout used in this study for verification testing is summarized in Fig. 5.1.

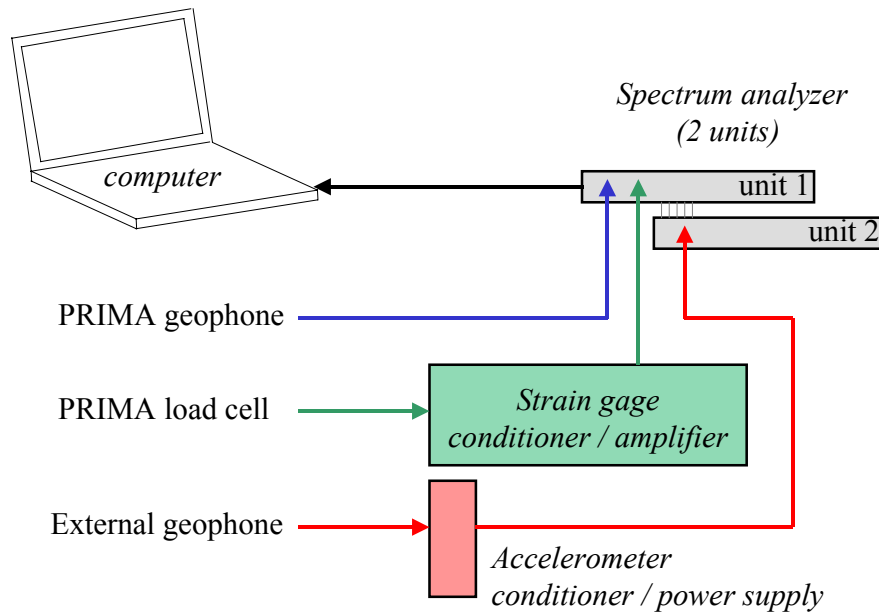


Fig. 5.1. BVT data acquisition

The proposed method, based upon the measurement of the zero-frequency components of the force and displacement records, is well-understood, however in practice a main limitation arises due to the sensors characteristics. As examined in Sections 2.4 and 3.3, in the low frequency range (typically 0 to 10/20 Hz), the sensor (geophone/accelerometer) output does not reflect the measured motion quantity. As a result, the value at zero frequency cannot be estimated directly from the measurements.

To overcome this problem, one must extrapolate experimental data in the low frequency range to obtain the value at zero frequency. It is well-known, however, that data extrapolation can be a dangerous process if reasonable controls are not applied. The best way to ensure a correct determination of the zero frequency value is to use a theoretical model as a guide for the extrapolation.

The remainder of this chapter presents the theoretical model used to extrapolate the data, as well as the frequency domain analysis tools used to estimate the beam's static stiffness.

5.1.1 SDOF model for the beam

The theoretical model chosen to guide the dynamic stiffness data extrapolation towards zero frequency is the SDOF system. We will assume for now that the beam motion accurately can be approximated by a SDOF system, at least for the low frequency range. The use of this particular model is motivated by its simplicity. Also, SDOF analogs are commonly used in structural vibration problems, such as determination of beams fundamental frequency. Note that no rigorous theoretical justification will be presented here. However, the relevance of this assumption is based upon previous analytical work, such as the analog SDOF system of a simply supported beam carrying a mass at mid-span and undergoing free vibrations in Stokey [29] and in Kármán [30], and will be justified a posteriori by the results obtained.

As a result, an alternative data interpretation method is proposed based upon the determination of the stiffness (i.e the spring constant) k of an equivalent SDOF system. In this method, the static stiffness $k_s = k$ is recovered from the time history of both load and displacement by fitting, in the low frequency range, a measured FRF to the corresponding FRF of the SDOF system.

During testing on the BVT, an impact shock produces a transient excitation of the beam containing various frequencies. It was found, however, that the BVT reacts to an impact load (applied to the receptacle) primarily through the fundamental mode of vibration. As a result, the SDOF simulation of the beam response pertains only to the lower vibration frequencies located around the fundamental resonant frequency. For higher frequencies, the SDOF system does not model the beam behavior well. Although the size of the useful frequency window could be adapted to each span of the tested beam, it is chosen in this study to match the range 10 – 150 Hz.

Fig. 5.2 illustrates the analogy tested beam / SDOF system. Following this outline, the equivalent mass m_{eq} corresponds to the total mass comprised between the beam and the point of measurement of the applied force. In other words, m_{eq} comprises the mass of the PRIMA device (enhanced setup) and the mass of receptacle, plus the mass of receptacle supports and clamping devices. Furthermore, the mass of the sensor(s) located on the receptacle and a (unknown) part of the mass of the cable assemblies also should be included.

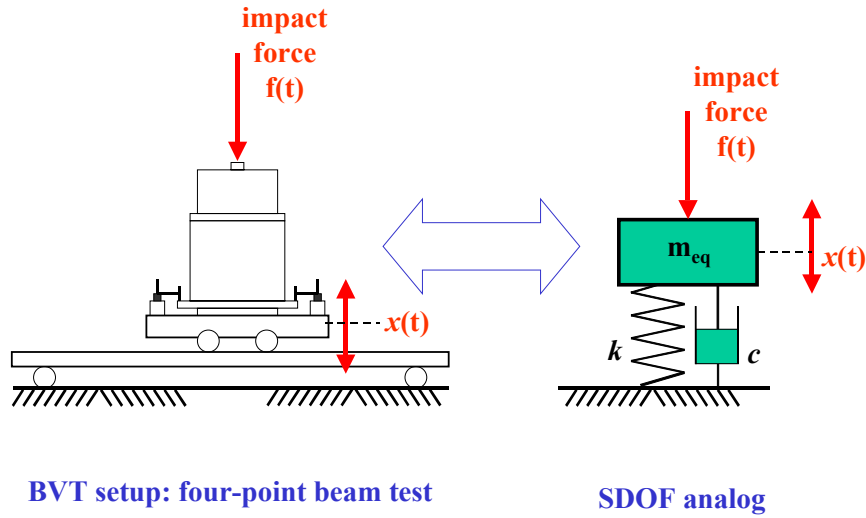


Fig. 5.2. SDOF analog for the BVT setup

5.1.2 Frequency domain analysis tools

In the ensuing analysis, the entire time history of the load and displacement signals is used as an input to the SDOF approximation of the beam response. During testing with the BVT, the beam response is linear, and so is the response of the SDOF equivalent system. This allows us to use the FRF for linear systems as defined in Section 2.5. Let us recall the definitions of the dynamic stiffness $K(\omega)$ and mobility $M(\omega)$ of a linear system, equations (32) and (28):

$$K(\omega) = \frac{F(\omega)}{X(\omega)} \quad (32)$$

$$M(\omega) = \frac{\dot{X}(\omega)}{F(\omega)} \quad (28)$$

where $F(\omega)$, $X(\omega)$ and $\dot{X}(\omega)$ are respectively the contact force, the displacement and the velocity at the PRIMA-BVT interface, in frequency domain. The advantage of using this method is that FRFs characterize the entire system, are unique (linear system), and are independent of the applied force. According to the approach of Section 2.5.5, which is built into the SigLab data acquisition system, the measured (average) FRF of choice is obtained directly from the spectral density functions estimates.

Let us recall at this point that FRFs are complex-valued functions, comprised of a real and an imaginary part. For this project the mobility function $M(\omega)$, both real and imaginary parts, is used to fit the experimental data. The mobility function is used because it corresponds directly to the quantities (velocity and force) being measured. The average $M(\omega)$ function can be obtained either directly from PRIMA sensors (geophone

and load cell) either from external sensors mounted on the calibration beam (accelerometer / geophone). The tests presented in this report are realized using the load cell from PRIMA and a geophone mounted on the receptacle.

Based upon the analytical solution for the mobility function $M(\omega)$ of a SDOF, presented in Section 2.5, an in-house Matlab code is used to fit the experimental mobility data to the theoretical $M(\omega)$ curve of a SDOF system and to obtain the optimal set of its fundamental properties, namely static stiffness k_s , damping ratio ξ and equivalent mass m_{eq} .

At this point the static stiffness of the SDOF, and thus that of the BVT, already has been estimated from the fitting process. However, it also can be directly read from the real part of the dynamic stiffness curve of the fitted SDOF system, at zero frequency:

$$k_s = \text{Re}\{K(\omega = 0)\} \quad (62)$$

Note that the SDOF dynamic stiffness function $K(\omega)$ can be constructed either from the fitted SDOF parameters, or by inverting the fitted $M(\omega)$ function to get the impedance function $I(\omega)$ and then multiplying $I(\omega)$ by $(i\omega)$.

The coherence function $\gamma^2(\omega)$, also introduced in Section 2.5, is a good indicator of the quality of the measurements and of the linearity of the system. A coherence significantly less than unity indicates presence of noise in the measurements, nonlinearity between input and output, or both. The coherence is therefore used to define the usable frequency range that can be employed for the fitting process and as a criterion to accept or reject a series of measurements. Typically, all the measurements for which the value $\gamma^2(\omega)$ is significantly below the unit value (less than 0.95 for this study) will be disregarded in the analysis.

5.2 Experimental procedure and results

5.2.1 Data acquisition setup

It has been shown previously that an independent data acquisition system is needed to capture the entire load and displacement time histories relevant to the BVT testing, which are characterized by an extended duration relative to field measurements. Therefore, the output plugs from both PRIMA's sensors, load cell and geophone, have been directly connected to an external data acquisition equipment described earlier. Doing so, however, one cannot access the sensors' calibration parameters that are embedded in the PRIMA's software. In this study, voltage output and corresponding velocity and force have been related using the values given by the sensor manufacturers. As mentioned earlier, an independent check using dead load calibration for the load cell and direct comparison for the geophone demonstrated that the sensors were accurate.

Fig. 4.1, 4.2 and 5.1 show the general experimental setup of the BVT. In the verification procedure, each test is composed of a series of ten measurements of the force from PRIMA's load cell and the induced motion velocity from PRIMA's geophone. The

data are sent directly to the SigLab analyzer where the mobility $M(\omega)$ is estimated using an FFT algorithm as a spectral average of the 10 measurements, together with the coherence function $\gamma^2(\omega)$, as depicted in Fig. 5.3.

Note that the measurements presented in Fig. 5.3 correspond to the configuration of long spans for the beam (50 cm to 70 cm) only. Examination of the coherence function in Fig. 5.3, plotted in the range 0 to 150 Hz, indicates that the useful range can be taken as 10 to 150 Hz. Note that a lower limit of 20 Hz would be even more conservative, but experience shows that this precaution is not necessary. The coherence degrades at very low frequency because the geophone's output is not linear: Recalling the geophone description given in Section 2.4, no accurate measurements can be expected at very low frequencies (below 10/20 Hz). For frequencies higher than 150/200 Hz, measurements are associated with an important decrease of the coherence function, which indicates that the response includes nonlinear effects, noise and stray vibrations. Therefore, the analysis is limited to frequencies up to 150 Hz.

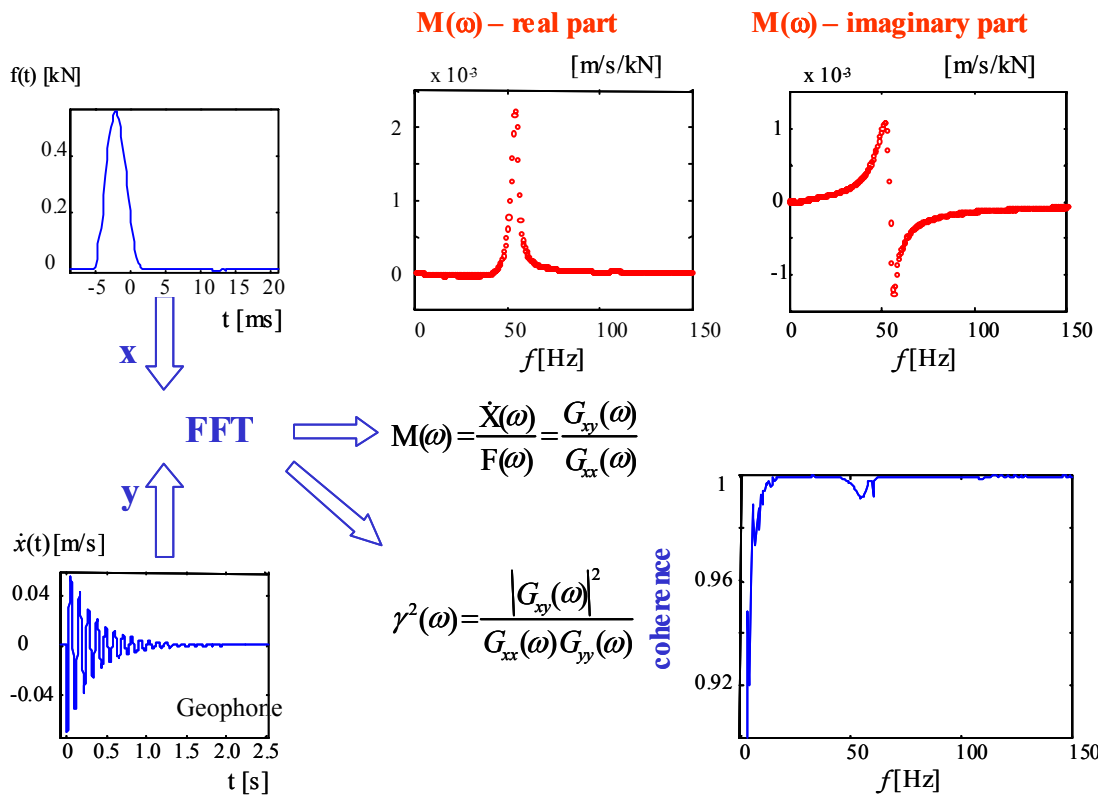


Fig. 5.3. Typical measurement sequence and output

Let us point out that, depending upon which channel is chosen as reference (i.e. input of the ideal linear system), the FRF resulting from velocity and force measurements can be either mobility $M(\omega)$ or impedance $I(\omega)$. Also, a very useful feature implemented in the SigLab analyzer software enables to integrate/differentiate directly the measured FFTs. The advantage is that $K(\omega)$ could be directly given as an output of the SigLab

analyzer from measurements of $I(\omega)$ and direct spectral differentiation (no additional data manipulation). For this project, however, the use of $M(\omega)$ is preferred.

5.2.2 Fitting process

Once the experimental $M(\omega)$ is recorded, an in-house Matlab code fits the measurements to the theoretical SDOF mobility function to estimate the system properties, k , ξ and m_{eq} . The program optionally can be called directly from the SigLab analyzer software after the test, so that the results are displayed on the same screen as the acquisition program. The fitting process follows an optimization method in which an objective function is being minimized. For this project, a built-in Matlab function, based upon an unconstrained nonlinear optimization method, is used. This method is a direct search method. It does not use numerical or analytic gradients. The built-in Matlab function finds the minimum of a scalar real-valued function of several variables, starting with an initial estimate. The minimum found is the local minimum of the objective function to minimize, in the vicinity of the initial estimate provided to the optimization process. The initial estimate can be a scalar, a vector, or a matrix. Consistent with current practice, the function minimized is the square of the difference between measurements and trial fitted curve.

Both the real and imaginary parts of $M(\omega)$ are used for curve fitting. The analytical expression used is given by equation (29). The initial parameters used to initiate the fitting process correspond to both automatic estimation of the fundamental frequency of the beam and initial guess (damping ratio and mass, and also frequency window width). The natural frequency of the SDOF analog is computed as being the fundamental frequency automatically estimated from the spectral data, using the peak in the real part of $M(\omega)$. Note that the fundamental frequency also could be estimated from the FFT of the velocity time history. The initial values for the SDOF damping ratio, equivalent mass and stiffness correspond to values comprised in the expected range. More precisely, the selected values are 10 kg for the SDOF equivalent mass and 1 percent damping ratio. An initial value for the stiffness of the SDOF analog is computed from the equivalent mass and the natural frequency estimate using equation (5).

As mentioned earlier, the appropriate frequency range is 10-150 Hz. However, to take into account the frequent drop in coherence function observed at the vicinity of the fundamental frequency (see in Fig. 5.1 at approximately 50 Hz), it is decided to exclude the point corresponding to the natural frequency, as well as two additional points on each side of the frequency spectrum. Using the foregoing scheme, the choice of an initial guesses for the mass and the damping ratio do not influence the fitting process, and a stable convergence of the minimization function is reached.

5.2.3 Estimated k_{est} from PRIMA vs. k_s using the mobility function

Verification tests on the enhanced PRIMA configuration and the techniques presented in the previous section were completed for spans of the BVT between 0.3 m and 0.7 m. Fig. 5.3 shows a typical measured mobility function $M(\omega)$. Fig. 5.4 shows the plots corresponding to the same data together with the corresponding fitted SDOF curves.

It can be seen from Fig. 5.4 that the SDOF model matches the experimental data well for longer beam spans. From this fitting process, the parameters of the equivalent SDOF system are effectively estimated. In particular, the stiffness k of the equivalent system, which corresponds to the static stiffness of the beam, is estimated.

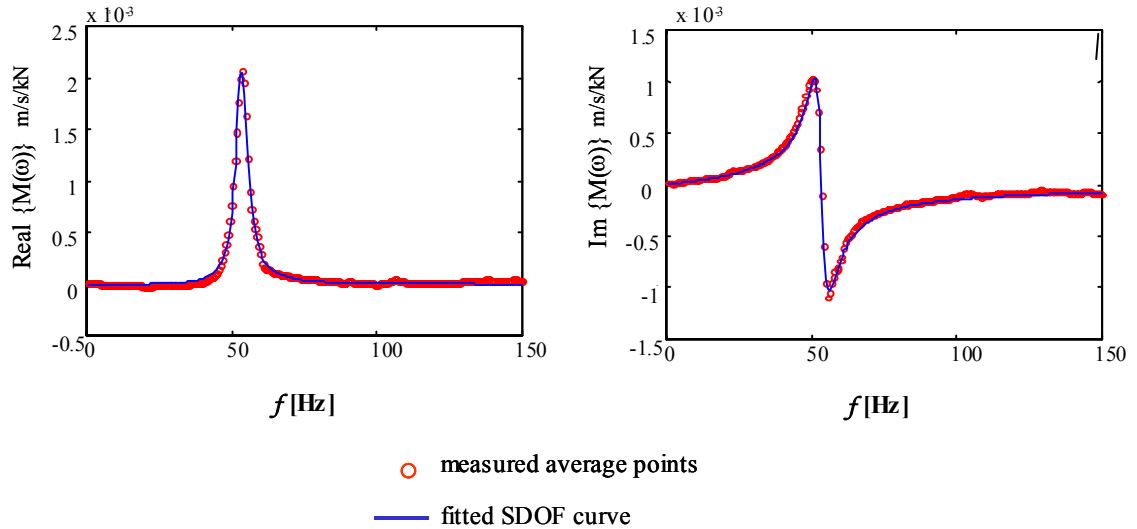


Fig. 5.4. Measured data and fitted SDOF curves - example of a 60 cm span beam

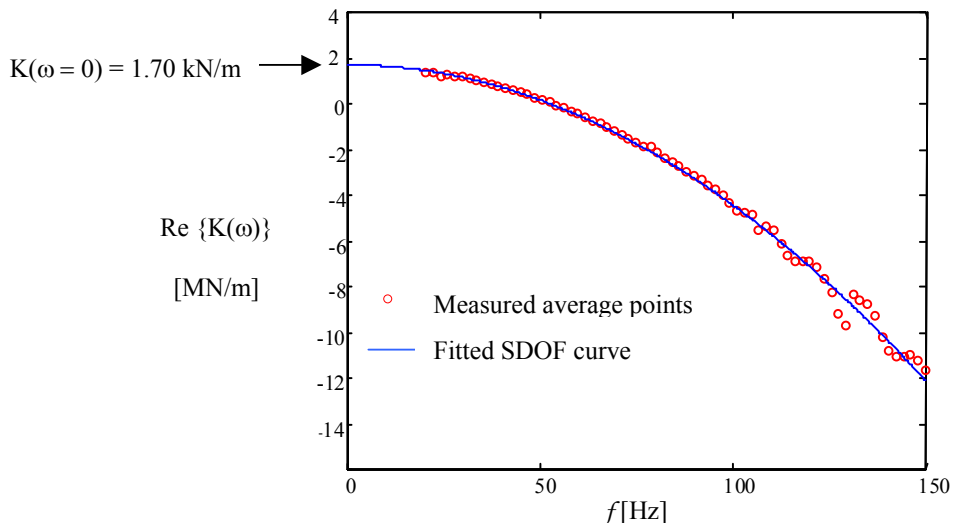


Fig. 5.5. Fitted SDOF real part of $K(\omega)$ – example of a 60 cm span beam

As mentioned earlier, using the values of the SDOF system resulting from the fitting process, it is possible to construct the curve corresponding to the real part of the dynamic stiffness $K(\omega)$ of the equivalent SDOF system. Fig. 5.5 presents such a plot,

corresponding to the beam span of 60 cm. From this curve the change of the stiffness with frequency is clear and can be used to estimate the static stiffness, at $f = 0$. The value of the static stiffness $k_{est} = 1.70$ MN/m obtained by this fitting process compares well with the true value which is for this 0.6 m span equal to 1.71 MN/m.

Table 5.1 shows the results associated with the fit of the experimental mobility data with the theoretical $M(\omega)$ function of a SDOF system for all beam spans. These results show that the proposed method is able to estimate the true static stiffness of the beam k_s within a few percent for the longer spans, namely $L = 0.5, 0.6$ and 0.7 m. Conversely, the results regarding the shorter spans ($L = 0.3$ and 0.4 m) show a poor agreement with the true value.

Beam span [m]	0.3	0.4	0.5	0.6	0.7
k_s [MN/m]	17.44	6.28	3.08	1.71	1.06
k_{est} [MN/m]	30.12	7.40	3.09	1.71	1.07
k_{est} / k_s	1.73	1.18	1.00	1.00	1.01

Table 5.1. Static stiffness estimates via fitting of the mobility function – undamped beam

The mismatch associated with the shorter spans can be associated with the particular geometry of the beam, which produces a very stiff beam with long cantilevers. For low spans, the cantilever parts of the beam, on each side of the supports, are long compared to the beam span. The presence of these long cantilever parts introduces additional significant masses away from the receptacle and therefore additional degrees of freedom, so that the SDOF analog is no longer appropriate.

The range of spans appropriate for verification tests is therefore 0.5 m to 0.7 m, for which the error ranges from 2 percent to 5 percent.

5.2.4 Beam with additional damping

During testing with PRIMA, the impact generates stress waves radiating away from the area of impact (source) in the tested support, which was the beam for this study and is the soil in field-testing situations. Would the support be constituted of a perfectly elastic material, the total energy imparted to the support and carried by the wave would be conserved without loss. However, the beam and soils do not behave purely elastically, energy is dissipated, and the waves' amplitude is attenuated (damped).

From Fig. 5.2, one may note that the damping of the BVT assembly, which results from material damping and energy dissipation at the mechanical contacts, is significantly lower than the observed in-situ damping (see Fig. 3.3).

In the case of soils, damping is generally very high. The attenuation of the stress wave amplitude results from two damping processes, material damping (conversion of elastic energy into heat) and radiation damping (e.g. Kramer [13]). Radiation damping,

also referred to as geometrical damping, is related to the reduction of the specific energy (elastic energy per unit volume) as the wave travels away from the source due to spreading of the energy over a greater volume of material.

The total damping in the beam, experimentally estimated in this study via the damping ratio of the equivalent SDOF system, does not exceed a few percent. As a result, the duration of motion during testing on the BVT is significantly longer than that observed in the field.

It is important to stress here that the need to provide additional damping to dissipate energy does not affect the validity of the stiffness estimation method. The static stiffness of the beam or its SDOF analog does not depend upon the amount of damping. Indeed, for the dynamic stiffness of the equivalent SDOF system with reference to equations (34) and (37), the real part is independent of the damping and the imaginary part is zero at zero frequency, which indicates that the static stiffness is independent of the amount of damping. Furthermore, as it will be seen in the following, tests showed that the addition of external damping on the beam does not affect the stiffness estimates.

However, anticipating a possible use of the BVT device as a tool for routine verification of PRIMA-type devices, we have to expect objections from the field-testing practitioners who might argue that the duration of the motion in BVT testing does not resemble the duration of the motion experienced in the field. To address this issue, it was decided to decrease the motion duration by adding some external damping to the beam.

5.2.4.1 Auxiliary dampers

Let us examine how damping can be added to the BVT using external devices. Damping devices such as auxiliary mass absorbers often are used (e.g. Reed [31]) to dissipate the vibration energy to reduce excessive vibrations in a structure. The simplest form of auxiliary damper is a SDOF system attached to the structure where additional damping is sought. In that case it is supposed that the amplitude of motion of the structure to be damped, the so-called primary structure, is unaffected by the presence of the auxiliary system, and that all the energy dissipation takes place in the damping element of the auxiliary system. Expressions to compute the energy dissipated by viscous damping per cycle of vibration in the case of a SDOF system submitted to steady-state vibrations, such as the one depicted in Fig. 2.5, can be found in the literature (e.g. Kramer [13]; Reed [31]).

It can be shown that for such a case, efficient energy dissipation is associated with an auxiliary system with a large mass, a small damping ratio and a stiffness tuned to $\beta = 1$. In other words, efficient energy dissipation will be obtained for a driving frequency close to the natural frequency of the auxiliary damper. For example, in the case of a beam with a span of 60 cm (measured fundamental frequency of about 50 Hz), the tuned value of the spring constant would be approximately 0.2 MN/m. As a result, a soft spring will be required for optimal energy dissipation.

5.2.4.2 External damping setup

To add some external damping to the beam without changing its static stiffness, it was decided to attach auxiliary damping devices on the beam's cantilever portions.

Before presenting the damping devices used for this study, let us first show that the static stiffness of the beam is not affected by their presence. Let us consider the additional masses corresponding to two identical damping devices positioned on the cantilever portions of the beam, as shown in Fig. 5.6.

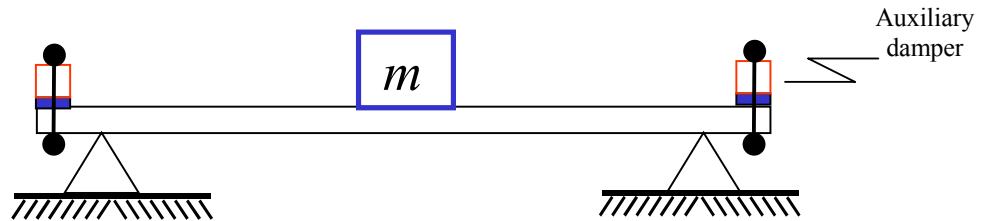


Fig. 5.6. Simplified layout of the simply supported beam with damping devices located on the cantilever parts

Before impacting the base of PRIMA represented by the mass m , the beam initial deformation is due to the mass m and also to the mass associated with the devices. This deformation state of the beam is the original state or equilibrium state. During testing, an additional deformation occurs due to the impact. However, the beam behaves as a linear elastic system and the deformation measured during testing corresponds only to the perturbation of the equilibrium state. In other words, the static stiffness of the linear elastic beam is not affected by the initial deformation state. As a result, adding some mass does not theoretically affect the static stiffness of the beam. However, the stiffness estimation is based upon the SDOF analog for the beam, so that the added mass should be small enough to avoid the introduction of supplementary degrees of freedom in the system.

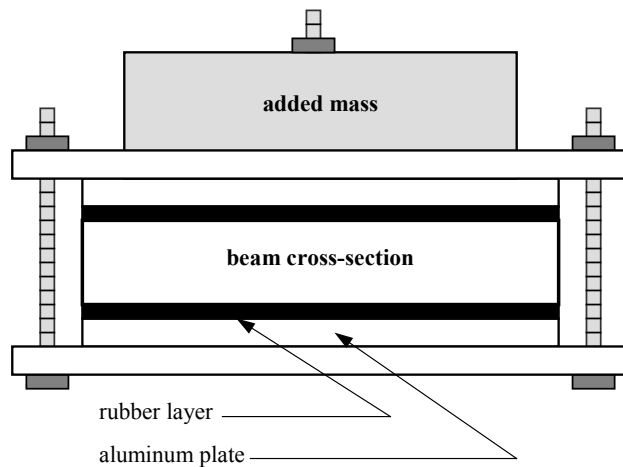


Fig. 5.7. Layout of a damping device located at the end of the overhanging part of the beam

Let us now describe the design of the damping devices. Based upon the guidelines for auxiliary damping systems presented in the previous section, damping devices with high vibration attenuation are associated with a small damping ratio, a large mass and a soft spring. However, a large mass would introduce an additional degree of freedom to the system. Therefore, a small mass needs to be used. As a result, the damping devices designed for the BVT are constituted of a small mass seating on a rubber layer and loosely connected to the cantilever portions of the beam, as shown in more details in Figs. 5.7 and 5.8. The loose connection is equivalent to the use of a soft spring and introduces a phase delay (responsible for the damping) between primary system and added mass motions. The rubber layers used are 10.16 cm wide, 8.5 cm long and 0.63 cm deep. They are supported by aluminum plates of same width and length. The assembly rubber layers plus aluminum plates is attached to the beam using an adjustable aluminum frame, on the top of which a mass is attached.



Fig. 5.8. Testing setup for the BVT with additional damping

5.2.4.3 Experimental results

Tests on the BVT showed that the efficiency of the auxiliary damping devices highly depends on the precise tuning of the devices. They also showed that the beam with smaller spans did not behave as a SDOF system due to the introduction of relatively important additional masses. As a result, the verification tests were conducted on the longer spans (0.6 m and 0.7 m) only.

For this study, a mass of 2.3 kg (5 lb) was used for each damping device. We did not attempt to estimate the exact tuning values, but focused on the attenuation effects. The stiffness of the connections was manually tuned, by adjusting the force in the nuts, in order to obtain the optimum vibration attenuation. Typical plots of the measured velocity are presented in Fig. 5.9, to show the reduction of the duration of the velocity time history due to the addition of the damping devices.

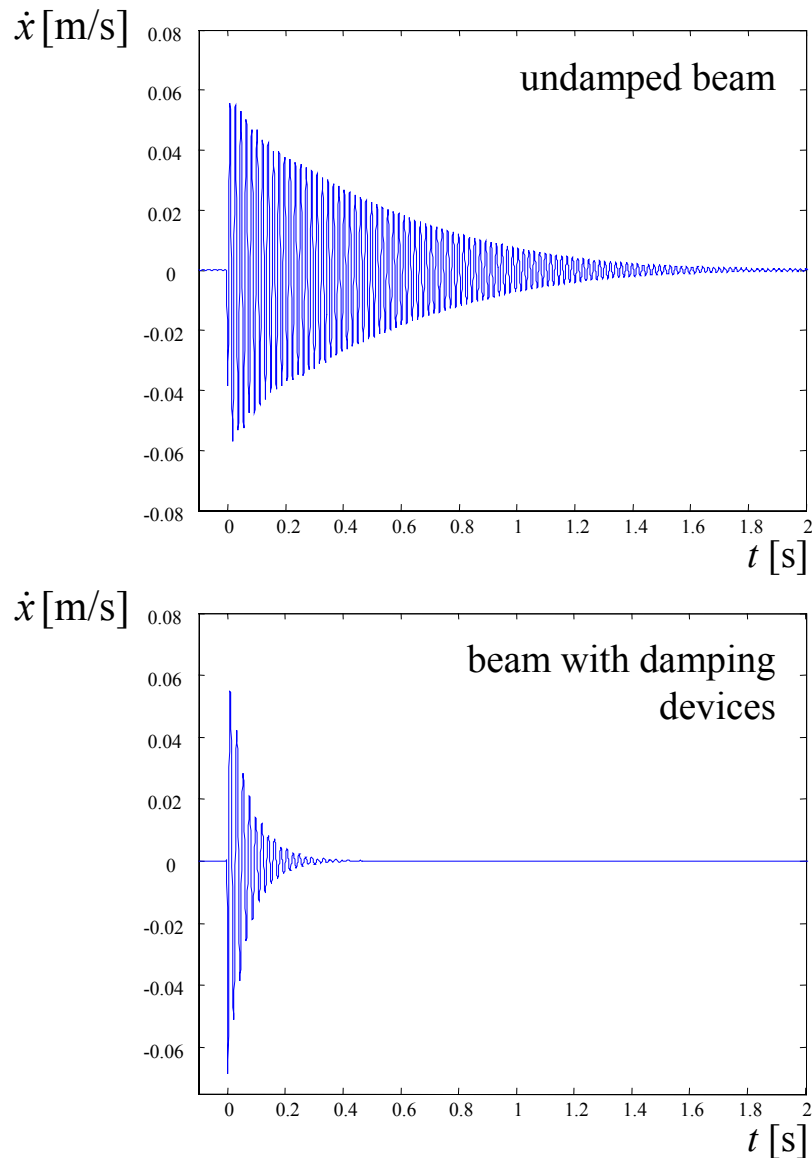


Fig. 5.9. Comparison of velocity time histories – undamped and damped beam setup

The damped beam stiffness was estimated using the same tools and procedures that were used for the case of the undamped beam. Table 5.2 presents the results of the beam stiffness estimation for the BVT with additional damping, and shows a good match between estimated values k_{est} and beam stiffness k_s . Comparison with Table 5.1 indicates that the featured damping devices do not have any significant effect on the accuracy of the results.

Beam span [m]	0.6	0.7
k_s [MN/m]	1.71	1.06
k_{est} [MN/m]	1.71	1.05
k_{est} / k_s	1.00	0.99

Table 5.2. Static stiffness estimates via fitting of the mobility function – beam with damping devices

5.3 BVT apparatus: summary and practical applications

Several departments of transportation throughout the world are preparing to use PFWD devices for quality assurance purposes. In this field, it is essential to use well-calibrated and rigorously validated devices. By design, the BVT can be used to effectively check the correctness and accuracy of stiffness estimates from PFWD devices.

5.3.1 PFWD PRIMA

This section showed that the true stiffness of the beam accurately can be estimated using PRIMA device, provided that the modified device (i.e. enhanced physical configuration of the device) is utilized for testing, and that a consistent (spectral-based) data interpretation method is used, rather than the peak method embedded in the original PRIMA data interpretation scheme.

Under these conditions, therefore, the BVT can be used to check and validate the performance of PFWD devices such as PRIMA, using a two-step procedure:

- 1) the calibration factors for the force and motion sensors, as used by the PFWD device data acquisition system, must be checked using the independent data acquisition system of the BVT,
- 2) the stiffness estimates can be directly verified against the true stiffness of the beam, using spans between 0.5 m and 0.7 m. A match between k_{est} and k_s within a few percents will indicate that the PFWD performance is satisfactory.

In the case of a mismatch between k_{est} and k_s , a recalibration of the sensors will be necessary. Note that in the case of PRIMA device, both the geophone and the load cell can be checked separately to determine the cause of the mismatch. As seen in Section 4.4.1, the load cell calibration factor easily can be verified under static loading using dead loads. Also, the output of the geophone can be calibrated during dynamic testing by comparison with the output of an independent BVT geophone, either in time domain, as presented in Section 4.4.1, or using frequency spectra.

A user's manual has been developed and is included as an appendix, to provide a support for routine testing using the BVT. This document describes a complete testing

procedure to verify the performance of PRIMA devices, and also presents some guidelines and testing procedures to verify the accuracy of the individual sensors embedded in PRIMA.

5.3.2 Other portable deflectometer devices

In this project, the PFWD verification effort was focused on the PRIMA device because it offers direct measurement of both force and velocity. Another advantage of PRIMA is that the device can be modified so that the impact load is low enough to allow for accurate measurements on the BVT.

Other deflectometer devices generally have specific characteristics in terms of (i) excitation type, such as impact (LOADMAN) or steady-state vibratory forcing (GEOGAUGE); (ii) force and motion measurement methods; and (iii) forcing magnitude and physical setup.

As a result, adaptations of the BVT device to particular deflectometer tool must be done on a case-by-case basis. However, a general restriction applies. The BVT can be adapted to check the stiffness estimates of other PFWD devices as long as they can operate with an impact energy comparable to the one used with the enhanced PRIMA configuration. Therefore, as mentioned in Section 4.3, the LOADMAN device, where the height of free fall of the weight is not adjustable, cannot be used on the BVT.

When aiming to check the performance of a given deflectometer device, one must distinguish between the estimated stiffness k_{est} from the device and the sensor accuracy. Indeed, the displayed k_{est} incorporates a data interpretation scheme specific to each device that might mask the effect of sensor calibration. Sensor accuracy can be checked only if the device allows for a direct independent check of each individual sensor. If not, a direct comparison k_{est} vs. k_s on the BVT can only check the overall device performance without distinction between the effects of sensor calibration and those of embedded data interpretation.

CHAPTER 6 - PRIMA DEVICE: ADDITIONAL CONSIDERATIONS AND RECOMMENDATIONS FOR FIELD USE

It was shown in this study, using the Beam Verification Tester (BVT), (i) that the peak method often used in practice for static stiffness estimation can lead to significant systematic errors and (ii) that reliable estimates of the static stiffness from PRIMA device measurements can be obtained only if the non-truncated load and velocity time histories can be extracted from the device and used as input to a consistent data interpretation based upon FRF zero-frequency estimates of dynamic stiffness and spectral average.

We now will investigate the possibility of implementing the concepts developed in the previous sections during field testing. It will be demonstrated that the peak method also can lead to systematic errors in the case of homogeneous and layered half-space. As a result, enhancements of the PRIMA analysis, hardware and software developed in conjunction with BVT testing need to be extended to field applications.

6.1 Theoretical comparison peak-based k_{est} vs. k_s for field profiles

6.1.1 Homogeneous half-space

In Section 4.4.2 the peak method was applied to the theoretical SDOF system. The results demonstrated that the ratio k_{est}/k_s was strongly and non-linearly dependent on the duration of the force pulse, T , relative to the natural period T_n of the SDOF system. Following the same logic, we will examine the relationship between k_{est}/k_s and T in the case of field-testing using PRIMA device as an example, where the foundation (i.e. base on top of subgrade) is modeled as a homogeneous elastic half-space. The steady-state load-displacement relationship for a rigid massive disk resting on the top of a homogeneous half-space, as depicted in Fig. 2.12, is given by equation (52)

$$X_0 = \frac{F_0}{\frac{1}{C_{vv}(\omega)} - m\omega^2} \quad (52)$$

where m is the mass of the footing, F_0 the maximum force amplitude, X_0 the maximum displacement amplitude, ω the driving frequency, and C_{vv} the massless vertical compliance function. In the case of testing with PRIMA, the force pulse is not steady state but can be approximated as a half-sine function. Decomposing the transient half-sine force pulse into a series of harmonic functions, equation (52) can be rewritten as

$$X(\omega) = \frac{F(\omega)}{\frac{1}{C_{vv}(\omega)} - m\omega^2} \quad (63)$$

where $F(\omega)$ is the Fourier transform of the applied force $f(t)$, $X(\omega)$ the Fourier transform of the displacement $x(t)$, and m the mass of the footing. Let us recall from equation (3) that the theoretical static stiffness k_s of a homogeneous half-space under the action of a rigid, frictionless circular punch of radius a is given by

$$k_s = \frac{4Ga}{1-\nu} \quad (64)$$

Let us now examine the procedure used to compute the “field” ratio k_{est}/k_s resulting from a known, i.e. prescribed, $f(t)$. The transient force time history is constructed from a known duration T and known maximum amplitude f_{peak} . Applying a FFT to $f(t)$ to get $F(\omega)$, and using the theoretical curves for $C_{vv}(\omega)$ presented in Section 2.6.1 (Pak and Guzina [12]), one can compute $X(\omega)$ using equation (63). The peak displacement x_{peak} is calculated as the maximum amplitude of the displacement $x(t)$ obtained from the inverse FFT of $X(\omega)$. The stiffness k_{est} , estimated using the peak method, is computed from equation (54) as

$$k_{est} = \frac{f_{peak}}{x_{peak}} \quad (54)$$

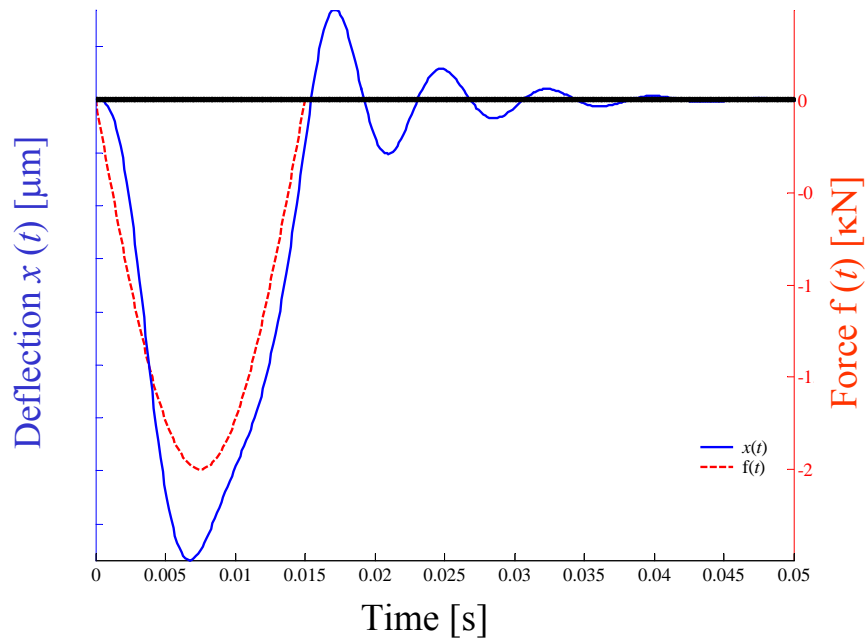


Fig. 6.1. Example of time history plots - homogeneous half-space

For given soil properties G and ν and given footing radius a , k_{est}/k_s is computed from equations (54) and (64). Note that G can be calculated from the given shear wave velocity c_s and soil's mass density ρ using equation (51). Fig. 6.1 shows an example of deflection time history computed for a prescribed force with duration $T = 15$ ms in the case of an elastic half-space with $c_s = 100$ m/s, $\nu = 0.30$ and $\rho = 1800$ kg/m³.

If the procedure is repeated for various values of force duration T , a plot of k_{est}/k_s vs. T can be constructed. Now, rather than using directly T , the dimensionless quantity \bar{T} , defined as

$$\bar{T} = T \frac{c_s}{a} \quad (65)$$

is preferred to present the results. Fig. 6.2 presents an example of the k_{est}/k_s vs. \bar{T} diagram, constructed assuming Poisson's ratio $\nu = 0.30$, and mass density $\rho = 1800$ kg/m³.

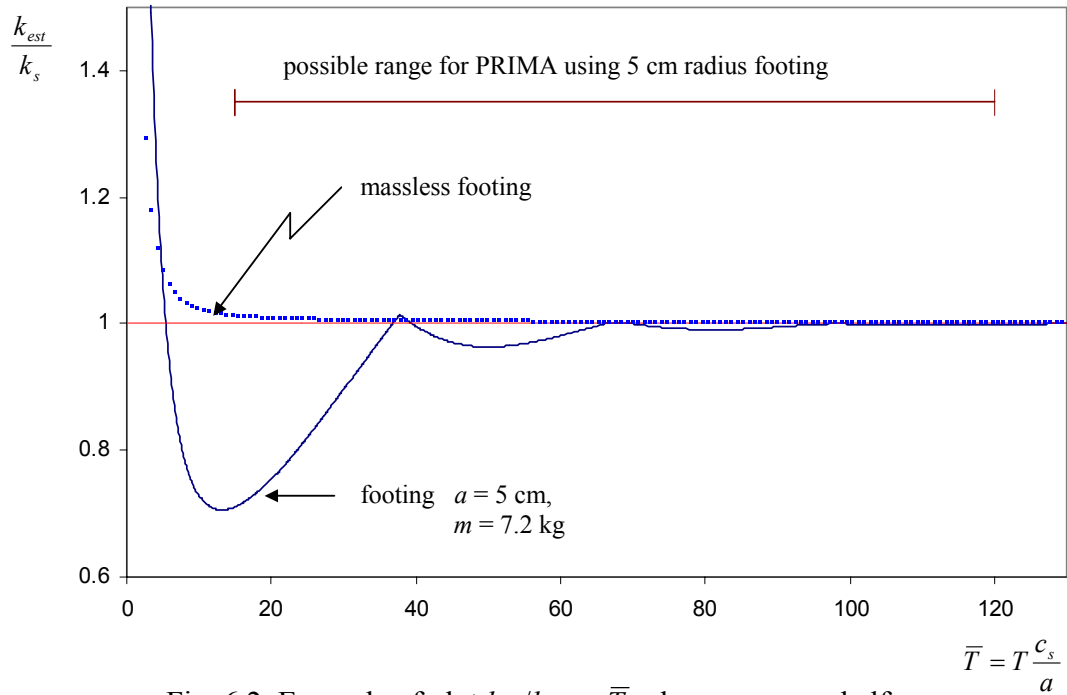


Fig. 6.2. Example of plot k_{est}/k_s vs. \bar{T} - homogeneous half-space

Fig. 6.2 presents only two curves. The first one corresponds to a massless footing and constitutes a theoretical limit as the mass decreases for a given footing ratio. One may note that this curve is independent of a , c_s and ρ . The second curve simulates the condition associated with a test using PRIMA device with the smallest loading plate (10 cm diameter). In this case the actual mass of the PRIMA footing (loading plate plus housing) is $m = 7.2$ kg. This configuration of PRIMA is the one that yields the greatest mismatch between k_{est} and k_s . For larger plates, and using the corresponding true footing mass, the curves tend toward the massless case curve. Computations showed that, for a

given plate diameter, the results for k_{est}/k_s vs. \bar{T} were independent of the shear wave speed c_s . Indeed, one can introduce an additional parameter, the mass ratio \bar{M} , defined as

$$\bar{M} = \frac{\rho a^3}{m} \quad (66)$$

In diagrams such as Fig. 6.2, \bar{M} can be used as a unique variable from which all the curves k_{est}/k_s vs. \bar{T} can be constructed. Possible field conditions are described with the following parameters: (i) for the half-space, c_s ranges from 50 m/s to 300 m/s, Poisson's ratio and mass density are assumed constants and (ii) for PRIMA device, the 10 cm diameter plate is prescribed and T ranges between 15 ms and 20 ms. Using these values, the range for \bar{T} covering most possible in-situ conditions is reported on Fig. 6.2 to describe the effect of the peak method on the results for the half-space model for realistic conditions.

It can be seen from Fig. 6.2 that the peak method also can lead to systematic errors when applied to a homogeneous half-space model. For the chosen example (10 cm footing diameter), the use of the peak method tends to overestimate the stiffness associated with very soft soils (low \bar{T}) and to underestimate the stiffness corresponding to soft to stiff soils (moderate values of \bar{T}). The ratio k_{est}/k_s tends towards unity only for very high values of \bar{T} . A similar trend, yet less accentuated, is observed for other footing diameters (i.e 20 cm and 30 cm). One may recognize that this trend is similar to the one observed in Fig. 4.8 in the case of the SDOF system (diagram k_{est}/k_s vs. T/T_n). In both cases there is no one-to-one relation between the error k_{est}/k_s and the support properties. As a result, the peak method cannot be used to produce an accurate index parameter. Therefore, for field-testing, using stiffness estimates from the peak method as index values could yield inaccurate interpretations.

6.1.2 Layered half-space

The half-space model rarely accurately describes in-situ profiles. However, the non-consistency of the peak method shown in the case of homogeneous half-space can be generalized to other situations. Indeed, it is known that the use of a static backcalculation from FWD measurements associated with the peak method can yield significant errors, especially in the case of a shallow stiff layer, as shown in Roesset and Shao [32]. It is further shown in Guzina and Osburn [7] that using a consistent data interpretation method, based upon zero frequency components, rather than the peak method, improves the consistency of the static backcalculation.

As a crude generalization, one could see that the accuracy of the peak method depends on the particular but *unknown in-situ profile* being investigated during routine testing. This fact has important implications since it means that 1) the peak method should not be used for estimation of the value of footing-on-soil stiffness without additional information on the in-situ profile, and 2) this method should not be used even for relative comparisons concerning unknowns soil profiles.

6.2 Proposal for PRIMA field-testing enhancements

Based upon the conclusions related to the data interpretation method, and the physical setup modifications of the PRIMA device discussed earlier, the use of PFWD PRIMA device could be enhanced for field-testing purposes associated with the conventional static backcalculation procedure. This section briefly explores the possibility of such enhancements. Development of an entire design for an enhanced method using PRIMA device would require a specific study. However, in summary, the proposed method would involve:

1. using the concepts of FFT, FRF, spectral average, and zero-frequency estimates,
2. defining an adequate theoretical FRF (e.g. footing-on-a-layered-half-space model),
3. utilizing the enhanced PRIMA setup,
4. adapting appropriate data acquisition system and associated software to measure experimental FRF functions using the entire force and velocity time histories from PRIMA,
5. developing programs for fitting the measured FFT with the chosen theoretical FFT and extracting the static stiffness.

6.2.1 Backcalculation analysis

The PFWD backcalculation analysis, as performed in practice, is based upon the use of the static stiffness as input to an elastostatic model to estimate the soil's Young modulus E . The key point is that the estimation of the static stiffness from the measurements should not be based upon peak force and displacement values but rather should use a consistent approach utilizing FFT, FRF, zero frequency components of dynamic stiffness and spectral averaging. In the case of the BVT, a SDOF system was used as theoretical model for the beam to extract the static components from the measured data. In the case of field measurements, the consistent method presented for the BVT can also be applied, provided that an appropriate half-space model is chosen to guide the extrapolation of measured data towards zero frequency.

For example, whenever an in-situ profile can be approximated as a homogeneous elastic half-space, the FRF $C_{vv}(\omega)$ presented in Section 2.6 can be used as reference model for fitting the experimental $C(\omega)$. Such method successfully was used by Pak and Guzina [12] in an experimental work using scaled models on a geotechnical centrifuge. This would constitute the basis of an improved data interpretation, using the same techniques as the laboratory beam verification. In other cases, such as the layered elastic half-space, the analysis would have to be performed using appropriate FRFs. For all cases, the measured and theoretical FRFs should be used in the fitting process to extract the true static footing-on- support stiffness. Note that the choice of the FRF to use is not limited to the compliance $C(\omega)$; other FRFs, such as the dynamic stiffness $K(\omega)$ can be

utilized. Also, the coherence function can be used as an index of the usable frequency range.

Note that the suggested analysis is based upon the force signal as measured by the load cell. However, due to inertial force of the deflectometer device, the true force transmitted to the soil is different from the force measured by the load cell. This issue does not affect the estimation of the static stiffness $k_s = K(\omega = 0)$ theoretically (zero acceleration and thus zero inertial force) but would affect the selected extrapolation procedure used to estimate the static stiffness from the measured dynamic stiffness. Indeed, the footing mass is embedded in the models chosen to guide the extrapolation of the measured data towards zero frequency (the output of the motion sensors cannot be used at very low frequency). For illustration purposes, let us examine how the effects of the footing mass were taken into account in this study. Concerning BVT testing, PRIMA mass was incorporated in the equivalent mass of the SDOF analog, which was estimated as a fitted parameter. In the theoretical example presented in Fig. 6.2, the prescribed force was applied on the top of PRIMA device, and the mass of the latter was taken into account in equation (63).

6.2.2 Hardware

a) PRIMA setup

With regards to the comments raised for the physical setup of PRIMA device in Section 3.4, it seems preferable, for quality assurance purposes, to use the enhanced configuration of the PRIMA device.

As a remainder, the so-called enhanced configuration is composed of the base of PRIMA only, and the load is applied using a rubber hammer. Using such a dynamic loading, not only the energy imparted to the soil is minimized, but also the dominant frequency of the force spectrum is increased, that is, a smaller force wavelength is produced. Such configuration therefore minimizes both the applied stress and the depth of penetration, resulting in small-strain estimates of the in-situ stiffness, which can be used to obtain an estimate for the in-situ equivalent homogeneous seismic elastic modulus. Dealing with such small-strain modulus, as discussed in Section 2.1, would be advantageous for both construction quality assurance and deterioration assessment applications. The shallower depth of penetration associated with the enhanced setup is appreciable in quality assurance of pavement construction where the modulus of the tested layer (e.g. base) needs to be checked only.

b) Data acquisition system

To perform a consistent analysis of the measured force and deflection data, non-truncated time histories need to be recorded. Furthermore, in PRIMA data acquisition system, the velocity automatically is integrated to yield the deflection time history. The integration process, however, is generally observed in practice to yield increasing inaccuracies (distorted displacement time histories) as the time record increases. Therefore, it is recommended that the velocity output of the PRIMA geophone be recorded.

The equipment used for data acquisition in the laboratory is not practical for field-testing. The consequence is that new pieces of hardware, more adapted to a daily utilization in the field, have to be found to perform data acquisition and FFT, to allow for spectral average and FRF estimate. The experimental setup for field-testing could resemble the one sketched in Fig. 6.3.

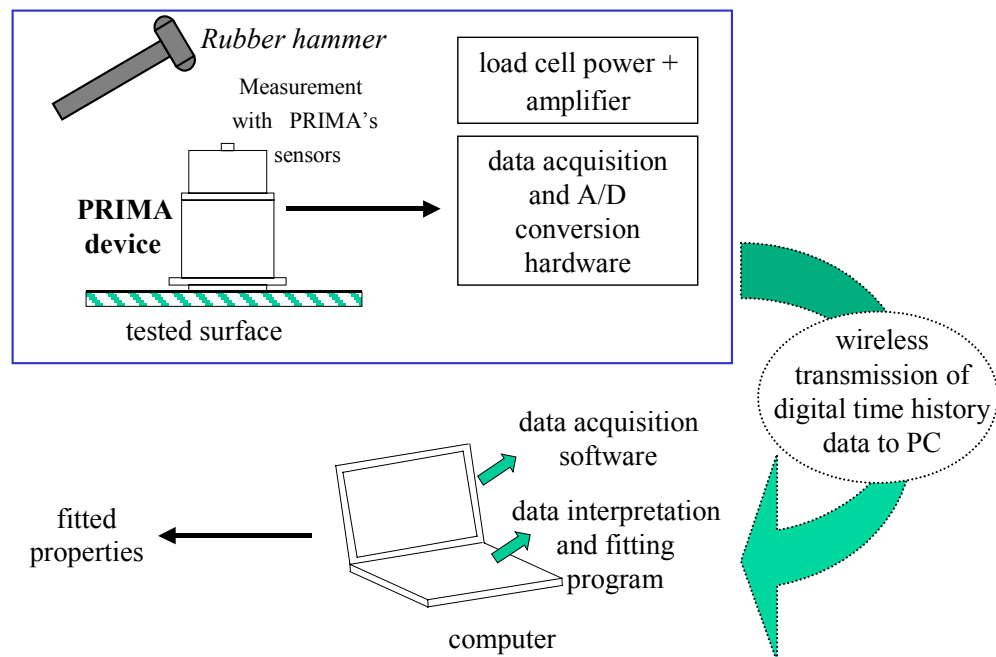


Fig. 6.3. Possible field-testing setup for PRIMA device

The exact definition of the necessary hardware would require a specific study. However, general ideas can be presented. For example, the use of an A/D converter and FFT card that can be directly inserted in a laptop would be advantageous. An external power source/amplifier for the load cell would also be needed.

To ensure a small force compatible with the linear system assumption embedded in the data analysis, the data acquisition system needs to include an automatic limitation of the force level. For example, the system could record the data only for force levels below a predefined threshold value.

Together with the field-adjusted data acquisition system, suitable pieces of software or programs would need to be developed to monitor data interpretation, spectral averaging, and FRF estimation.

CHAPTER 7 - CONCLUSIONS

The study's main purpose was to design and develop a laboratory tool for verification of the performance of PFWD devices used for quality assurance purposes in pavement construction. This study also aimed to examine possibilities to enhance the performance (physical setup and data interpretation) of existing PFWD devices.

A particular PFWD device, PRIMA 100, was chosen as example and an associated verification testing setup was proposed. The verification test for the PRIMA device is based upon the Beam Verification Tester (BVT) apparatus, which is a simply supported beam assembly. The BVT apparatus has been developed at the University of Minnesota for the Minnesota Department of Transportation (Mn/DOT). This apparatus is intended for verifying the performance of PRIMA 100 devices. Using the BVT associated with the spectral analysis presented in the report, tests also can be conducted to check whether the calibration factors of the sensors of PRIMA devices, as given by the manufacturer, are accurate. The objective of the verification tests is to detect the potential occurrence of deterioration of the sensor's accuracy during the life of the field-testing device.

For the featured PRIMA device, the calibration of the internal force and velocity sensors proved to be satisfactory. However, it was demonstrated that the data interpretation method embedded in the device, based upon peak values, introduces significant systematic errors, in terms of the estimated support stiffness, both in the case of BVT and field testing.

To obtain consistent results from the device during verification testing on the BVT, an alternative data interpretation scheme was used. Based upon an enhanced device setup and spectral analysis of dynamic signals, it was shown that the static stiffness of the beam modeled as a SDOF system could be accurately recovered experimentally, for appropriate span length, of both undamped and damped beams. As a result, the BVT apparatus is proposed as a routine tool to check the performance of PRIMA devices. Also, extension of the BVT use to other devices is discussed. Finally, a basis for the enhancement of PRIMA device in field-testing situations is proposed. Enhancements are based upon the same consistent data interpretation method than the ones used for the BVT.

The key conclusions and recommendations stemming from this research are:

1. PFWD devices such as PRIMA deflectometer constitute an effective and reliable tool for load and deflection measurements. It appears, however, that the traditional data interpretation scheme, so-called peak method, used to estimate the static footing-on-soil stiffness from these measurements, is capable of producing systematic errors and therefore needs to be replaced.
2. In this study, the original data interpretation, based upon peak values, was replaced by a consistent dynamic method in order to estimate the static footing-on-support stiffness using the reaction support offered by the BVT apparatus. The modified data interpretation is based upon spectral analysis

and relies on a SDOF analog as theoretical guide. In addition to this first modification, the physical setup of the device itself is also replaced with a simplified, yet enhanced, setup that enables testing with small impact energy. The BVT apparatus proves to be a potentially useful tool for routine verification of the performance of PRIMA 100 devices.

3. Furthermore, similar enhancements of PRIMA device for field-testing situations can be investigated. In that case, the spectral-based data interpretation should incorporate an adequate theoretical model (such as the footing-on-a-layered-half-space model, and replace the SDOF analog used for the beam).
4. For quality assurance purposes, field in which stiffness estimation focuses on the top layer of pavement profiles, the enhanced physical setup presented in this study is recommended. In addition to the advantage of offering a shallower depth of investigation (compared to that associated with the original falling weight setup), the use of the enhanced setup aims toward the estimation of the seismic modulus, comparable to that stemming from geophysics investigation methods.

This research focused on a laboratory assessment of the performance of PRIMA 100 device. Applications to field-testing for this device, as well as extension to other portable deflectometer devices could only be touched on briefly. Specific complementary studies to address these issues would be necessary to optimize the use of deflectometer devices. Further investigations could encompass the following propositions:

1. The BVT apparatus could be adapted on a case-by-case basis to other devices for performance assessment.
2. Further studies are necessary to develop the data analysis techniques, as well as the necessary hardware and software adaptations, required for the consistent and enhanced field operation of PRIMA 100 and similar PFWD tools.
3. The traditional data interpretation (i.e. the peak-based method) can produce systematic errors. Nevertheless, it presents the advantage to be simple and robust. A field-testing study should be conducted in order to examine the performance of the proposed enhancements in field conditions.
4. There is a need to investigate the relations between seismic modulus, obtained from field-testing, and resilient modulus, used in pavement design. On-going laboratory research at the University of Minnesota aims to examine correlations between resilient modulus and small strain modulus.

REFERENCES

- [1] “Resilient Modulus of Unbound Granular Base/Subbase Materials and Subgrade Soils,” *Long-Term Pavement Performance (LTPP)*, Protocol P46, U.S. Department of Transportation, Federal Highway Administration, Virginia, 1996.
- [2] Lytton, Robert L., “Backcalculation of Layer Moduli – State of the Art,” *Nondestructive Testing of Pavements and Backcalculation of Moduli, ASTM STP 1026*, A.J. Bush III and G. Y. Baladi, Eds., American Society for Testing and Materials, Philadelphia, pp. 7-38, 1989.
- [3] Chen, Dar-Hao, Bilyeu, John, and He Rong, “Comparison of Resilient Modulus between Field and Laboratory Testing: A Case Study,” *Proceedings of the 78th Annual Meeting of Transportation Research Board Annual Meeting*, 25 pp., January 10th-14th, Washington, D.C, 1999.
- [4] Siekmeier, John A., Young, D., and Beberg, D., 1999, “Comparison of the Dynamic Cone Penetrometer with Other Tests During Subgrade and Granular Base Characterization in Minnesota,” *Nondestructive Testing of Pavements and Backcalculation of Moduli: Third Volume, ASTM STP 1375*, S. D. Tayabji and E. O. Lukanen, Eds., American Society for Testing and Materials, West, Conshohocken, Pennsylvania., 1999.
- [5] McKane, Ryan, “In Situ Field Testing of Mechanical Properties,” University of Minnesota, *48th Annual Geotechnical Engineering Conference Young Engineer Paper Competition*, Feb. 18, 2000.
- [6] Van Gurp, Christ, Groenendijk, Jacob, and Beuving, Egbert, “Experience with Various Types of Foundation Tests,” *Fifth International Symposium on Unbound Aggregates in Roads (UNBAR5)*, 21st-23rd June 2000, Nottingham, United Kingdom, 2000.
- [7] Guzina Bojan B. and Osburn, Robert H., “An Effective Tool for Enhancing the Elastostatic Pavement Diagnosis,” *Transportation Research Record 1806*, pp. 30-38, 2002.
- [8] Lepert, Ph., Simonin J.M., and Meignen, D., “An Alternative Approach to Bearing Capacity: Impulse Dynamic Investigation,” *Proceedings of the Fourth International conference on the Bearing Capacity of Roads and Airfields*, Vol. 1, July 17th – 21st Minneapolis, MN, 1994.
- [9] Stolle, Dieter F.E. and Peiravian Farideddin, “Falling Weight Deflectometer Data Interpretation Using Dynamic Impedance,” *Canadian Journal of Civil Engineering*, Vol. 23, Issue 1, 1996.

- [10] Briaud, Jean-Louis and Lepert, Philippe, “*WAK Test to Find Spread Footing Stiffness*,” *Journal of Geotechnical Engineering*, ASCE, Vol. 116 (3), p. 274-286, 1990.
- [11] Hardin, Bobby O. and Drnevich, Vincent P., “*Shear Modulus and Damping in Soils: Design Equations and Curves*,” *Journal of Soil Mechanics and Foundation Division*, ASCE, Vol. 98 (SM7), p. 667-693, 1972.
- [12] Pak, Ronald Y.S. and Guzina, Bojan B., “*Dynamic Characterization of Vertically Loaded Foundations on Granular Soils*,” *Journal of Geotechnical Engineering*, ASCE, Vol. 121 (3), p. 274-286, 1995.
- [13] Kramer, Steven L., *Geotechnical Earthquake Engineering*, Prentice-Hall Inc, New Jersey, 1996.
- [14] Richart, F. E., Jr., Hall, J. R., Jr., and Woods, R. D., *Vibration of Soils and Foundations*, Prentice-Hall, Inc, New Jersey, 1970.
- [15] Seed, Bolton H., Wong, Robert T., Idriss, I. M. and Tokimatsu, K., “*Moduli and Damping Factors for Dynamic Analyses of Cohesionless Soils*,” *Journal of Geotechnical Engineering*, ASCE, Vol. 112 (11), pp. 1016-1032, 1986.
- [16] Sokolnikoff, Ivan S., *Mathematical theory of elasticity*, Second Edition, McGraw-Hill Book Company, Inc, York, Pennsylvania, 1956.
- [17] Craig, R. F., *Soil Mechanics*, Sixth Edition, E & FN Spon, an imprint of Chapman & Hall, London, United Kingdom, 1997.
- [18] Meirovitch, Leonard, *Fundamentals of Vibrations*, Third Edition, McGraw-Hill Companies, Inc., New York, 2001.
- [19] Inman, Daniel J., *Engineering Vibration*, Second Edition, Cyril M. Harris Editor, Prentice Hall, Inc., Upper Saddle River, New Jersey 07458, 2001.
- [20] Wilson, Edward L. and Clough, Ray W., “*Dynamic Response by Step-by-Step Matrix Analysis*,” *Symposium on the Use of Computers in Civil Engineering*, Laboratorie Nacional de Engenharia Civil, Lisbon - Portugal, 1-5 October, 1962, pp. 45.1 - 45.14.
- [21] Bendat, Julius S. and Piersol, Allan G., *Random data analysis and measurement procedures*, Third Edition, *Wiley series in probability and statistics*, John Wiley & sons, Inc., 2000.
- [22] “*Estimating Transfer Functions with SigLab*,” Application Note, DSP Technology Inc., available at <http://www.dspt.com/sig/slap5.pdf>, 1996.
- [23] Luco, Juan E. and Westmann, Russell A., “*Dynamic response of circular footings*,” *Journal of the Engineering Mechanics Division*, ASCE, Vol. 97, pp. 1381-1395, 1971.

- [24] Pak, Ronald Y.S. and Gobert, Alain T., “*Forced Vertical Vibration of Rigid Discs with Arbitrary Embedment,*” *Journal of the Engineering Mechanics Division*, ASCE, Vol. 117 (11), pp. 2527-2548, 1991.
- [25] Clemen, Rene, “*Guidelines for Calibration of Falling Weight Deflectometers,*” Carl Bro Pavement Consultants, Denmark, available at <http://www.pavement-consultants.com/pdf/trondheim.pdf>.
- [26] Lardner, Thomas J. and Archer, Robert R., *Mechanics of Solids, an Introduction*, Third Edition, Cyril M. Harris Editor, McGraw Hill, Inc., New York, 1994.
- [27] Dally, James W. and Riley, William F., *Experimental Stress Analysis*, Third Edition, Cyril M. Harris Editor, McGraw-Hill, 1991.
- [28] “*Errors Due to Misalignment of Strain Gages,*” Technical Note, TN-511, Measurements Group Inc., Raleigh, NC, also available at http://www.vishay.com/brands/measurements_group, 1983.
- [29] Stokey, William F., “*Vibration of System having Distributed Mass and Elasticity,*” *Shock and Vibration Handbook*, Third Edition, Cyril M. Harris Editor, McGraw-Hill Book Company, pp. 7-1 – 7-43, 1988.
- [30] Kármán, Theodore von and Biot, Maurice A., *Mathematical Methods in Engineering*, First Edition, McGraw Hill Book Company, Inc., New York, 1940.
- [31] Reed, Everett F., “*Dynamic Vibration Absorbers and Auxiliary Mass Dampers,*” *Shock and Vibration Handbook*, Third Edition, Cyril M. Harris Editor, McGraw-Hill Book Company, pp. 6-1 – 6-37, 1988.
- [32] Roesset, Jose M. and Shao, Ko-Young, “*Dynamic Interpretation of Dynaflect and Falling Weight Deflectometer Tests,*” *Transportation Research Record* 1022, pp. 7-15, 1985.

Appendix A:

User's Manual for the Beam Verification Tester (BVT)

-

**Technical information and experimental procedure for
PRIMA device verification testing**

Appendix A:

User's Manual for the Beam Verification Tester (BVT)

-

**Technical information and experimental procedure for
PRIMA device verification testing**

This user's manual is an appendix of the report "Enhancements and Verification Tests for Portable Deflectometers" and should be used only in conjunction with this report.

The Beam Verification Tester (BVT) apparatus has been developed at the University of Minnesota for the Minnesota Department of Transportation (Mn/DOT). This apparatus is intended for verifying the performance of Portable Falling Weight Deflectometer (PFWD) PRIMA 100 devices. Using the BVT associated with the spectral analysis presented in the report, tests can also be conducted to check whether the calibration factors of the sensors of PRIMA devices, as given by the manufacturer, are accurate or not. The objective of the verification tests is to detect the potential occurrence of deterioration of the sensor's accuracy during the life of the field-testing device.

This user's manual presents the apparatus, as delivered to Mn/DOT, the necessary complementary equipment references, and the procedure to follow for routine testing of PRIMA devices.

A 1 - DESCRIPTION OF THE BVT APPARATUS ELEMENTS

A 1.1 Listing of the elements delivered

The PRIMA deflectometer verification tester apparatus is delivered to Mn/DOT with:

- one PRIMA 100 device, with a unique central geophone, two additional 20 cm diameter plates and two cable assemblies (this device is the one being used for the study),
- one manufacturer installation software (PRIMA 100 software 2001) on CD,
- one verification steel beam (dimensions: 4" x 5/8" x approximately 93 cm),
- one support steel beam, machined to receive the supports of the verification steel beam at several spans,
- two supports for the verification beam (each comporting a rectangular steel mounting, a hardened steel rod, and two adjustable clamps),
- one receptacle for PRIMA device with its two supports (each comporting a hardened steel rod, and two adjustable clamps) and two adjustable clamps on the top surface to secure the deflectometer device; the receptacle is equipped with four screw to center PRIMA device,
- a removable annulus to ameliorate the seating of PRIMA device on the receptacle,
- two removable damping device assemblies,
- one external geophone fixed on the top of the receptacle with its cable assembly, operating manual and calibration certificate. The geophone mounted on the BVT is an IMI Sensors (a PCB Piezotronic div.) industrial ICP[®] accelerometer model VO622A01, where VO stands for Velocity Output. The sensitivity of the sensor delivered with the BVT, as given by the manufacturer, is 3854 mV/m/s at 100 Hz,
- all necessary screws to assemble the various elements and rubber buffer pieces to ameliorate the quality of the contact between clamps and steel structures,

- cable assemblies necessary to connect sensors and data acquisition system (2 special cable assemblies plus two BNC cable assemblies),
- one rubber hammer with additional rubber tip,
- one software package comprising:
 - the programs necessary to perform the consistent data interpretation presented in the report and obtain an estimate of the stiffness of the beam, and to compare the output from PRIMA geophone, using PRIMA software, and the output of the external IMI geophone, independently acquired,
 - the reference SigLab files for the beam stiffness estimation application and for the acquisition of the external IMI geophone time history alone,
 - some examples of measured data files.

The programs are written in Matlab, and the reference files are SigLab “.vna” files.

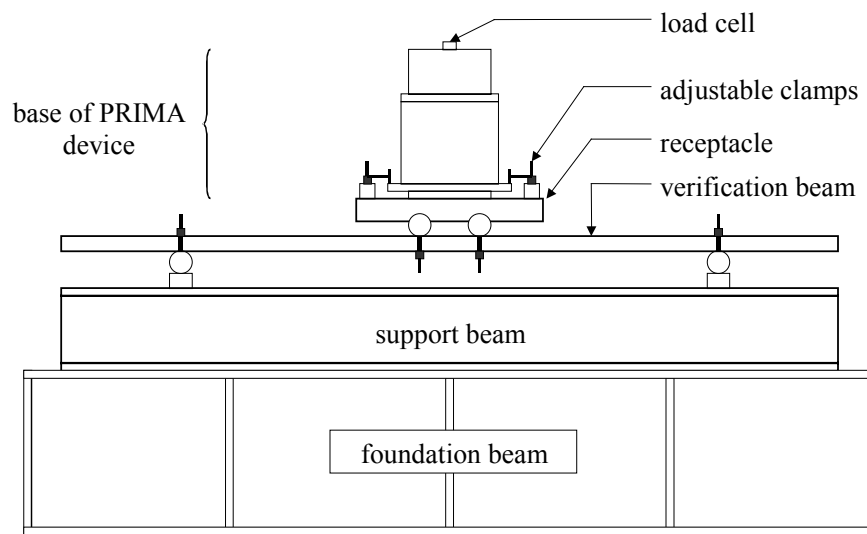


Fig. A.1.1. Sketch of the verification setup

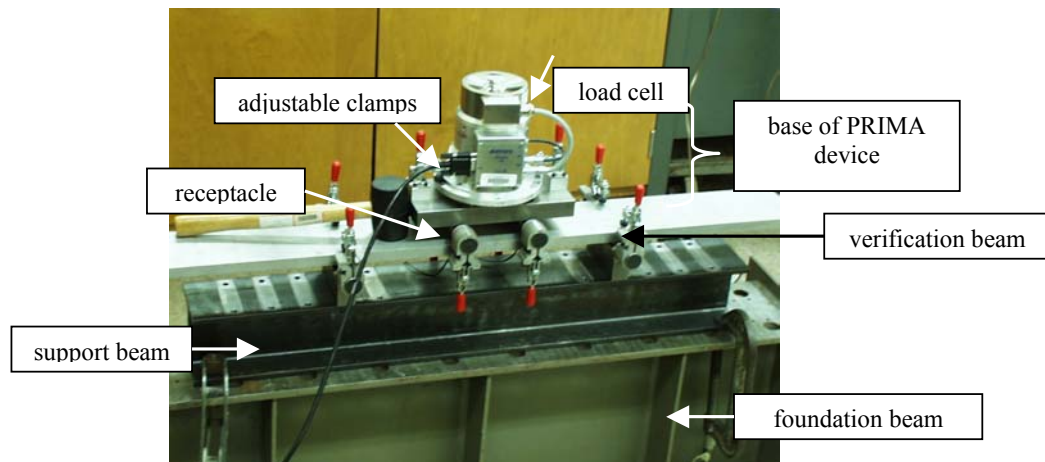


Fig. A.1.2. Verification setup



Fig. A.1.3. Testing setup for the BVT with damping devices

For the sake of clarity, the reader will find displayed on the previous page and above some figures (Fig A.1.1, Fig A.1.2 and A.1.3) borrowed from the body of the report. It will be easier for the reader to identify the elements detailed in this users guide.

A 1.2 Additional elements needed

A 1.2.1 Foundation of the BVT

The BVT is delivered with its machined support beam, but without the foundation beam used for the evaluation testing (comparable to a ‘W12x35’ type steel beam, 39” long, 6.5”wide and 12.5”deep). The support beam needs to be fixed onto a rigid foundation. We recommend fixing the apparatus either to a heavy beam (steel or better, concrete) as shown in Fig A.1.1 and A.1.2, either directly to the testing facilities concrete slab. A good coupling between the BVT apparatus and its foundation is necessary.

A 1.2.2 Data acquisition hardware

Most parts of the acquisition system are not delivered with the BVT and will therefore need to be obtained separately. These parts were not purchased as part of the Mn/DOT contract.

The necessary hardware to be used with the BVT to acquire the data from PRIMA device is as follows:

- a laptop computer (desktop possible with special adaptations) under Windows system,
- a second computer (optional, as explained next page)
- an analog/digital (A/D) converter and spectrum analyzer: two-channels DSPT SigLab unit model 50-21. This model is a 50 kHz bandwidth analyzer. Other SigLab models, featuring a 20 kHz bandwidth, could also be suitable (Model 20-22 for 2 channels and Model 20-42 for 4 channels),
- an Adaptec SCSI card to connect the SigLab analyzer to the laptop,

- a conditioner/power supply for the ICP geophone: PCB Line Powered Signal Conditioner Model 482A22,
- a signal conditioner/ amplifier for PRIMA's load cell: 2-channels Vishay Measurements group strain gage conditioner model 2120 coupled with a model 2110A power supply, together with the appropriate housing.

The particular brands and models given above are the ones used for this study. The user is free to choose alternative hardware. Nevertheless, the program associated with this study, as well as the procedures described in this guide apply only to the referenced material. The precise model for the SCSI card will depend on the exact model of SigLab analyzer, the type of computer, and the operating system installed on the computer. Please contact SigLab for the exact card specifications.

For this verification study two SigLab model 50-21 units were used, offering a total of four channels. However, for routine testing, a unique two-channel unit is sufficient. As a result, this users guide will focus on procedures using a two-channel unit, and the data interpretation programs delivered with the BVT assume a two-channels unit.

The tests realized for the study were conducted using two computers:

- a desktop to acquire data directly from PRIMA device, as intended by the manufacturer (PRIMA's sensors connected to PRIMA's electronics and to the computer using PRIMA's software),
- a laptop to monitor measurements from the independent data acquisition system. The particular laptop used did not have the connections necessary to plug the manufacturer's PRIMA cable assembly.

For routine testing, the use of a unique computer would be more convenient. However, this option could not have been tested during the research phase. The user will have to investigate the possibility to use a single computer to record simultaneously data from PRIMA device using the original configurations and data from an external geophone using the external data acquisition system. The data interpretation can be performed on any computer, provided that the delivered software package plus the test data files are correctly installed.

A 1.2.3 Specific software packages

The SigLab acquisition system needs to be used with the following software packages:

- SigLab software (normally delivered with the SigLab spectrum analyzer),
- Matlab[®] software.

In addition, Matlab[®] software is also used for the programs written for enhanced data interpretation.

A 1.3 Detail of the cable assemblies

Connections and cables used to connect the sensors to the data acquisition system are:

- IMI geophone to PCB power supply: 10' PCB cable with BNC termination, model 052AE010AC,
- PCB power supply to SigLab analyzer: usual BNC cable,
- PRIMA's geophone to SigLab analyzer: special cable with BNC connector at one end, and the 2 pins female LEMO connector ref. PHG.1B.302 at the other end. The BNC connects to the SigLab and the female LEMO plug to the geophone (via its male LEMO plug FGG.OB.302).
- PRIMA's load cell to the Vishay strain gage conditioner: the 6 pins female LEMO connector ref. PHG.1B.306 at one end, and a Vishay model 2120-A50 input plug. The LEMO plug connects to the load cell (via its LEMO plug FGG.1B.306) and the Vishay plug to the Vishay strain gage conditioner,
- Vishay strain gage conditioner to SigLab: usual BNC cable.

Particular care must be taken with the cable assemblies comporting the female LEMO plug and the Vishay connector. They have been assembled and wired especially for PRIMA device sensors plus associated output cable assemblies and the particular strain gage conditioner used for testing.

A 2 - GENERAL INSTALLATION PROCEDURES

A 2.1 BVT apparatus installation

A 2.1.1 Undamped beam

- fix the support beam on its foundation,
- screw the verification beam supports on the location corresponding to the span chosen for the test (50, 60 or 70 cm),
- clamp the verification beam on its supports, and clamp the receptacle on the verification beam. Proceed with caution to locate beam and receptacle at the exact required positions: the receptacle supports should be placed at 5 cm on each side of the mid-span of the beam; the beam should be centered on its supports,
- place the removable annulus in-between the four guiding screws located on the top surface of the receptacle.

Note that the BVT is designed for five different beam spans, ranging from 30 cm to 70 cm. However, we strongly recommend using only the two or three longer spans for verification testing purposes.

A 2.1.2 Damped beam

The additional damping should be used only for 60 cm and 70 cm spans. The installation of the (optional) damping devices is described here. However, it is recommended to run some tests with the undamped configuration prior to installing the damping devices. The damping devices must be added at the end of the cantilever parts of the beam, as shown in Figs A.1.3 and A.2.1.

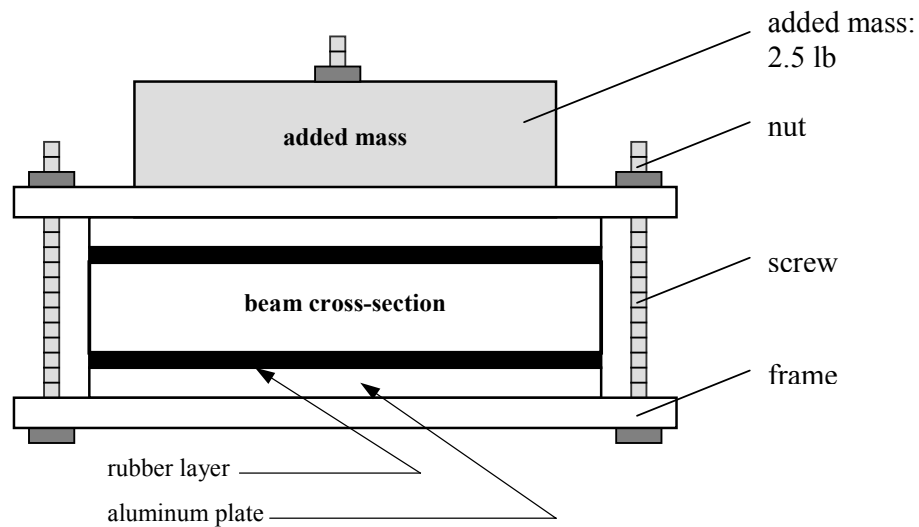


Fig. A.2.1. Layout of a damping device located at the end of a cantilever part of the beam

For each of the two damping devices, proceed as follows:

- assemble the frame (leave enough room to place beam + rubber layer + aluminum plates),
- position rubber layer and aluminum plates on each side of the beam,
- place the frame and adjust the nuts on the screws in order to clamp the assembly to the beam; the clamping force should be small, that is, the assembly should be loosely attached to the beam,
- assemble the screw for the added mass on the top of the frame, place the mass with a washer and a nut on the screw,
- the damping device is now attached to the beam and ready to be tuned.

The tuning of the damping devices is addressed in Chapter A7.

A 2.2 PRIMA installation

- utilize the enhanced (i.e. modified) setup: disassemble the PRIMA device in order to take the cap of the load cell off and utilize only the base,
- the selected plate diameter is the 10 cm diameter (no additional plate on the base). Remove any additional loading plate,
- set down the base of PRIMA device on the top of the removable annulus and secure the device with the two clamps of the receptacle.

A 2.3 Strain gage conditioner/amplifier

Make sure that the initial setup of the Vishay strain gage conditioner/ amplifier is adequate (refer to the conditioner users guide).

General testing routine overview:

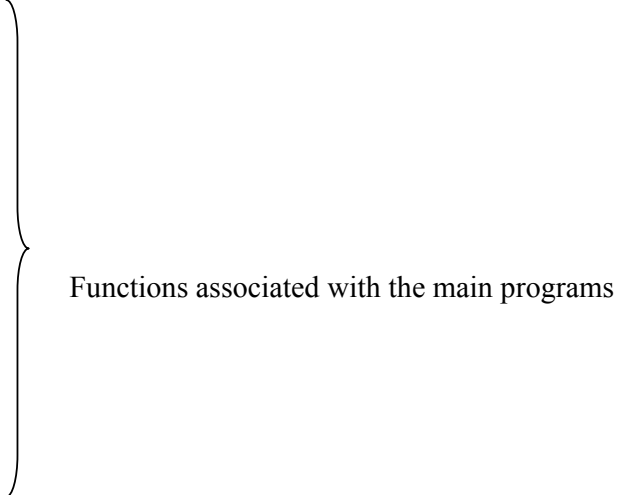
- turn on the conditioner a few minutes before testing,
- verify that the sensor is plugged in and that the output cable is connected to the data acquisition system,
- turn on the *excitation* on the channel being used,
- adjust bridge *excitation* and *gain* to the desired level, and adjust the *amplifier zero*,
- turn on the *excitation* on the channel being used and adjust the *balance*,
- the conditioner is ready for measurements.

A 2.4 Data acquisition hardware starting sequence

- check the connections between all the elements of the data acquisition system,
- plug on power cables of laptop, SigLab analyzer and conditioners,
- check the settings on the conditioners,
- plug the SCSI card in the laptop,
- connect the SCSI card and turn the SigLab analyzer on,
- once the SCSI card is inserted and the SigLab turned on, start the laptop,
- connect sensors and cables,
- turn on the conditioners.

A 2.5 Software packages installation

Concerning SigLab and Matlab software packages, please refer to the manufacturers recommendations. A data analysis software package is provided with the BVT apparatus. The programs have been written to search for files in specific locations, so we recommend that the installation instructions be followed. All the programs are regrouped in the folder “*BVT*”. This folder should be copied directly under the C hard drive of the computer. Under “*C:/BVT*” the user should find the following folders and files:

- **Matlab_programs** : comports the specific program package for data analysis
 - BVTmobility.m : main program for stiffness comparison
 - PrimaCompGeo.m : main program for velocity comparison
 - arondi.m
 - average.m
 - fitBVTmobility.m
 - getPrimaFileFunction.m
 - IMIvel_adjust.m
 - input_test_number.m
 - input_test_yes_no.m
 - shift_time_PRIMA.m
 - offsetcorrectionIMI.m
 - offsetcorrectionPrima.m
 - offsetcorrectionLoopIMI.m
 - offsetcorrectionLoopPrima.m

Functions associated with the main programs
- **SigLab_reference_files**
 - BVTgeophoneref.vna
 - BVTmobilityref.vna
- **Measurements**
 - PRIMA_files
 - Examples : subfolder with two examples
 - g70Example.crv,
 - g70Example.pkv
 - SigLab files
 - Examples : subfolder with three examples
 - 50mobilityExample.vna
 - 70mobilityExample.vna
 - g70Example.vna

Note that the examples in “*C:\BVT\Measurements\PRIMA_files\Examples*” have also been copied directly under the sub-directory “*C:\BVT\Measurements\PRIMA_files*” to enable the user to use these files with the program “*PrimaCompGeo.m*”. The special location where the data files should be recorded, as well as the requirements on their name, will be addressed in subsequent sections.

In order to be able to run the data analysis programs, the user will have to specify to Matlab[®] software their exact location. To do so, under the File menu of Matlab[®] software, select *Set Path*. In the *Set Path* window, select *Add with subfolders* and choose the entire “*C:\BVT*” folder. Save the changes and close the window. As a result, the “*C:\BVT*” folder is located at the top of the Matlab[®] software folder listing.

The program included in the package has been written to simplify as much as possible routine measurements and analysis. The major drawback with simplified programs is that they do not allow for much flexibility. Modifications of the programs or development of more sophisticated codes could be useful for an eventual future advanced use.

A 3 - PRELIMINARY CONSIDERATIONS

A 3.1 PRIMA’s sensors calibration factor

For the PRIMA device tested for this study, the calibration factors obtained from the manufacturer were

- load cell: 2 mV/V for 20 kN,
- geophone: 28.8 V/m/s.

Since the sensors will not be used in conjunction with PRIMA’s software and calibration parameters associated with PRIMA’s electronics, these calibration factors may need to be modified. The calibration parameters embedded in PRIMA software cannot be accessed, but they are thought to be accurate and are not susceptible to variations. Therefore, the accuracy of the sensors alone will have to be independently verified.

In the case of the geophone, which will be directly connected to the SigLab analyzer, the value of 28.8 V/m/s can be kept as is.

In the case of the load cell, however, a new calibration factor has to be derived. The load cell signal is conditioned and amplified using the Vishay device and the calibration factor needs to be correspondingly adjusted. For the research study, the Vishay strain gage conditioner was used with a bridge excitation of 10 V and a gain of 2000. Using this setup, the theoretical calibration value for the load cell is therefore 2 V/kN or 0.5 kN/V.

These calibration factors are the ones that will be verified using the BVT.

A 3.2 Applying the force to PRIMA device

With reference to the enhanced configuration of the device, the force is applied by using the rubber hammer. The operator should always impact the top of the load cell with the rubber tip added to the hammer, since it provides an impact that minimizes the “ringing” of the entire BVT plus PRIMA assembly. The force of the shock does not have to be very high. As a guideline, if the impact is too strong, the entire apparatus will produce audible high frequencies. Note that such sounds can also be an indicator of insufficient clamping of the various components of the BVT apparatus. A strong impact might also exceed the capability of the data acquisition system and produce an overload in SigLab. The impact must however be strong enough to trigger the data acquisition system. Also, it is important to impact the center of the load cell as precisely as possible, and to provide a force as vertical as possible, in order to avoid any non-symmetrical effect. Such effects are detrimental to the accuracy and precision (repeatability) of the analysis, which assumes a vertical mode only. The operator will most likely develop an intuitive understanding of the adequate way to impact the beam with experience.

A 3.3 Expected accuracy

The accuracy of the results depends upon both the accuracy of the sensors and the characteristics of the data acquisition system. Let us examine some guidelines to estimate an expected maximum accuracy for the results.

Using PRIMA device or the independent data acquisition setup with the appropriate settings, the resolution of the data acquisition system is not an issue.

The specifications of the sensors for PRIMA device, as given by the manufacturer, are:

- Load cell:
 - frequency range: 0 - 400 Hz,
 - accuracy: $\pm 1\%$,
 - resolution: 0.01 kN.
- Geophone
 - max. displacement: 2200 μm ,
 - frequency range: 0.2 - 300 Hz,
 - accuracy: better than $\pm 2\%$,
 - resolution: 1 μm .

The load cell is a HBM Force transducer (model C2 AD1/2t) with a nominal force of 2 kN. It is guaranteed by HBM with an accuracy class of 0.1 % and a resolution of 0.1 % of full scale or 1000 divisions or 20 N. These specifications are conservative because guaranteed. Measurements using the setup in Section A3.1 showed an output accuracy better than 10 N.

In the general case, the accuracy of the measurements cannot be better than the resolution of the less accurate sensor, i.e. the geophone with an accuracy of 2 %. As a result, the results from the tests should not reasonably be expected with accuracy better than 2 - 3 %.

A 4 - BEAM STATIC STIFFNESS VERIFICATION: BVT

MOBILITY TEST

In this test the measured static stiffness k_{est} of the beam is verified against its known true value k_s . The stiffness k_{est} is estimated from the measured mobility from PRIMA's sensors output (recorded using the independent data acquisition system) and using the consistent data interpretation embedded in the data analysis software provided with the BVT apparatus.

A 4.1 Experimental setup

This test involves the BVT apparatus, both PRIMA's sensors plus the independent data acquisition system. The additional IMI geophone and the manufacturer PRIMA's software are not needed. Set up the BVT apparatus and PRIMA device as specified in Section A2 - GENERAL INSTALLATION PROCEDURES. Disconnect the sensors from the PRIMA electronic box by disengaging the LEMO plugs, and connect the later to the special cable assemblies designed for this purpose.

Connections scheme (see FIG. A4.1):

- PRIMA geophone directly connected to a SigLab input,
- PRIMA load cell connected to an input of the Vishay strain gage conditioner; output of the conditioner connected to a SigLab input,
- IMI geophone connected to an input of the ICP signal conditioner; output of the conditioner connected to a SigLab input,
- SigLab output connected to the SCSI card inserted in the laptop.

Refer to Section A1 for the cable assembly type to use in each case. In the case of a two channel SigLab analyzer, only two sensors can be used simultaneously.

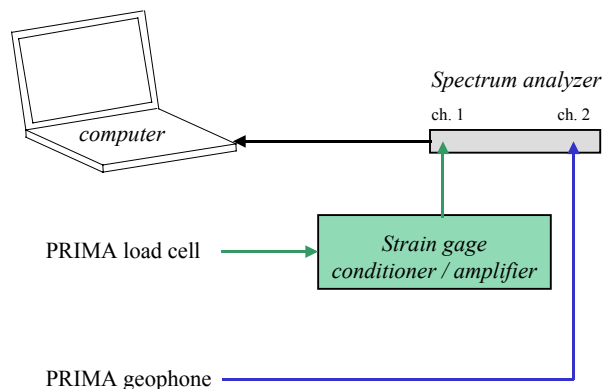


Fig. A4.1. BVT mobility test setup

A 4.2 Data acquisition

The program developed for routine beam stiffness estimation has been written for the channel arrangement presented in Table A 4.1:

SigLab channel number	1	2
PRIMA sensor	Load cell	Geophone

Table A 4.1. SigLab channels setup

Once the entire data acquisition hardware is connected and turned on, open the SigLab software and select the option “*vna*” under the Network menu (SigLab version 3.2). Once the SigLab reference *.vna* file is launched, the user can open the reference file provided with the BVT apparatus, file “*BVTmobilityref.vna*”.

Once the reference file is open, we recommend to promptly saving the file under a name chosen for the particular test sought. It is necessary to observe the same nomenclature convention than the one embedded into the data interpretation program. Following this approach, the name of the file should always starts with the number corresponding to the span of the beam in cm. For example, the name of a file corresponding to a 60 cm span beam could be “*60device2test5.vna*”, as opposed to “*70device2test5.vna*” for a test performed on a 70 cm span beam. Also, the file should be saved under the directory “*C:\BVT\Measurements\SigLab_files*”. The user is free to create subdirectories to organize the files.

Two plotting windows are displayed in the *.vna* file. The upper window will display the real part of the mobility function, whereas the lower one is a plot of the coherence function. The system is setup to average the results for a series of ten measurements, using an addition scheme. No overlap between measurements is allowed. The analysis window is “Boxcar”. Measurements with overload are disregarded. Each measurement is triggered using the geophone in channel 2, with a trigger value of + 9 %. The trigger value is set so that the software starts recording the data after the motion due to the shock with the hammer is sensed. The maximum input voltage is set at only 2.5 V for the geophone for triggering purposes. The data acquisition bandwidth is set at 1 kHz and the record length at the maximum, i.e. 8192 points. These values represent a good compromise between spectral resolution and necessity to sample over a period longer than the time needed for the motion signal to decay. In this case, the frequency resolution 0.313 Hz and the sampling period is 3.2 s. It is important to recall that sampling entire time history from the geophone is a key point in the data analysis. It may therefore be necessary in some cases to reduce the bandwidth or to adjust the delay in order to sample the entire time histories. We strongly recommend extreme care when adjusting the sampling parameters. The option “Every Frame” indicates that each measurement is ready to be triggered after the end of the sampling period corresponding to the previous measurement.

The user now has to input the tested calibration factors of PRIMA’s sensors, as defined in Section A3. As a reminder, the calibration values to be tested in the case of the studied PRIMA device are 28.8 mV/m/s for the geophone and 0.4905 kN/V for the load cell (when used with the specified conditioner settings). Open the *MC setup* menu and adjust, if necessary, the values corresponding to the sensitivity of geophone and load cell. Note that the

load cell channel uses a DC coupling whereas the geophone channel is AC coupled. Click on Apply and Close to return to the main window. To start the test, click on the button Avg. The system is now ready to acquire a series of 10 measurements and to perform the spectral average.

Apply the first impact with the rubber hammer as described in Section A3.2.2. Wait until the vibration in the beam dies out before impacting the beam for the second measurement. When ready, impact the beam again, and repeat until the series of ten measurements is completed.

Once the measurement series is recorded, save the file. In the case where the coherence function is significantly below one in the frequency range 10/20 Hz to 150/200Hz, the series of measurement can be considered as suspect, should not be taken into account but rather replaced by a new measurement series.

In this study, voltage output and corresponding velocity and force have been related using the values given by the sensors manufacturers.

As mentioned earlier, an independent check using dead load calibration for the load cell and direct comparison for the geophone showed that the output of the sensors was accurate. For future use, however, we would recommend preliminary checks and, if necessary, adjustment of the calibration factors.

Check the balance on the Vishay conditioner before each test series. The conditioner frequently shows a small drift, so that frequent adjustments are needed.

Close all programs and turn off the data acquisition system when the test series are completed.

A 4.3 Data interpretation

Open Matlab[®] software. Run the program “*BVTmobility.m*” provided with the BVT device. This program will analyze a given experimental data file to estimate the stiffness of the beam corresponding to this file.

The “*BVTmobility.m*” program is written to adjust the parameters of a theoretical model of the beam to the measured data, in the frequency window ranging from 10 Hz to 150 Hz. The theoretical model is a Single Degree Of Freedom (SDOF) system. All the data points in the 10 to 150 Hz window are used in a fitting process, except five points centered on the fundamental frequency of vibration of the beam.

Once the program runs, the user is prompted to choose the file to be analyzed. From this point on, the program is automatically executed. After a few seconds, the results are displayed on the Matlab[®] Command Window and illustrated by five plots. The main displayed results are the beam estimated stiffness and the percentage error between this estimate and the known true stiffness of the beam. The values of the true stiffness of the beam have been experimentally obtained by the procedure explained in the report. They are reported in Table A 4.2.

Beam span [m]	0.3	0.4	0.5	0.6	0.7
k_s [MN/m]	17.44	6.28	3.08	1.71	1.06

Table A 4.2. Values of k_s

The plots display the average measured data and fitted curves for both real and imaginary parts of the complex mobility function, the associated coherence function, the velocity time history corresponding to the last measurement in the series, and a theoretical dynamic stiffness curve constructed from the fitted parameters.

A 4.4 Results comparison and level of significance

The stiffness estimates resulting from the tests on the BVT, as presented in the previous sections, should be compared to the true values (see Table A4.2) keeping in mind that a minimum level of significance should be defined in order to validate or not the accuracy of the tested calibration factors. As a guideline associated with the comments mentioned in Section A3, the accuracy of PRIMA's sensors can be considered satisfactory when the mismatch between true and estimated stiffness do not exceed approximately 3 %.

In the case when the static stiffness verification test shows a significant mismatch between the true stiffness of the beam and its estimation using PRIMA's sensors (as presented in Section A3, an individual check for each of PRIMA's sensors might be useful. The corresponding tests are presented in the following sections.

A 5 - PRIMA'S LOAD CELL CALIBRATION TEST

The load cell's sensitivity can be simply checked using a dead weight calibration. To do so, the user needs a set of known masses. The PRIMA has to be connected to the Vishay conditioner for which the setup is identical than the one used in Section A4. In that case, however, the output can be directly read using a Voltmeter connected to the output of the Vishay conditioner, rather than using SigLab.

For this test, PRIMA device can be set up on the BVT or directly seated on a rigid surface. We suggest using the PRIMA device with the cap of the load cell and its rubber buffers assembled on the top of the base, with the guiding rod removed, so that the load can be applied. Doing so, the first mass is centered on the top of the rubber buffer. Depending upon the size of the masses, the user might need an intermediate support. The other masses can be added successively one over each other.

Measuring the output voltage for different levels of loading will enable the user to estimate the sensitivity of the load cell, which corresponds to the slope of the load vs. load experimental curve.

In the research study, such static calibration using dead weights indicated a calibration factor of 0.506 kN/V. The difference with the theoretical value derived in Section A3 is approximately 1.2 %. With regards to the experimental setup, it is therefore considered for the presented case that using the given value of 0.5 kN/V is satisfactory.

A 6 - PRIMA'S GEOPHONE CALIBRATION TEST

The verification of PRIMA's geophone calibration (sensitivity) is a little more involved. First it must be recognized that what needs to be checked is not only the output of the geophone itself, but rather the output of the geophone as given by PRIMA's. Indeed, PRIMA's data acquisition incorporates 1) a filter correction in the low-frequency range to compensate for sensor's non-linearity and 2) the integration of the velocity signal to yield a deflection time history.

A 6.1 Procedure for testing the displayed PRIMA's geophone output

A 6.1.1 Experimental setup

This test involves the BVT apparatus, both PRIMA's sensors, plus PRIMA's data acquisition and software, the independent data acquisition system, and the additional IMI. In this test, the output from PRIMA device, given by the manufacturer's software will be verified against the output of the IMI sensor, obtained using the SigLab analyzer. With regards to the comments of Section A2, this test might require a second computer solely devoted to PRIMA measurements (see "Solution 2" in Fig A6.1). This would be the case if the laptop used with the SigLab analyzer cannot record simultaneously the data from the two different data acquisition systems.

Set up the BVT apparatus and PRIMA device as specified in Section A2 - GENERAL INSTALLATION PROCEDURES. Connect PRIMA's sensors to the PRIMA electronic box. Connect the IMI geophone to the independent data acquisition system.

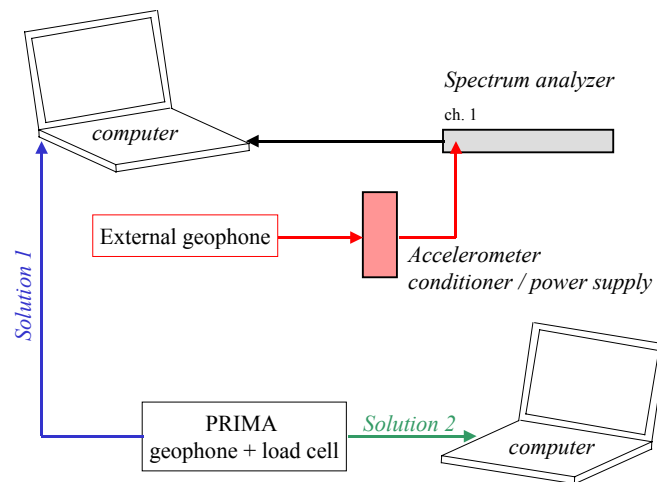


Fig. A6.1. BVT mobility test setup

Connections scheme (see Fig. A6.1):

- PRIMA geophone directly connected to PRIMA's electronic box,
- PRIMA load cell directly connected to PRIMA's electronic box,
- PRIMA electronic box connected to the adequate computer ports, using the PRIMA's manufacturer cable,
- IMI geophone connected to an input of the ICP signal conditioner; output of the conditioner connected to the SigLab input number one,
- SigLab output connected to the SCSI card inserted in the laptop.

Refer to Section A1 for the cable assembly type to use in each case.

A 6.1.2 Data acquisition

The reference SigLab program to use for routine PRIMA's geophone calibration checking test is the provided program "*BVTgeophoneref.vna*". Note that the IMI geophone must be connected to the channel number one in the SigLab analyzer as specified in the reference *vna* file and in the data analysis program.

Once the entire data acquisition hardware is connected and turned on, open the SigLab software, select the option "*vna*" under the Network menu (SigLab version 3.2), open the reference file "*BVTgeophoneref.vna*", and save it under a name chosen for the particular test sought. In order to adopt the nomenclature convention defined in the data analysis program, the name of the file for this test should always starts with the letter g followed by the number corresponding to the span of the beam in cm. Following this approach, the name of a file corresponding to a 60 cm span beam could be "*g60device2test5.vna*", as opposed to "*g70device2test5.vna*" for a test performed on a 70 cm span beam. The distinction in the nomenclature for this test and for the test of Section A4 will prevent any confusion during data analysis. Here again, the file should be saved under the directory "*C:\BVT\Measurements\SigLab_files*" or under any eventual subdirectory created under this path.

Two plotting windows are displayed in the *.vna* file. The upper window is setup to display the time history velocity measured by the IMI geophone, whereas the lower one is a plot of the amplitude of its Fourier transform (frequency amplitude spectrum). For this test no average process is embedded in the procedure. Measurement is manually triggered using a value of + 9 % for channel 1.

The maximum input voltage is set at only 2.5 V for the geophone for triggering purposes. The data acquisition bandwidth is set at 20 kHz and the record length at the maximum, i.e. 8192 points. Since PRIMA's software will sample data over a maximum period of 120 ms, there is no need to sample the entire time history with the SigLab analyzer. Also, precise adjustment of the sampling parameters is less critical for this test than it was for the beam stiffness test. In this case, a high time resolution is preferred. A poor resolution in frequency is of no consequence for the test based on a time domain comparison. Unless the IMI geophone is replaced by another reference sensor or recalibrated, there is no need to change the sensitivity entered in the *MC setup* menu. The sensor is AC coupled. As a reminder, the calibration factor of the IMI geophone used for the study and delivered with the BVT apparatus is equal to 3.859 V/m/s. To start the test, click on the *On* button of the trigger and then on the *Inst.* button. The system is now ready to record the data.

Let us turn towards the PRIMA software. For information about the software, please consult the manufacturer's users guide. Start the program and verify that its parameters are meeting the requirements of the test setup. In particular, select the option "*Save time history data*", check the entered plate radius (should be 50 mm) and the duration of the data acquisition. The user may want record using the maximum 120 ms time window to obtain more points to compare with the IMI geophone. It should be pointed out that this might not yield a better comparison since the integration performed in PRIMA's data acquisition might induce a distortion of the displacement time history. This effect is generally observed when dealing with signal integration; it increases with the number of points being integrated. Also check the triggering level for the load cell. The level should be set low enough to meet the test conditions. For example, choose a trigger of 30 kg. Once the parameters are checked, exit the setting window. The system should be ready for testing.

At this point both data acquisition systems are ready for testing. Apply the impact with the rubber hammer as described in Section A3.2.2. As a result, both SigLab analyzer and PRIMA's software should be triggered and start sampling the data. If only one of the systems is triggered, the user will have to stop the test and reset the triggered system for a new impact. Both systems must record the same impact test.

Once the test is completed, save the SigLab file and the PRIMA's software files. Save PRIMA's software files under the directory "*C:\BVT\Measurements\PRIMA_files*", with the same name than the SigLab file. Two files are generated by PRIMA's software: a data file with extension "*.crv*" and a results display summary file with the extension "*.pkv*". Only the "*.crv*" file will be used for the test purpose; the "*.pkv*" file can be either erased or kept for the user's records. To provide an example, the measurements PRIMA file corresponding to the test saved under the name "*g70device2test5.vna*" for the SigLab file should be saved as "*g70device2test5.crv*". Also note that in the case of the PRIMA files the user should not create any sub-directory under the directory "*C:\BVT\Measurements\PRIMA_files*", and save the files under the root. The reason for this restriction is that the data analysis program will automatically search for the file at this specific path location. Finally, when saving the file under the name of an existing file, always select replacing rather than appending. Always use a file with a unique measurement test.

Close all programs and turn off the data acquisition system when the tests are completed.

A 6.1.3 Data interpretation

The data analysis program to use for routine PRIMA's geophone calibration checking test is the provided program "*PrimaCompGeo.m*". This program opens SigLab and PRIMA files, reads the data and draws the velocity time histories associated with each file on the same plot. The velocity from PRIMA is not recorded on the file "*.crv*", but the displacement is. Using "*PrimaCompGeo.m*", the velocity signal is automatically computed from the displacement using a differentiation scheme.

Under Matlab, run the program "*PrimaCompGeo.m*". The user will be prompted to choose the SigLab file to analyze. Once the file is chosen, the program opens automatically the SigLab file and the associated PRIMA file. The program includes some options to modify the recorded time histories, namely a signal offset correction and a signal "time shifting" feature.

The offset correction is useful to remove the DC component eventually present in the signal (when the signal is not "centered" on the time axis). It is based upon a trial and error process in which the user is visually guided by time history plots.

The signals from PRIMA and from SigLab analyzer do generally not begin at the same time, which causes difficulties for a direct comparison. The program includes an option to “shift” in time the entire signal from PRIMA. Using here again a visual trial and error process, a delay can be estimated and the two signals can be approximately superposed for comparison purposes. Upon reaching a satisfactory superposition, the user confirms the correction and the program displays a final plot featuring both geophones time histories for the time window –15 ms to 200 ms.

The user can use the featured plot as a tool to draw conclusions regarding PRIMA’s geophone output accuracy. When doing so, it should be kept in mind that the superposition is often not perfect, even for a well-calibrated sensor, because the IMI geophone is not centered on the receptacle. For this reason, if the impact is not perfectly vertical, a rocking mode of vibration is excited and the motion of the IMI geophone will be biased.

A 6.2 Overview of the procedure for testing PRIMA’s geophone alone

Checking the output of PRIMA’s geophone alone will not yield any information on the quality of the displayed deflection during in-situ testing. However, a straightforward comparison between PRIMA’s geophone output and the output of the IMI geophone can also be performed using the BVT apparatus. The main steps of the procedure to follow are presented here. Both sensors are connected to the SigLab analyzer. Here again the SigLab software *vna* option is used, with the calibration factor of each sensor entered in the corresponding channels. Since there is not reference file provided for this test, the user will have to create its own file setup. Upon performing an impact test with BVT and PRIMA devices setups similar to those used in Section A4, one can display on the same plot both geophones’ time histories. A mismatch between both signals will indicate a calibration defect.

A 7 - DAMPED BEAM

Tests with the damped beam are similar to tests with the undamped beam described in the previous Chapters. The installation of the (optional) damping devices is described in Section A1.2.1.2. The tuning of the attachment of the devices is addressed in this last Chapter because it requires prior knowledge of BVT testing and practice with the data acquisition system.

The clamping force needs to be accurately tuned in order to obtain satisfactory results. This condition can only be reached using successive trials. The tuning process is successful when a significant reduction of the duration of vibration during testing can be noticed. To do so, the user will have to perform tests using Matlab to displays the duration of the geophone signal during testing. To provide the user with a guideline, tests using the undamped beam (for spans of 60 cm and 70 cm) showed durations of the velocity signal of the order of 2 – 3 s. Using an appropriate tuning of the clamping force, the signal duration was of the order of 20 – 50 ms. Remember that using the featured clamping devices with a 2.5 lb mass a loose connection is required.

A 8 - MANUFACTURER CONTACTS

- DSPT SigLab dynamic spectrum analyzer – Spectral Dynamics, Inc.
<http://www.dspt.com>
<http://www.spectraldynamics.com>
- IMI – Industrial Monitoring Instrumentation.
imi@pcb.com
<http://www.imi-sensors.com>
- IMI accelerometer/geophone signal conditioner - PCB PIEZOTRONIC, Inc.
gep@pcb.com
<http://www.pcb.com>
- LEMO plugs – LEMO Inc.
<http://www.lemo.ch>
LEMO USA Inc.
<http://www.lemousa.com>
lemous@lemousa.com
- Matlab[®] software - The MathWorks, Inc.
<http://www.mathworks.com>
- PRIMA 100 device
Carl Bro Pavement Consultants
http://www.pavement-consultants.com/dl_fwd.php
Keros Technology
<http://www.keros.dk/Engelsk/PRIMA100/index.htm>
- SCSI cards – Adaptec, Inc.
<http://www.adaptec.com>
- Strain gage conditioner/amplifier - Measurements Group - Vishay Intertechnology, Inc.
http://www.vishay.com/brands/measurements_group/main.html